Copy

RM A57E22

NACA RM A57E22

RESEARCH MEMORANDUM

SOME EFFECTS OF AILERON DEFLECTION ON THE STATIC LATERAL AND DIRECTIONAL AERODYNAMIC CHARACTERISTICS OF FOUR CONTEMPORARY AIRPLANE MODELS

By Willard G. Smith and Peter F. Intrieri

Ames Aeronautical Laboratory
Moffett Field, Calif.

CLASSIFIED DOCUMENT

This material contains information affecting the National Defense of the United States within the meaning of the espionage laws, Title 18, U.S.C., Secs. 793 and 794, the transmission or revelation of which in any manner to an unauthorized person is prohibited by law.

NATIONAL ADVISORY COMMITTEE
FOR AERONAUTICS

WASHINGTON

July 23, 1957

NACA RM A57E22

NATIONAL ADVISORY COMMITTEE FOR AERONAUTICS

RESEARCH MEMORANDUM

SOME EFFECTS OF AILERON DEFLECTION ON THE STATIC LATERAL AND DIRECTIONAL AERODYNAMIC CHARACTERISTICS OF FOUR CONTEMPORARY AIRPLANE MODELS

By Willard G. Smith and Peter F. Intrieri

SUMMARY

This report presents some effects of aileron deflection on the static lateral and directional aerodynamic characteristics of four airplane models which are representative of aircraft capable of flight at supersonic speeds. The results are presented for subsonic Mach numbers ranging from 0.60 to 0.90 and for supersonic Mach numbers ranging from 1.20 to 1.90. In these tests the angle of attack was varied from -4° to $+12^{\circ}$ while the angle of sideslip was held at zero. The Reynolds numbers of the tests were from 1 to 4 million based on the mean aerodynamic chord of the wing.

The results presented are limited to the most pertinent aerodynamic effects of ailerons contributing to the lateral and directional characteristics of each airplane type. The four models tested, with the exception of one aileron configuration, appear to meet current military rolling performance requirements through the speed range of this investigation. Each of the models exhibits generally favorable yawing moments with deflected ailerons. Aileron interference is shown to have a direct influence upon fuselage and tail loads and, consequently, upon the lateral and directional characteristics. Further, the strength of this interference is greater for inboard ailerons than for outboard ailerons.

INTRODUCTION

Since airplanes capable of flight at supersonic speeds are generally characterized by short-span wings, the ailerons are placed in close proximity to the fuselage and tail. Deflection of these ailerons may produce large changes in loading not only on the wing but also on the fuselage and tail. These aileron induced interference loads can significantly influence the lateral and directional characteristics of present day supersonic aircraft.

It is the purpose of this report to present data showing the effects of aileron deflection on the static lateral and directional aerodynamic characteristics of four contemporary airplane models which have been under investigation recently in the Ames 6- by 6-foot supersonic wind tunnel. These data were obtained from unrelated developmental wind-tunnel tests of predetermined model configurations specified by the military services wherein the stability was of primary importance. Hence, these data do not represent a systematic investigation of aileron effects but the results do summarize some of the current information pertinent to this study. The static lateral and directional stability characteristics of these models with controls undeflected are presented in reference 1.

NOTATION

All results are presented in standard coefficient form with the forces and moments referred to the body axes. The sign convention used to denote forces, moments, and angles is shown in figure 1. (See table I for moment center location.) The notation and definitions used in this report are as follows:

C_l rolling-moment coefficient, $\frac{\text{rolling moment}}{qSb}$

C_m pitching-moment coefficient, $\frac{\text{pitching moment}}{qS\bar{c}}$

C_n yawing-moment coefficient, $\frac{\text{yawing moment}}{qSb}$

C_Y side-force coefficient, $\frac{\text{side force}}{qS}$

ΔC_l increment of rolling-moment coefficient, (C_l for deflected ailerons minus C_l for undeflected ailerons)

ΔC_m increment of pitching-moment coefficient, (C_m for deflected ailerons minus C_m for undeflected ailerons)

ΔC_n increment of yawing-moment coefficient, (C_n for deflected ailerons minus C_n for undeflected ailerons)

ΔC_Y increment of side-force coefficient, (C_Y for deflected ailerons minus C_Y for undeflected ailerons)

[redacted]

M	free-stream Mach number
S	total wing area including the area formed by extending the leading and trailing edges to the vertical plane of symmetry, sq ft
V	true airspeed, ft/sec
b	wing span, ft (unless otherwise noted)
$\bar{c}$	mean aerodynamic chord of the wing, ft (unless otherwise noted)
p	rolling angular velocity, radians/sec
$\frac{pb}{2V}$	wing-tip helix angle, radians
q	free-stream dynamic pressure, lb/sq ft
α	angle of attack measured between the projection of the relative wind in the plane of symmetry of the model and the wing chord plane, deg
δ_a	aileron deflection (perpendicular to hinge line), deg (positive downward)

Subscripts

l	left
r	right
t	total

APPARATUS

Wind Tunnel and Equipment

The experimental results presented were obtained in the Ames 6- by 6-foot supersonic wind tunnel. This wind tunnel is of the closed-return, variable-pressure type in which the stagnation pressures can be varied from 2 to 17 pounds per square inch absolute. At the time of these tests, Mach numbers from 0.60 to 0.90 and from 1.20 to 1.90 could be

obtained. Recent modifications have extended the Mach number range. A complete description of the wind tunnel prior to these modifications is given in reference 2.

The models in each case were sting-mounted with the plane of movement of the system horizontal to utilize the most uniform stream conditions (see ref.2). The aerodynamic forces and moments were measured with an electrical strain-gage balance enclosed within the model. The electric unbalance in the strain-gage circuits was registered by recording type galvanometers which were calibrated by applying known loads to the balance.

The models used in these tests were of polished metal construction. Each model was fitted with simple, unsealed ailerons which could be set at several fixed deflection angles. The primary geometric characteristics of the four models are presented in table I. For simplicity, these models will be referred to as models A, B, C, and D (see fig. 2) for the remainder of this report.

TESTS AND PROCEDURE

The ranges of Mach number, Reynolds number, angle of attack, and aileron deflection were different for each of the four models investigated since, as previously stated, the data presented herein were obtained from unrelated tests. All Mach numbers investigated were within the range of 0.60 to 0.90 and 1.20 to 1.90. Data for subsonic Mach numbers were obtained for models A and B only and the minimum supersonic Mach number was higher for the larger models (B and D) in order that the shock waves reflected from the tunnel walls would not intersect any part of the model. The angle-of-attack range was generally from -4° to $+12^\circ$ in 2° increments. The effects of variation of sideslip angle were not investigated; results are presented for zero sideslip. The Reynolds numbers for these tests, based on the mean aerodynamic chord of the wings, were all within a range of from 1 to 4 million. Data were obtained for only three or four aileron deflection angles taken at increments of about 10°. The largest deflection angle was 25°.

In order that the results for the four models be consistent and somewhat comparable, all the results except the basic data are presented for aileron deflections which produce a positive rolling moment. Since only one aileron was deflected, the results for the other aileron were obtained by reversing the signs of the rolling-moment, side-force, and yawing-moment coefficients. For example, the yawing moment produced by a 10° up aileron on the left wing is assumed equal and of opposite sign to that of a 10° up aileron on the right wing. This manipulation is based on the model's symmetry about the XZ plane.

The stream curvature present in the vertical plane of the wind tunnel (ref. 2) was acting in the yaw plane of the model since, as noted previcusly, the models were pitched in the horizontal plane. The effects of these stream irregularities manifest themselves in these results as large side-force and yawing-moment coefficients and, to a lesser extent, rolling-moment coefficients at zero aileron deflection. Corrections for these stream effects were not made to the results because this investigation was concerned primarily with incremental data for aileron deflections and because the validity of the corrections might be doubtful for these large stream effects. It is believed that although the absolute level of yawing-moment, side-force, and rolling-moment coefficients is in error, due to stream effects, the incremental coefficients for the various aileron deflections are essentially correct. All the results do include corrections for the effects of the tunnel walls at subsonic speeds (ref. 3).

RESULTS

The results of these tests are grouped according to models. In order to facilitate identification of the model to which the data in a particular graph pertain, a sketch of the model is shown at the top of each graph. The form of presentation for each model is as follows:

1. Dimensional sketch of the model.

2. Detail drawing of the aileron.

3. Variation of rolling-moment, side-force, and yawing-moment coefficients with angle of attack.

4. Variation of the incremental control effectiveness parameters, ΔC_l, ΔC_Y, and ΔC_n, at $\alpha = 0^\circ$ with Mach number.

For models A and B the variations of pitching-moment coefficient with angle of attack and ΔC_m with Mach number are presented.

DISCUSSION

It is the intent to discuss herein only the broad aspects of the effects of aileron deflection on the static lateral and directional characteristics of each particular model, and to point out the pertinent aerodynamic factors contributing to the results.

Since these four models represent airplane prototypes, the rolling capabilities of the ailerons are of interest. The aileron effectiveness

parameter (pb/2V) was computed for each model with the use of experimental rolling-moment coefficients and theoretical values of damping in roll (refs. 4 and 5). The variation of pb/2V with Mach number, at an angle of attack of 0° and a total aileron deflection of 20°, is presented in figure 3. Aeroelastic effects were not considered in obtaining these results and the damping contribution of the tails were neglected. The roll response for a single degree of freedom of the four airplanes was computed using the data of figure 3 and mass characteristics which were believed to be representative in each case. The aileron response characteristics are presented in figure 4 in terms of the total aileron deflection necessary to roll each airplane 100° in one second, assuming a step aileron deflection.

An evaluation of the rolling performance of these airplanes can be made by comparing the predicted rolling characteristics presented in figures 3 and 4 with the minimum rolling performance requirements listed in the current military flying qualities specifications (ref. 6). Stated briefly, the requirements are: pb/2V = 0.09 below minimum combat speed and at high speed the airplane must roll 100° in one second. The rolling performance predictions presented in figures 3 and 4 indicate that all the models, except model B with inboard ailerons, are capable of meeting the roll requirements of reference 6 with total aileron deflections of 40° or less.

Model A

Model A is of particular interest, in this group of four models, because of the high wing and low horizontal tail location on the fuselage. A three-view drawing of the model is shown in figure 5(a). Figure 5(b) shows a detailed drawing of the right aileron. Further details concerning the geometric characteristics are presented in table I.

Experimental rolling-moment, side-force, and yawing-moment coefficients are presented in figures 6 and 7 for several aileron deflection angles through the angle-of-attack range for the complete model and wing-fuselage configuration. These data are summarized as functions of Mach number in figure 8.

The increments of rolling-moment coefficient (fig. 8) for the complete model and wing-fuselage combination show that the aileron induced loads on the tail reduce the roll capability of the ailerons by about one third.

The effects of aileron deflection on the directional characteristics of model A are presented in figure 8. The complete model experiences favorable yawing moment, that is, positive yawing moment with a positive rolling moment. This favorable yawing moment is due largely to the

aileron induced loads on the tail which exceed the effects of aileron drag. The yawing-moment coefficient for a total differential aileron deflection of 20° is approximately equivalent to that resulting from a sideslip angle of 7° at subsonic speeds and 3° at supersonic speeds (ref. 1). For the wing-fuselage configuration, a small positive side force results from either a positive left aileron deflection or a negative right aileron deflection, due to air loads acting on the fuselage below the plane of the ailerons. These side forces would tend to give negative yawing moments. However, in the case of the negatively deflected right aileron, the effect of aileron drag is greater than the interference effect and a positive yawing moment results.

A continual decrease with increasing angle of attack in the increment of side-force and yawing-moment coefficients due to deflected ailerons is evident in the results for the complete model presented in figure 6. Comparison of the results for the complete model (fig. 6) with those for the wing-fuselage configuration (fig. 7) indicates that the side force induced on the vertical tail by the deflected aileron is in the opposite direction to that induced on the fuselage. Further examination of the results shows that it is the aileron-fuselage interference loads which vary with angle of attack while the induced loads on the tail remain nearly constant. The nature of this aileron-fuselage interference appears to be due to the high wing location since the other three models do not show this same relationship between fuselage and tail load.

The pitching moment due to an aileron deflection will be considered an interference effect since ailerons on airplanes of this type are generally not used for longitudinal control. The variation of pitching-moment coefficient with angle of attack for several aileron deflections for the complete model and for the tail-off configuration is shown in figure 9. A differential aileron deflection of -10° and +10° produces a resultant pitching moment of practically zero through the speed range of this investigation (fig. 8).

Model B

Model B, unlike the preceding model, has a horizontal tail mounted high above the wing chord plane. The low aspect ratio midwing is basically unswept. A three-view drawing of this model is presented in figure 10(a). The model was equipped with both an outboard and an inboard aileron. A detailed drawing of these ailerons is presented in figure 10(b). Further details concerning the geometric characteristics of model B are presented in table I.

The data are arranged in two groups. The first group presents the data for the outboard aileron for the complete model and wing-fuselage

combination (figs. 11 and 12). The second consists of data for an inboard aileron (figs. 13 and 14) for the complete model and model without the horizontal tail.

Relatively poor roll effectiveness is obtained with the inboard ailerons especially at supersonic speeds. The small increments of rolling moment obtained with this aileron (fig. 15(b)) are largely attributable to the short distance from the aileron to the moment center location.

Deflection of either inboard or outboard ailerons (fig. 15) produces favorable yaw. A much greater side force and yawing moment results, however, from a deflection of the inboard aileron due to its closer position to the vertical tail. This effect of spanwise location of ailerons is further emphasized here by the fact that the deflection angle of the inboard aileron was smaller than that of the outboard aileron. The outboard-aileron interference loads on the vertical tail, obtained by comparing results for the model with and without the tail (fig. 15(a)), decrease with increasing supersonic speed. Above a Mach number of 1.7 no outboard-aileron interference effects on the tail were observed, since the tail was outside the Mach lines from the inboard end of the aileron. Data are not available for the inboard aileron tail-off configuration to further this analysis. Further inspection of the data shows that for the outboard aileron a negative deflection gives a greater side force and yawing moment than a positive deflection, but for the inboard aileron the reverse is true.

The variation, with angle of attack, of side force due to deflection of the outboard aileron for model B (figs. 11 and 12) is somewhat different from the variation shown for model A. In contrast to model A, the aileron induced loads on the fuselage and vertical tail are additive for model B and although the fuselage loads increase slightly with angle of attack, the aileron induced side force on the complete model remains essentially constant.

The longitudinal trim change for the complete model resulting from the deflection of the outboard ailerons (fig. 15(a)) shows practically no change with Mach number. The trim change resulting from deflection of the inboard ailerons (fig. 15(b)) does vary with Mach number, and becomes negative at a Mach number of about 1.7. The horizontal tail in both cases decreases the increment of pitching moment due to deflected ailerons (fig. 16).

Model C

Model C, in contrast to models A and B, has no horizontal tail. The wing plan form of this model is basically triangular, but modified by rounded tips and indented trailing edges. The ailerons extend along the whole exposed trailing edge of the wing. A three-view drawing of the

model is presented in figure 17(a). A detailed drawing of the left aileron is presented in figure 17(b). Further details concerning the geometric characteristics of model C are presented in table I.

The variations of rolling-moment, side-force, and yawing-moment coefficients with angle of attack are presented in figure 18 for several aileron deflections. These data are summarized in figure 19 as functions of Mach number.

Plus and minus aileron deflections produce proportionally the same rolling moments. This proportionality holds up to an aileron deflection of -20°.

Model C experiences favorable yawing moment with aileron deflection in the Mach number range of this investigation (fig. 19). These results indicate that for equal aileron deflections of opposite sign, the net yawing moment will be essentially zero. However, ailerons on this airplane are also used for longitudinal control, and at normal trim conditions, the control surface deflections will be negative. For rolling maneuvers at these trim conditions, the resulting unequal negative deflections will produce favorable yawing moments (figs. 18 and 19).

Two interesting effects of aileron deflection on the lateral and directional characteristics were observed for this model. Both are directly associated with the relatively close proximity of the aileron and vertical tail, typical of most tailless airplanes. First, there was a marked decrease in the incremental tail load, due to the deflected aileron, with increasing angle of attack. This is apparent, at least for negative deflections, in figure 18 from the variation of side-force and yawing-moment coefficients with angle of attack for several aileron deflections. Secondly, figure 18 shows that the increments of side force and yawing moment for aileron deflections of -20° and -25° are much larger proportionally than would be expected from, for example, the increments for a deflection of -10°. Both of the foregoing effects are due to changes in the tail load caused by relocation of the shock wave from the aileron. As the angle of attack increases, the shock wave from a deflected aileron will bend back because of the accelerated flow over the upper surface of the wing, thus reducing the area of the vertical tail which is influenced by the pressure field of the aileron. As the deflection angle of the aileron increases, the shock wave detaches and moves forward. This exposes a greater portion of the tail to the pressure field of the aileron with a consequent increase in aileron induced load. At a Mach number of 1.9, both of these effects are less apparent since the shock waves are swept back so that a relatively small portion of the vertical tail is influenced by pressure disturbances from the ailerons.

Model D

This model is comparable to the preceding model in that it is also basically a triangular wing airplane with no horizontal tail. A small vertical stabilizing surface extends from the external store, but it is believed to be sufficiently forward of the ailerons so as to have no effect on the results presented herein. A three-view drawing of the model is presented in figure 20(a) and a detailed drawing of the right aileron is presented in figure 20(b). Further details concerning the geometric characteristics of model D are presented in table I.

Although data for this model are available for only two supersonic Mach numbers, these data show very nearly the same trends for comparable aileron deflections as did the results for the preceding model both in the variations with angle of attack (fig. 21) and the incremental data (fig. 22).

Model D experiences favorable yawing moment with deflected ailerons for the Mach number range of this test. This model, like model C, has negative control deflections at normal trim conditions. Unequal negative aileron deflections, for rolling at these trim conditions, produce favorable yawing moment (fig. 22).

The increments of side force and yawing moment for a negative 5° aileron deflection are considerably larger than for a positive 5° deflection. This probably results from the detachment and forward movement of the compression wave from the negatively deflected aileron. The influence of this aileron is then felt over a larger part of the vertical tail than that of the positively deflected aileron with its attached expansion wave.

Since in this test both the right and left ailerons were deflected, the results offer an opportunity to verify superposition of the effects of the ailerons at supersonic speeds. The sum of the effects of a -5° left aileron deflection and a $+5^\circ$ right aileron deflection (fig. 21) is nearly equal to the effects for a total aileron deflection of $\pm 5^\circ$.

CONCLUDING REMARKS

The results of this investigation show the pertinent effects of aileron deflections on the static lateral and directional aerodynamic characteristics of four contemporary airplane models. Each of the models, except model B with inboard ailerons, has sufficient aileron effectiveness to meet current military rolling performance requirements. All models tested exhibited, in varying degree, favorable yawing moment with aileron

deflection. Aileron interference effects are shown to have a direct influence upon fuselage and tail loads and consequently upon the lateral and directional characteristics of the airplane. The magnitudes of these effects were found to be greater for the ailerons extending farthest inboard.

Ames Aeronautical Laboratory
National Advisory Committee for Aeronautics
Moffett Field, Calif., May 22, 1957

REFERENCES

1. Smith, Willard G., and Ball, Louis H.: Static Lateral-Directional Stability Characteristics of Five Contemporary Airplane Models From Wind-Tunnel Tests at High Subsonic and Supersonic Speeds. NACA RM A55J03, 1956.

2. Frick, Charles W., and Olson, Robert N.: Flow Studies in the Asymmetric Adjustable Nozzle of the Ames 6- by 6-Foot Supersonic Wind Tunnel. NACA RM A9E24, 1949.

3. Silverstein, Abe, and White, James A.: Wind-Tunnel Interference with Particular Reference to Off-Center Positions of the Wing and to the Downwash at the Tail. NACA Rep. 547, 1935.

4. Jones, Arthur L., and Alksne, Alberta: A Summary of the Lateral-Stability Derivatives Calculated for Wing Plan Forms in Supersonic Flow. NACA Rep. 1052, 1951.

5. DeYoung, John: Theoretical Antisymmetric Span Loading for Wings of Arbitrary Plan Form at Subsonic Speeds. NACA Rep. 1056, 1951.

6. Anon.: Flying Qualities of Piloted Airplanes. Military Specification MIL-F-8785(ASG), Sept. 1, 1954, including Amendment 2, Oct. 17, 1955.

[redacted]

TABLE I.- PRIMARY PHYSICAL CHARACTERISTICS OF THE WIND-TUNNEL MODELS

	Model A	Model B	Model C	Model D
Wing				
Plan form	Sweptback	Unswept	Modified triangular	Modified triangular
Aspect ratio	3.4	2.5	2.02	2.1
Moment center, $\bar{c}$	0.287	0.25	0.25	0.25
Area[1], ft^2	.662	1.406	2.728	5.338
Mean aerodynamic chord, ft	.495	.799	1.288	2.128
Vertical tail				
Area[1], ft^2	.1758	.421	.468	.712

Physical Characteristics of the Ailerons

	Model A	Model B		Model C	Model D
Aileron					
Plan form	Tapered	Inboard tapered	Outboard tapered	Constant chord	Tapered
Ratio of aileron area to 1/2 wing area	0.109	0.058	0.049	0.088	0.12
Sweep of hinge line, deg	26.5	0	0	16.9	0
Centroid in % semispan	41.4	35.7	79.3	60.2	42.1

[1]Total area with leading and trailing edges extended to longitudinal axis.

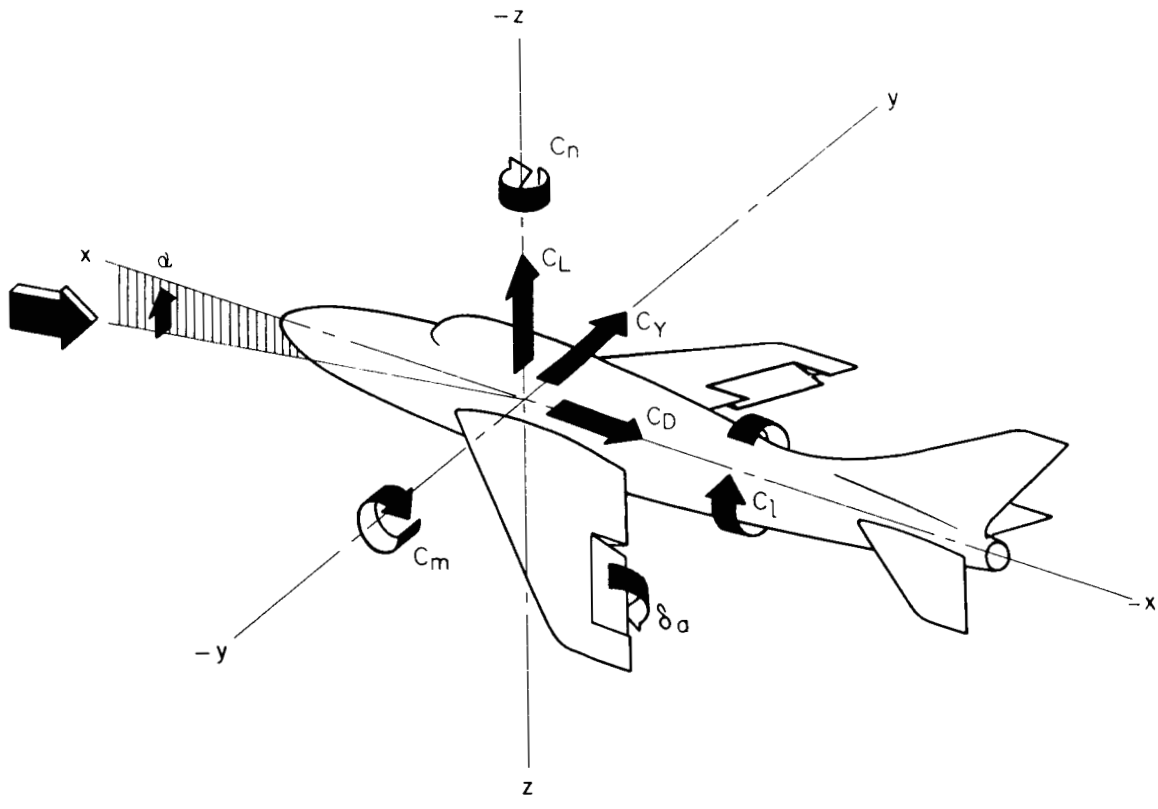

Figure 1.- Airplane axes; positive forces, moments, and angles.

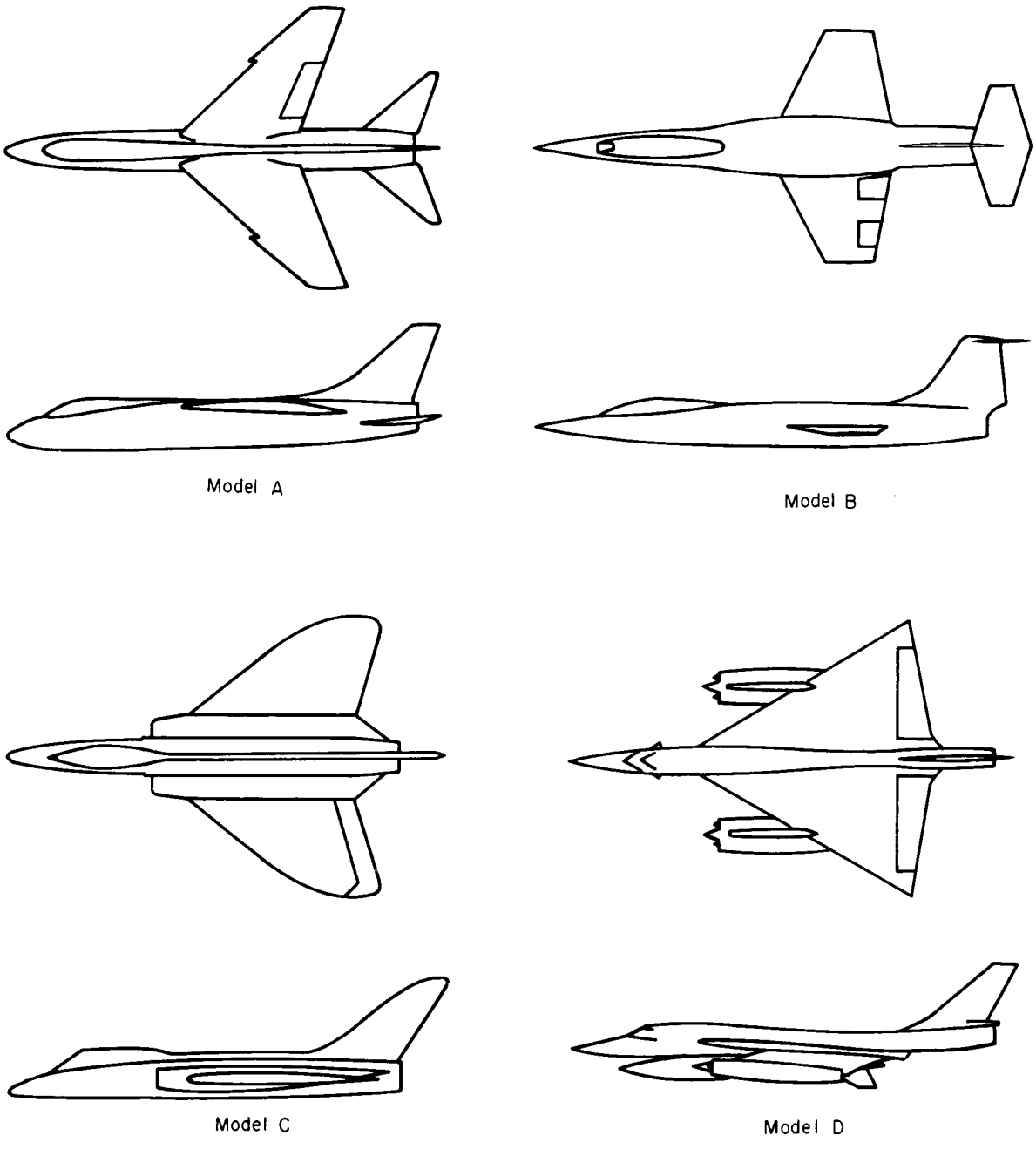

Figure 2.- General arrangement of the four models tested.

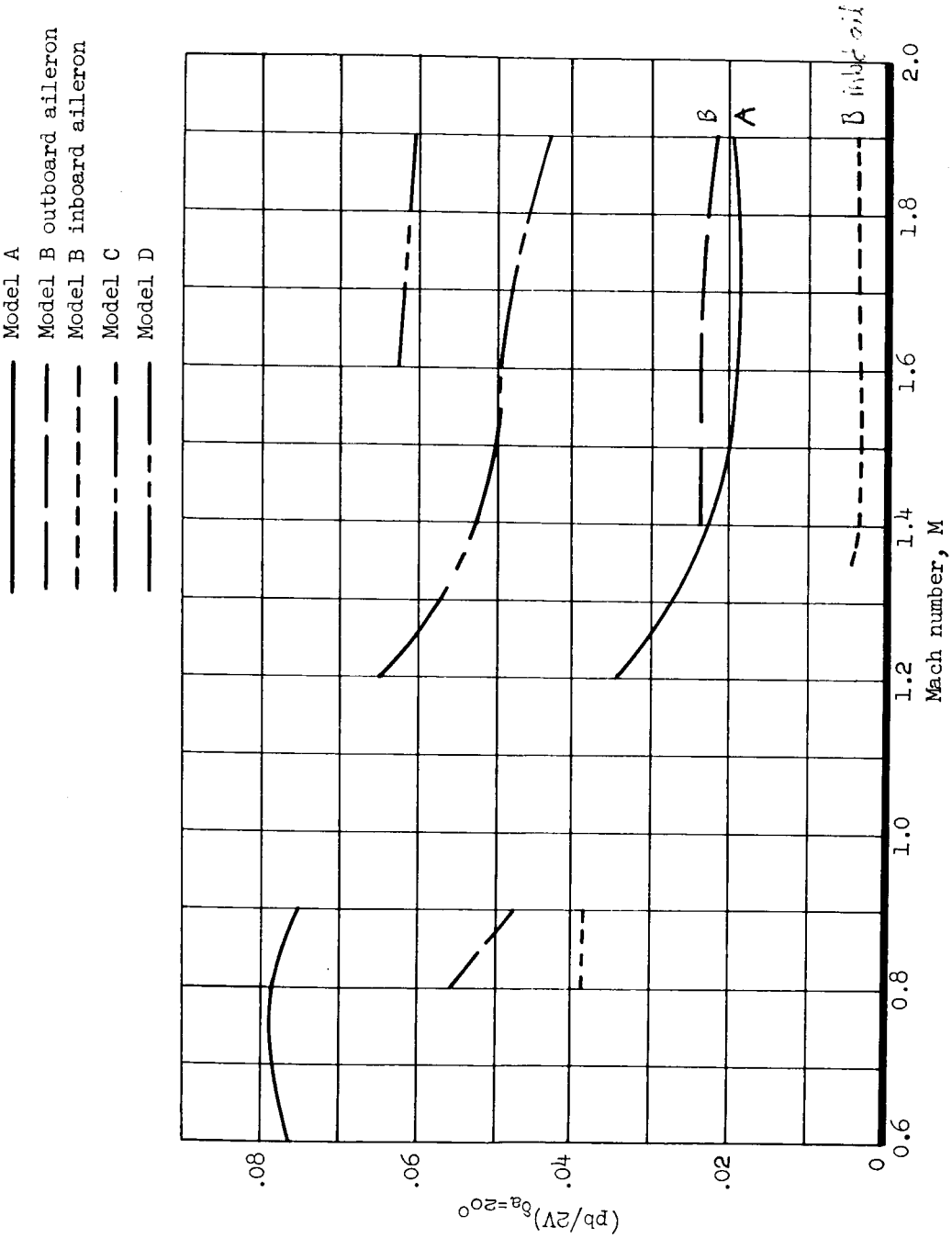

Figure 3.- Variation of aileron effectiveness with Mach number for a total aileron deflection angle of 20°; $\alpha = 0^o$.

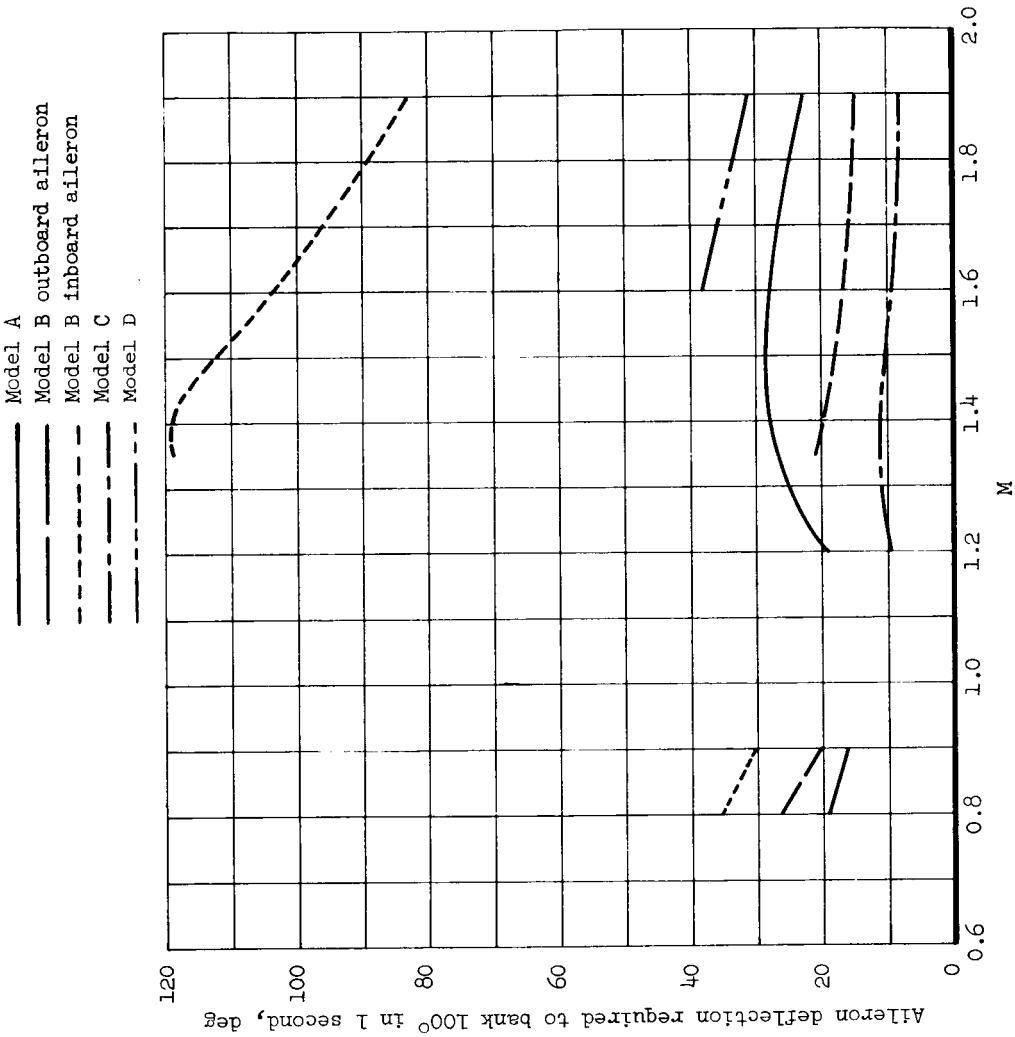

Figure 4.- Variation of total aileron deflection required to attain a bank angle of 100° in one second; single degree of freedom, step aileron deflection, $\alpha = 0°$.

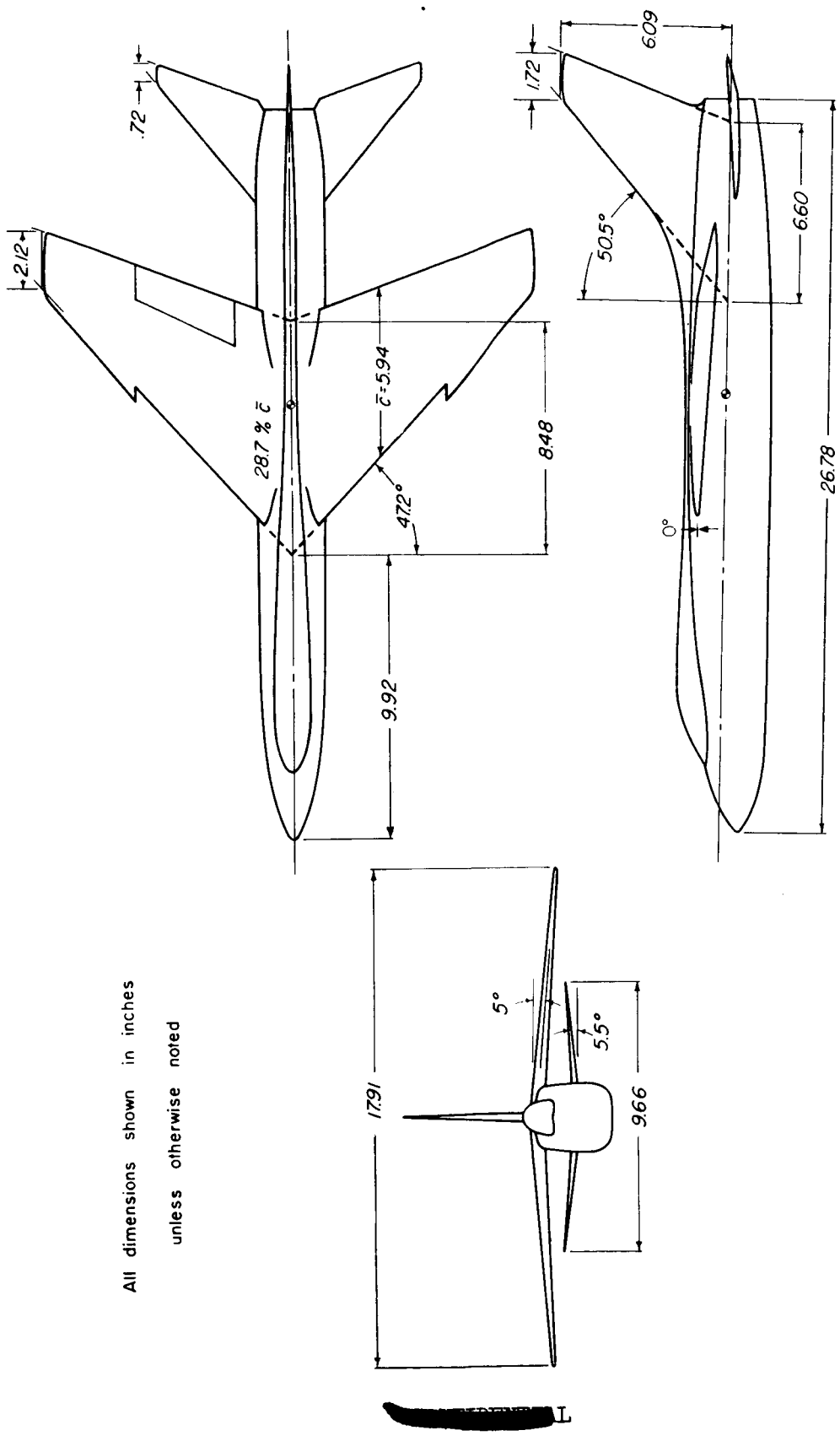

(a) Three-view drawing.

Figure 5.- Dimensional sketch of model A.

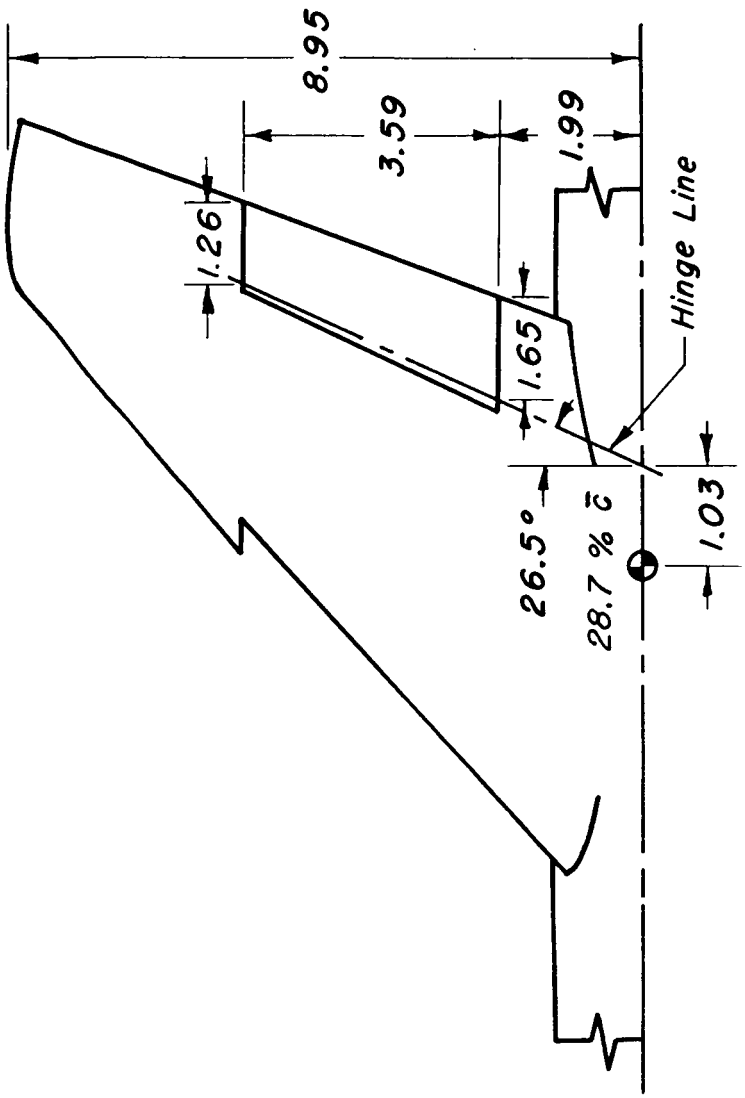

(b) Aileron detail.

Figure 5.- Concluded.

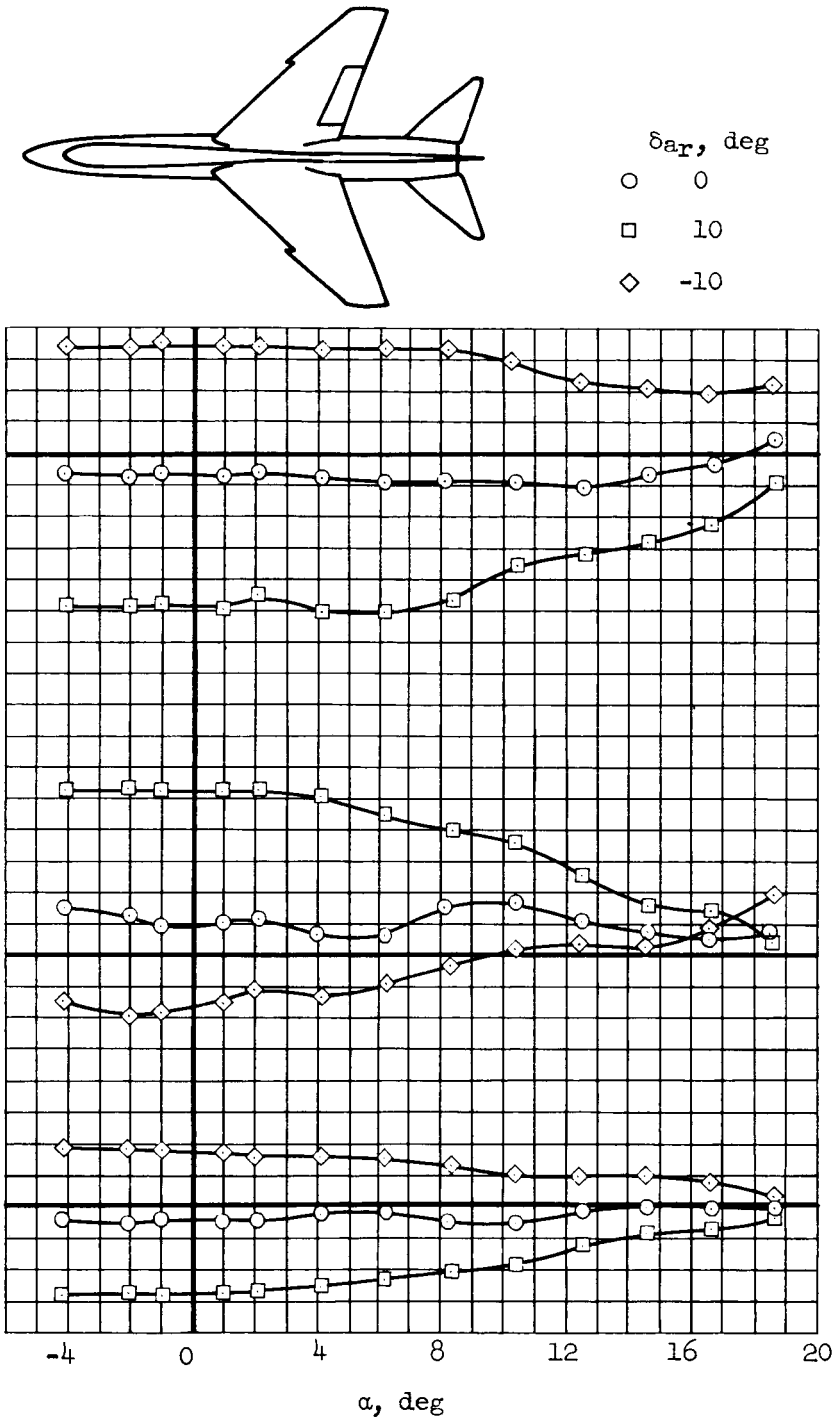

(a) M = 0.60

Figure 6.- Variation of C_l, C_Y, and C_n with angle of attack for model A.

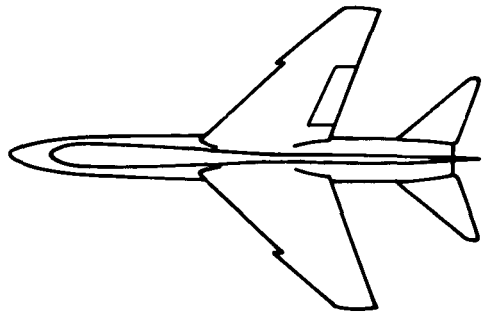

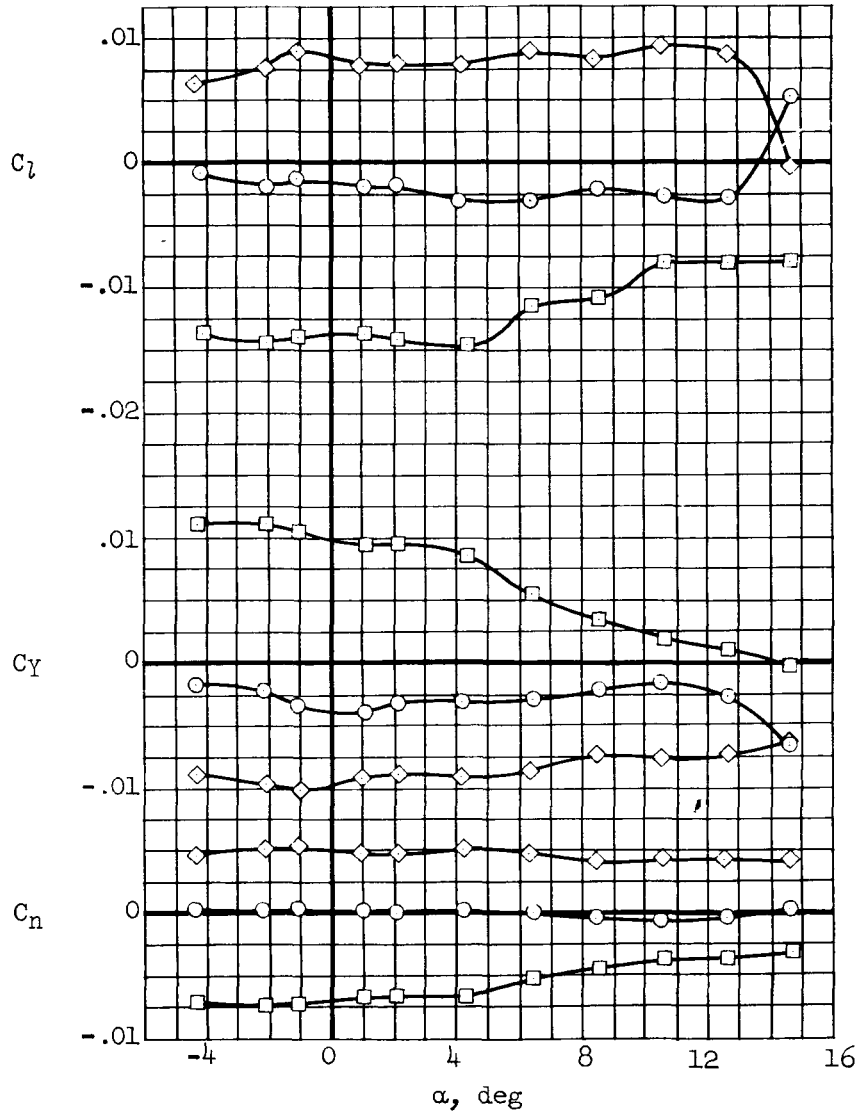

(b) M = 0.90

Figure 6.- Continued.

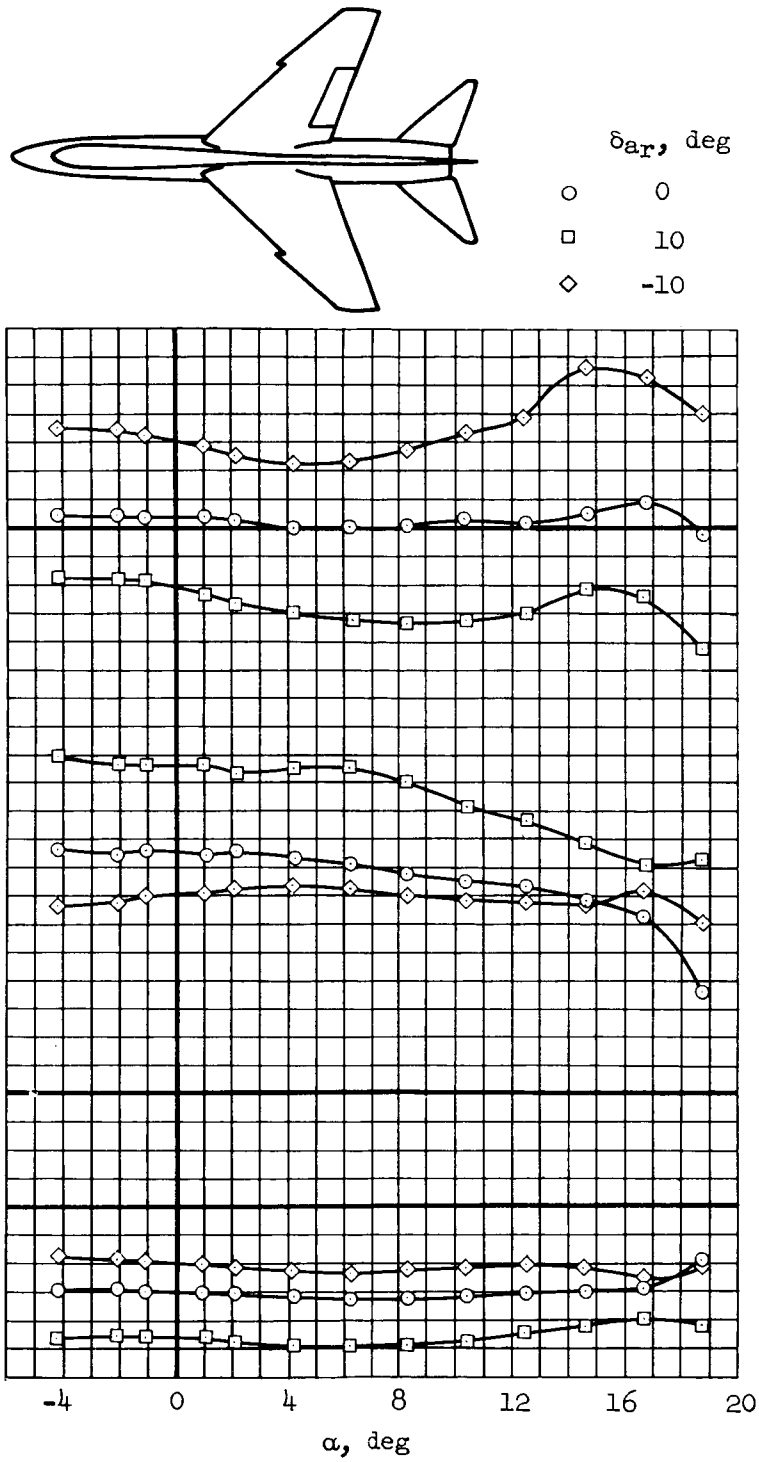

(c) M = 1.20

Figure 6.- Continued.

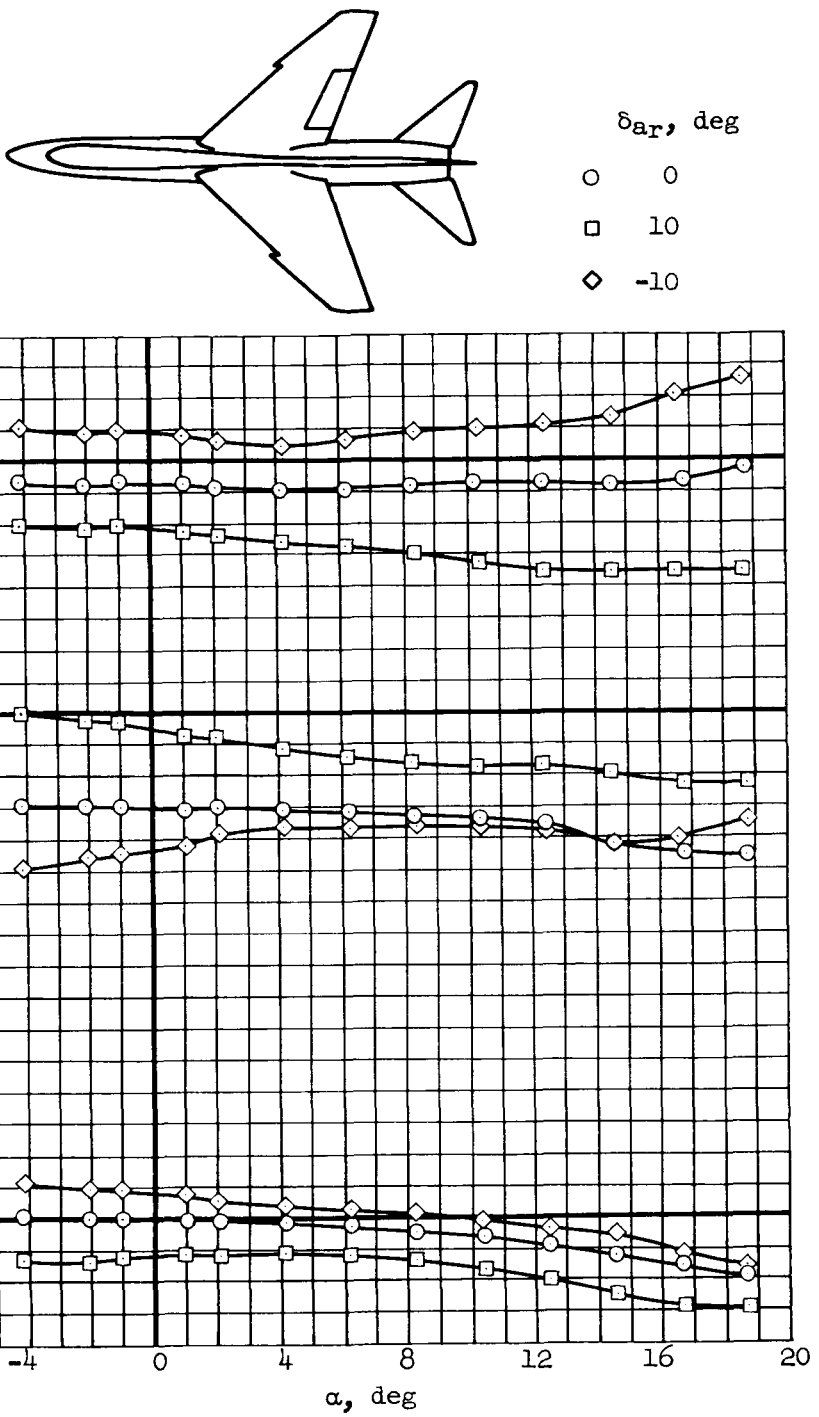

(d) M = 1.40

Figure 6.- Continued.

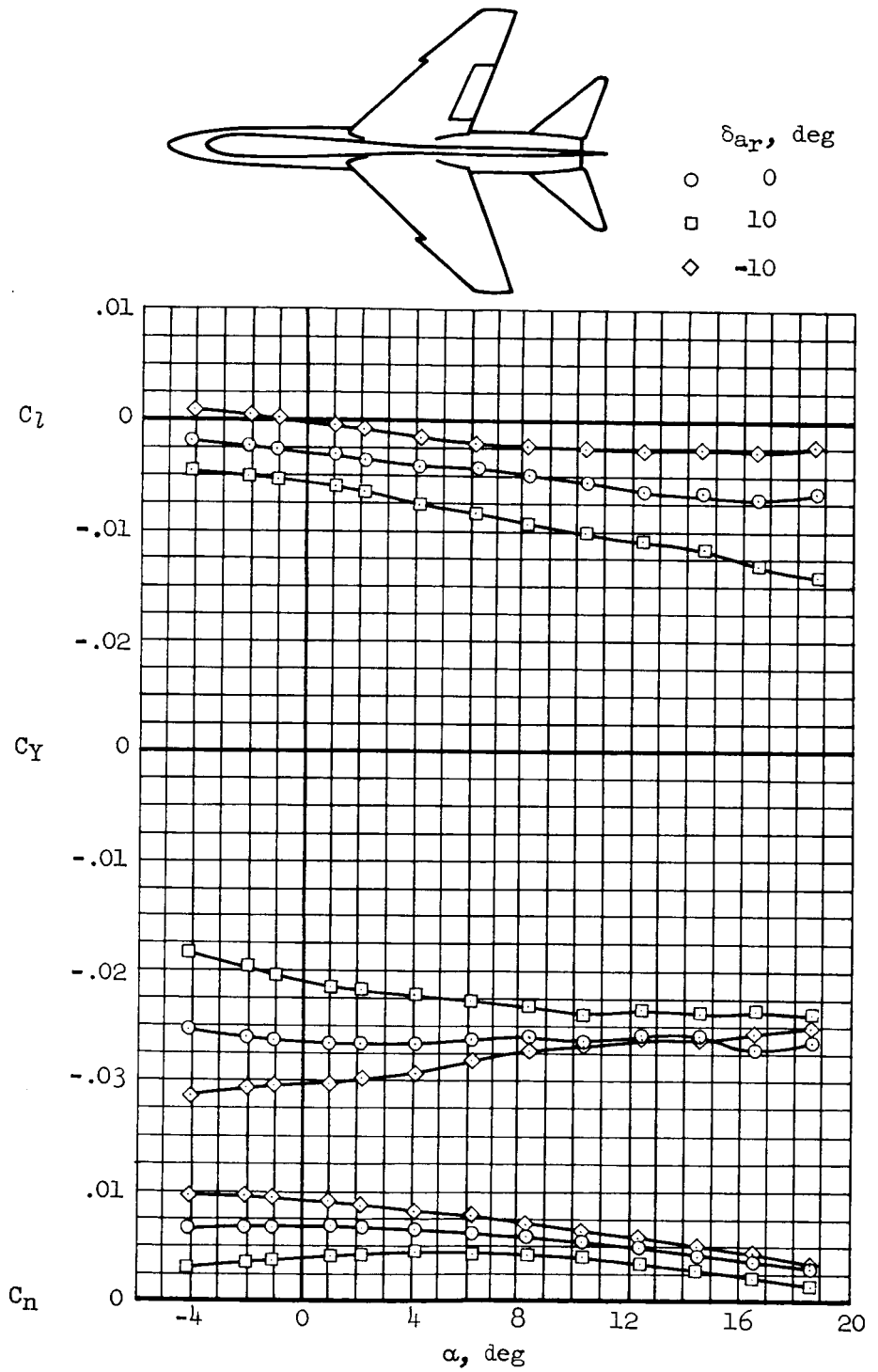

(e) M = 1.60

Figure 6.- Continued.

[redacted]

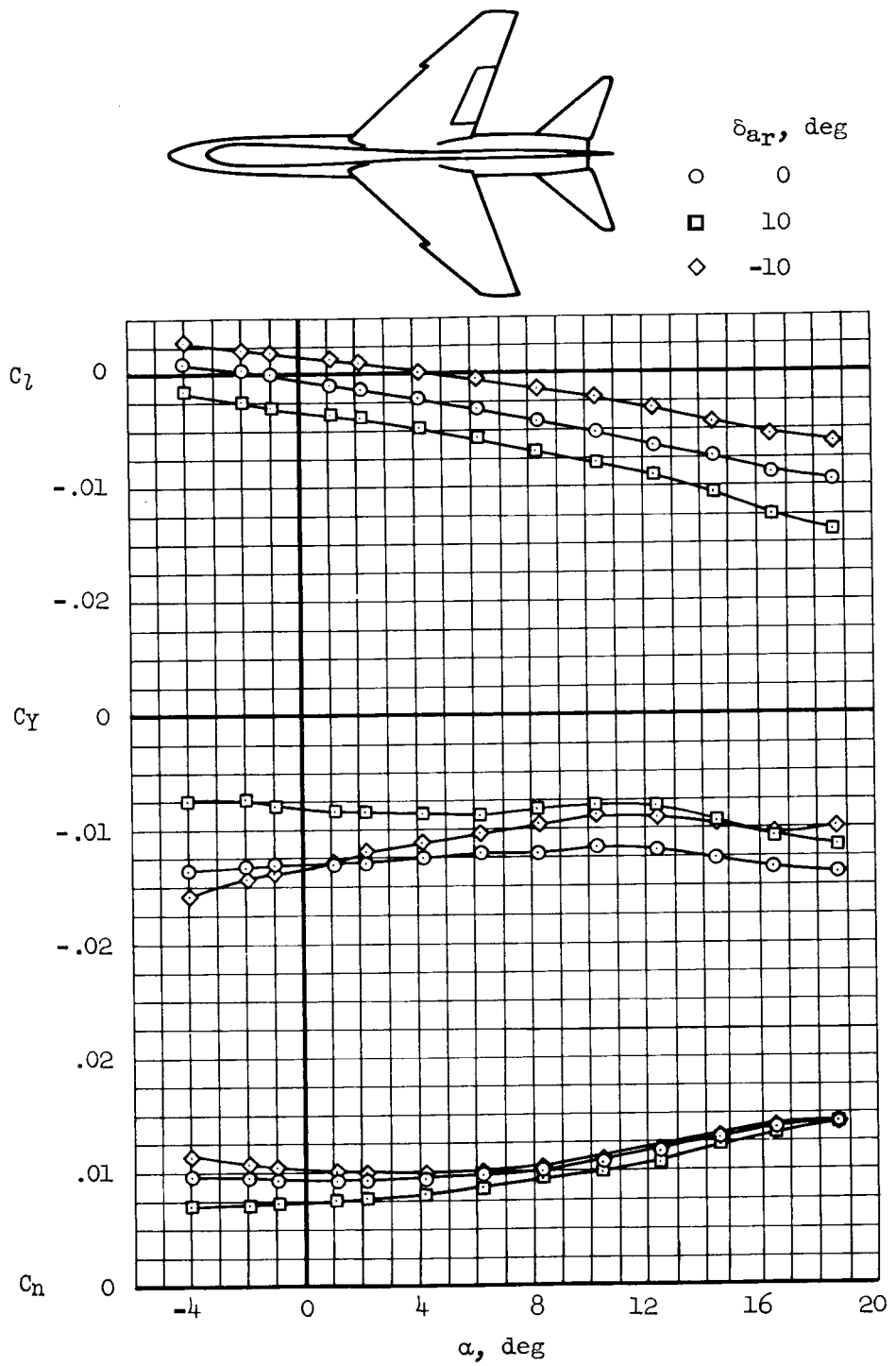

(f) M = 1.90

Figure 6.- Concluded.

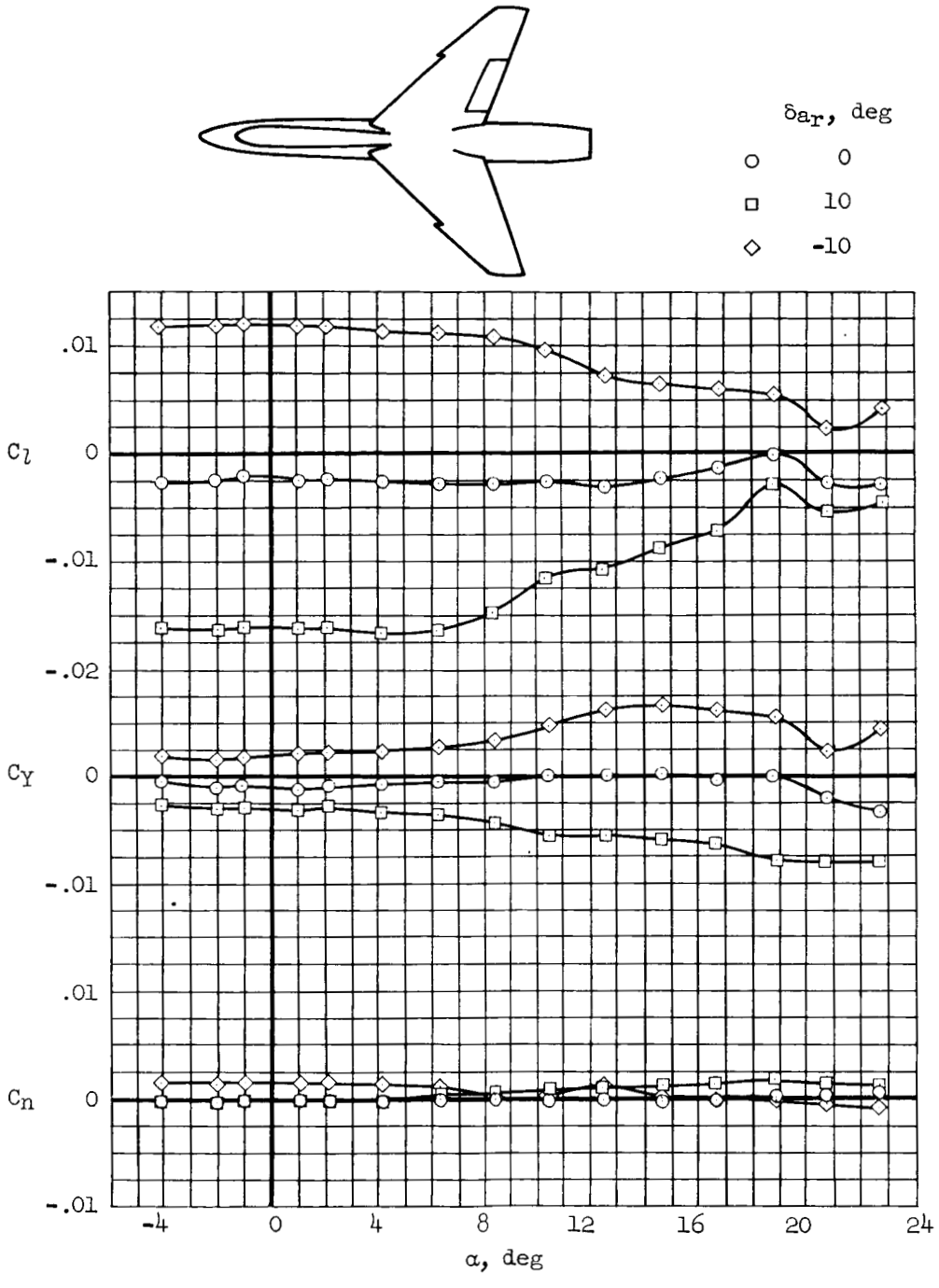

(a) M = 0.60

Figure 7.- Variation of C_l, C_Y, and C_n with angle of attack for model A with the tail removed.

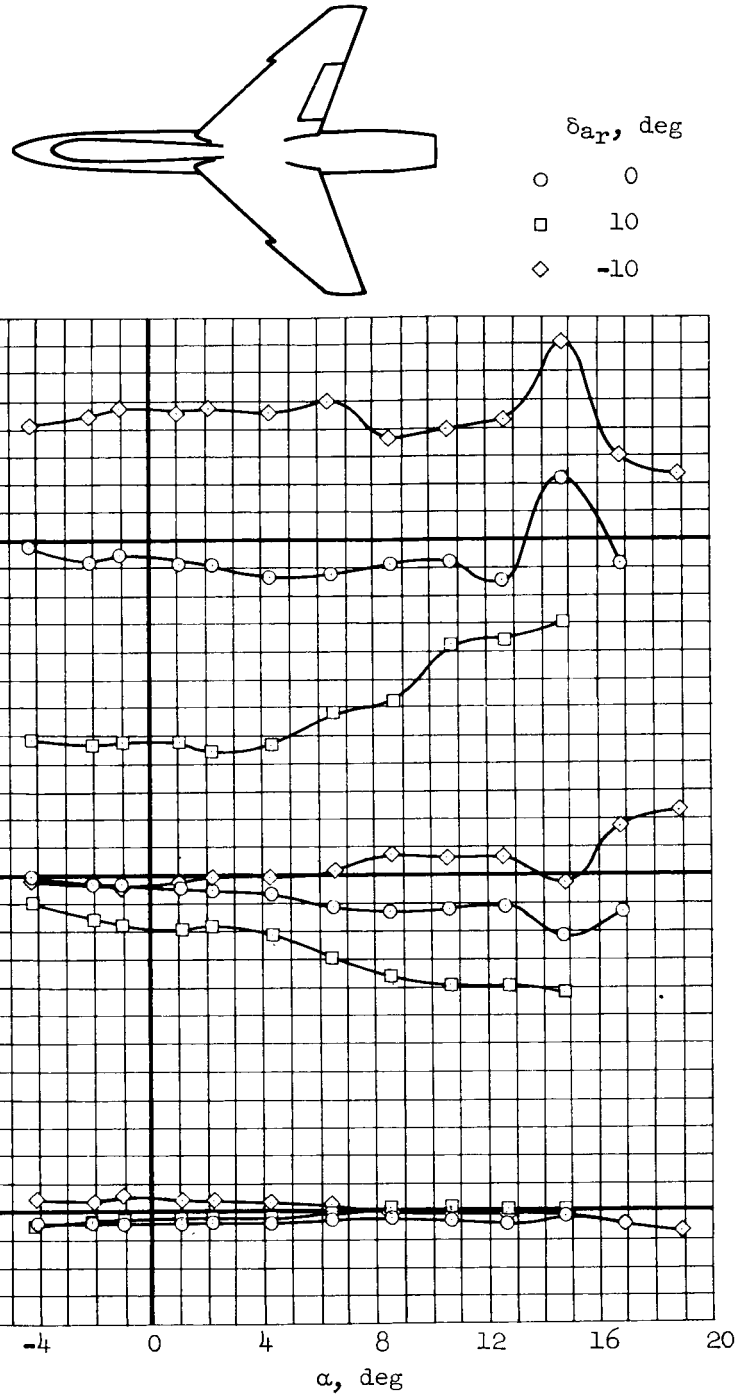

(b) M = 0.90

Figure 7.- Continued.

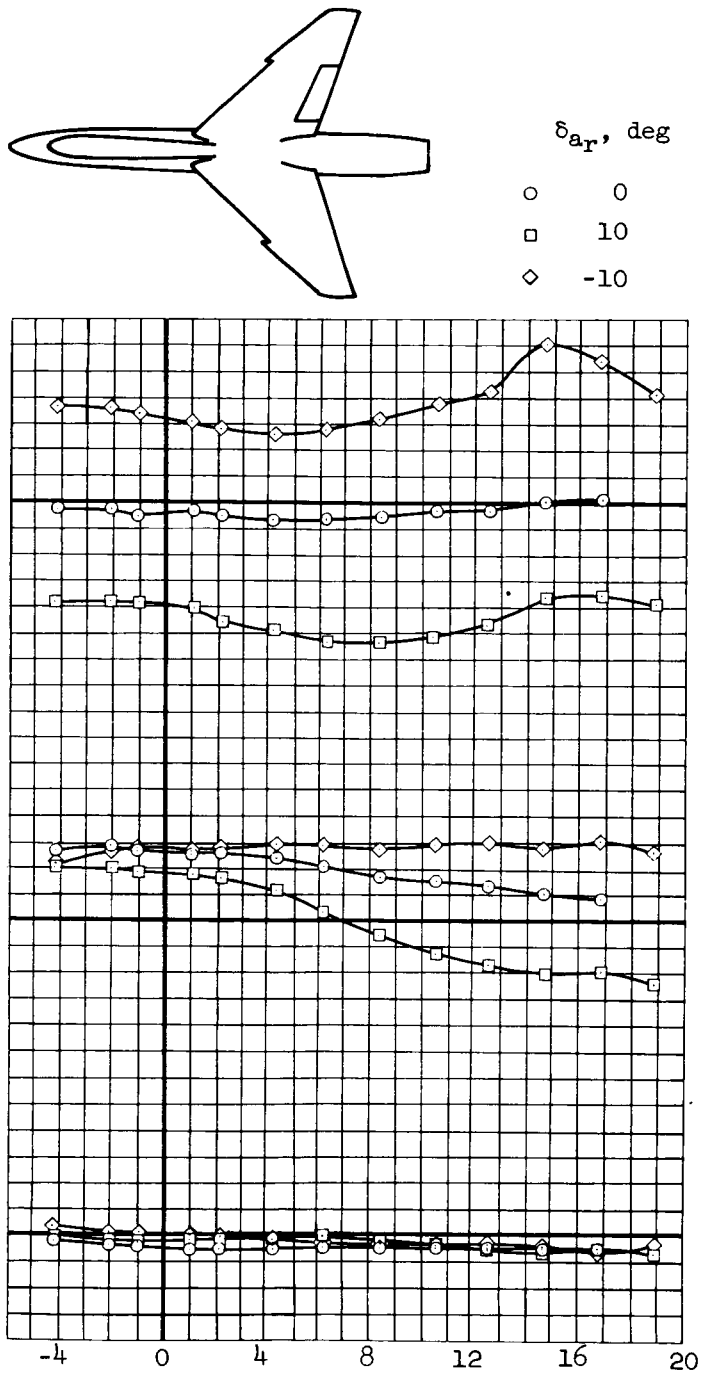

(c) M = 1.20

Figure 7.- Continued.

[redacted]

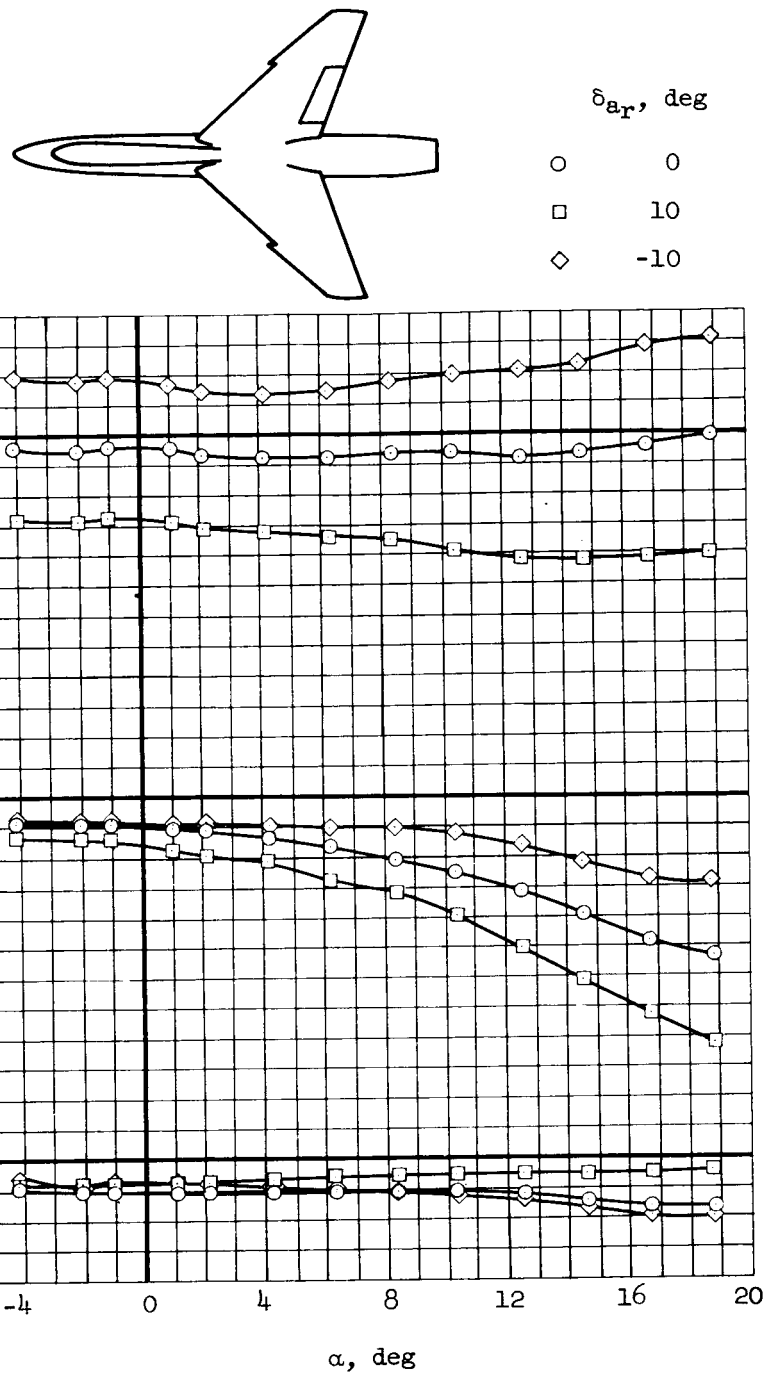

(d) M = 1.40

Figure 7.- Continued.

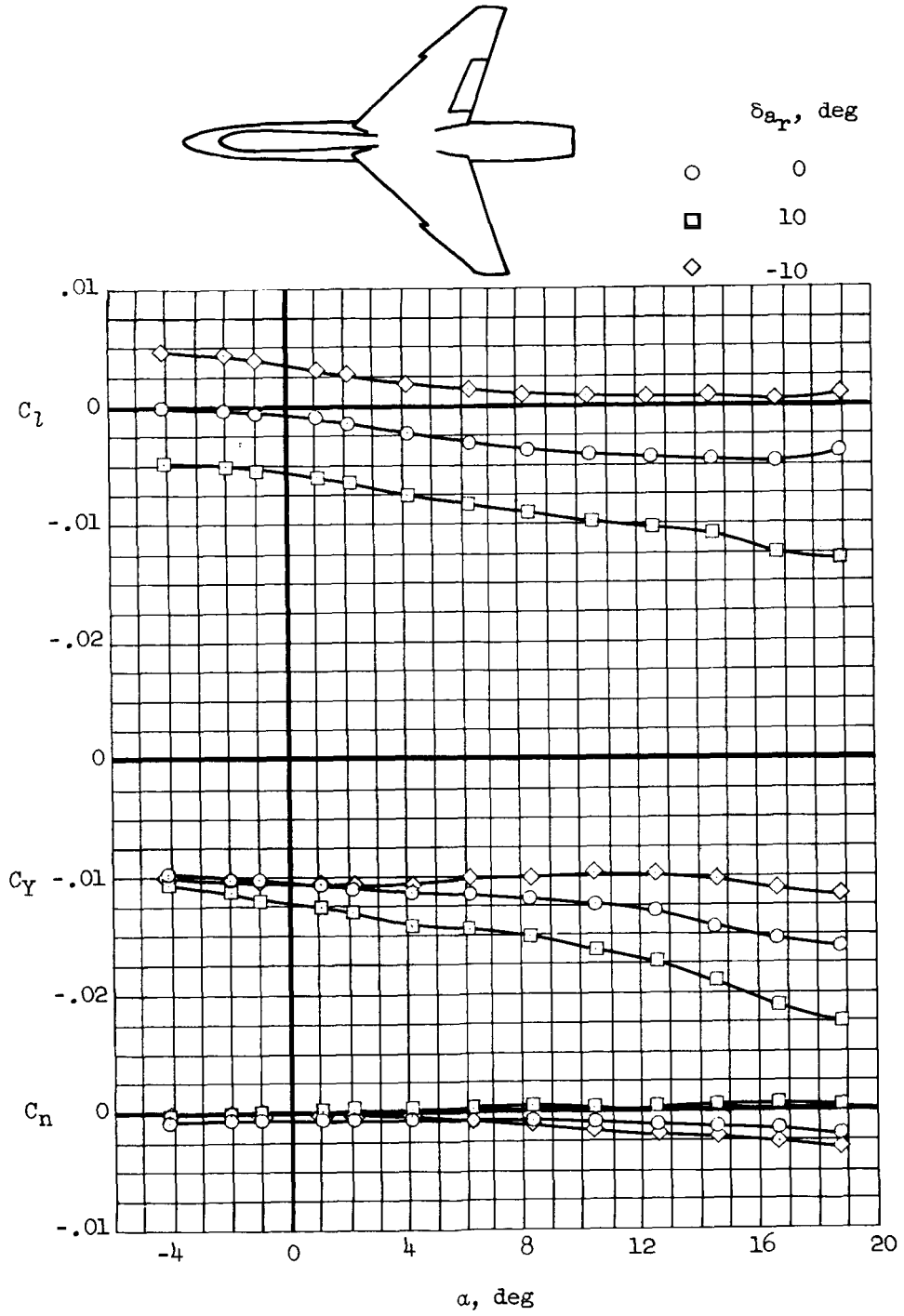

(e) M = 1.60

Figure 7.- Continued.

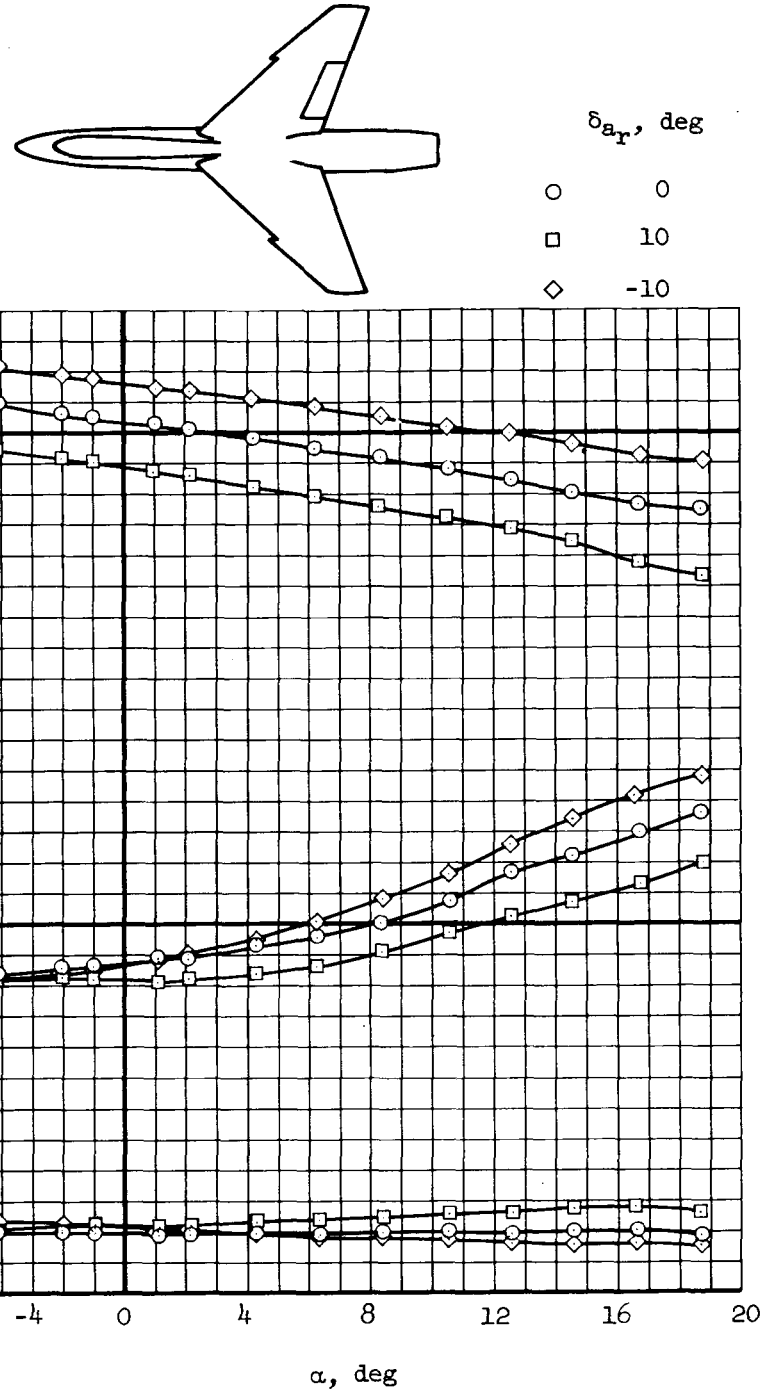

(f) M = 1.90

Figure 7.- Concluded.

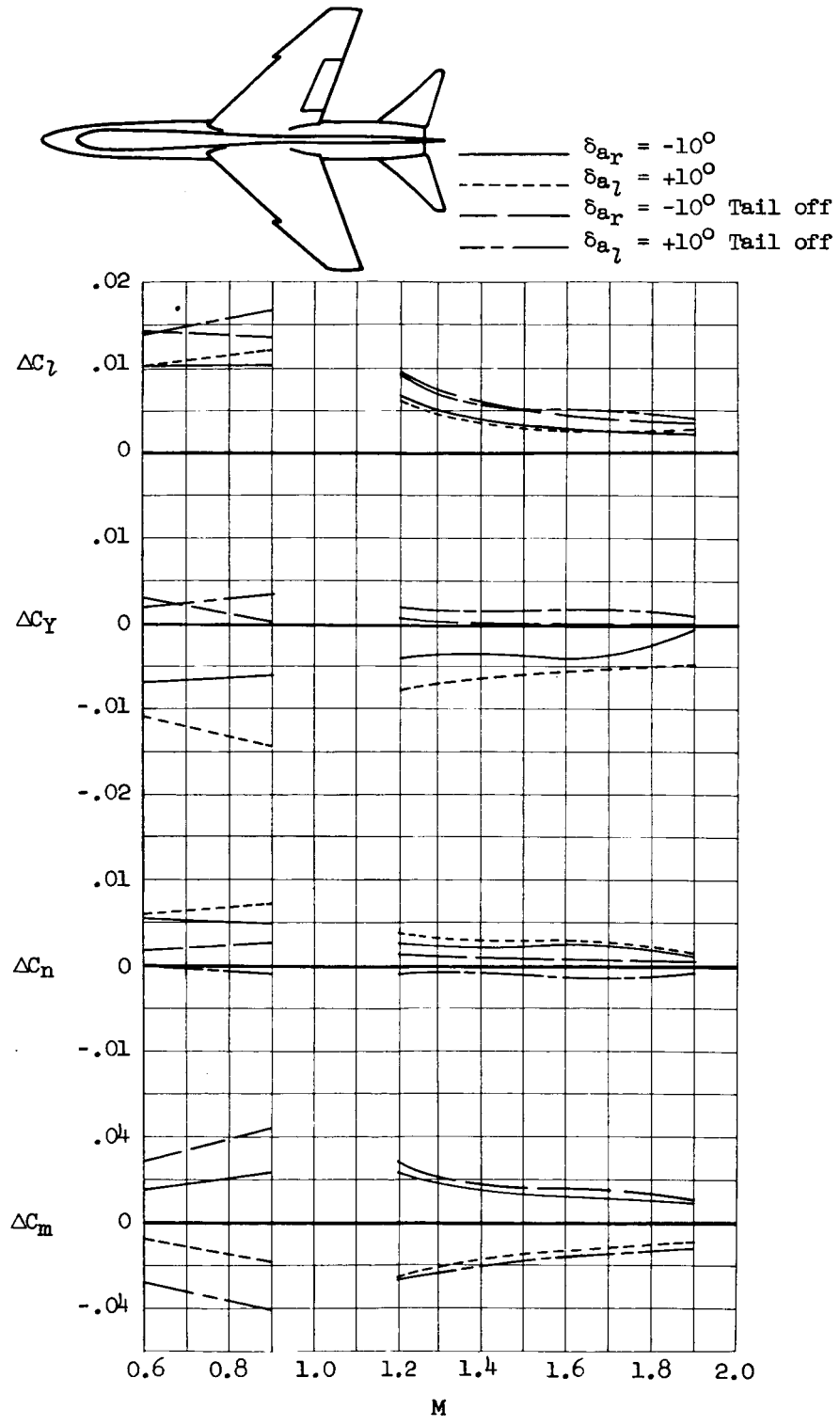

Figure 8.- Variation of ΔC_l, ΔC_Y, ΔC_n, and ΔC_m with Mach number for model A; $\alpha = 0^\circ$.

[redacted]

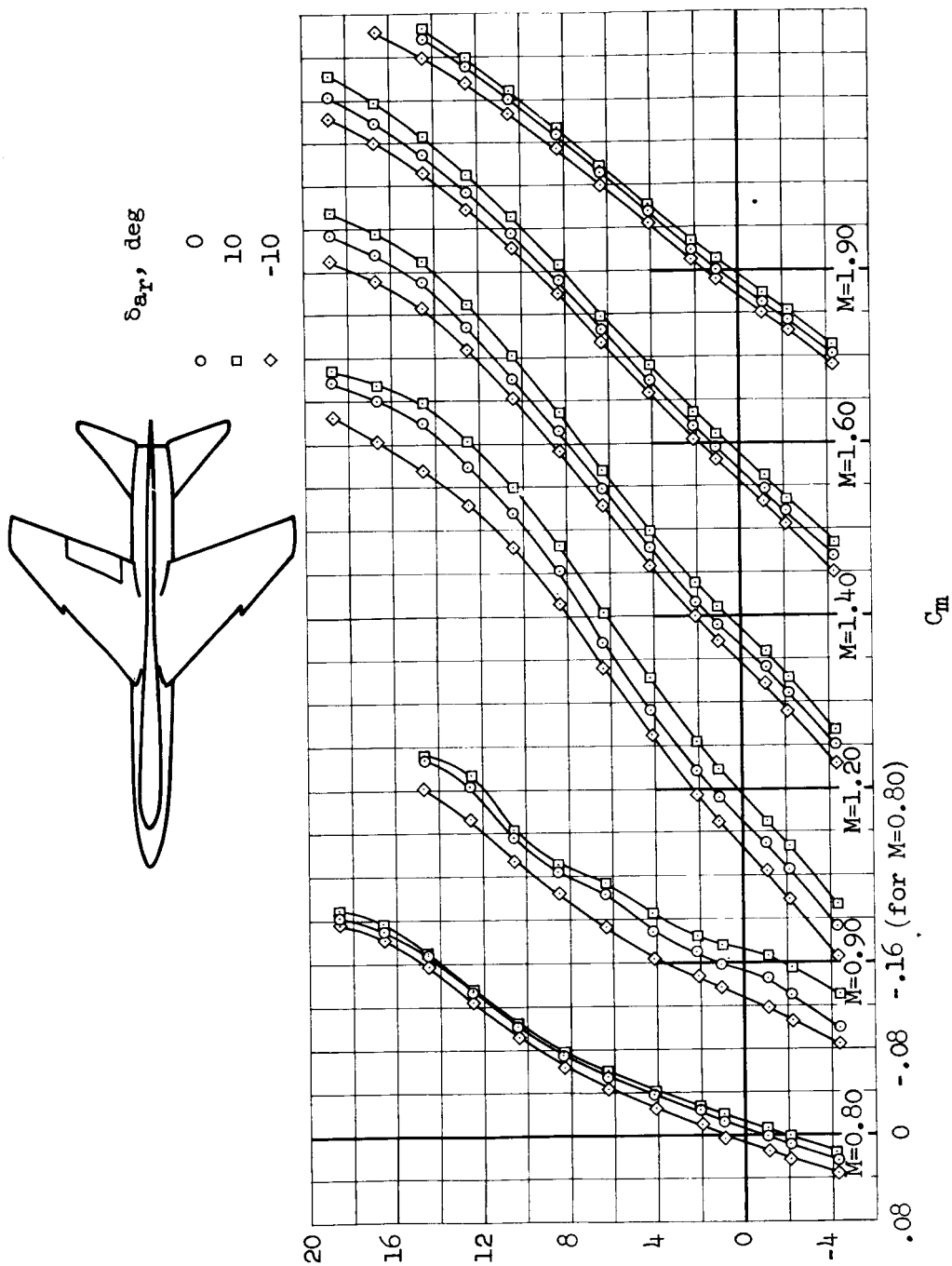

(a) Complete model.

Figure 9.- Variation of C_m with angle of attack for model A.

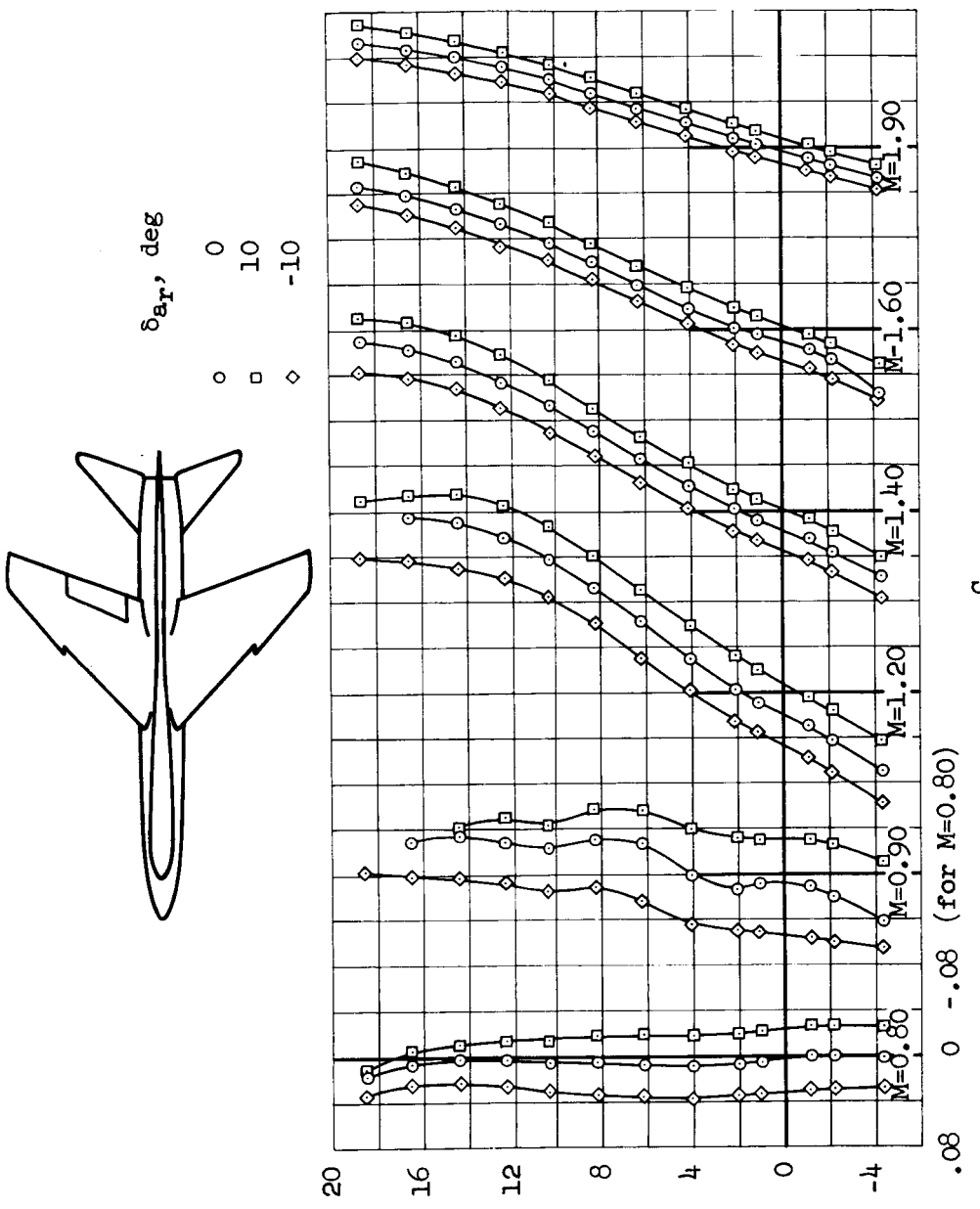

(b) Tail-off configuration.

Figure 9.- Concluded.

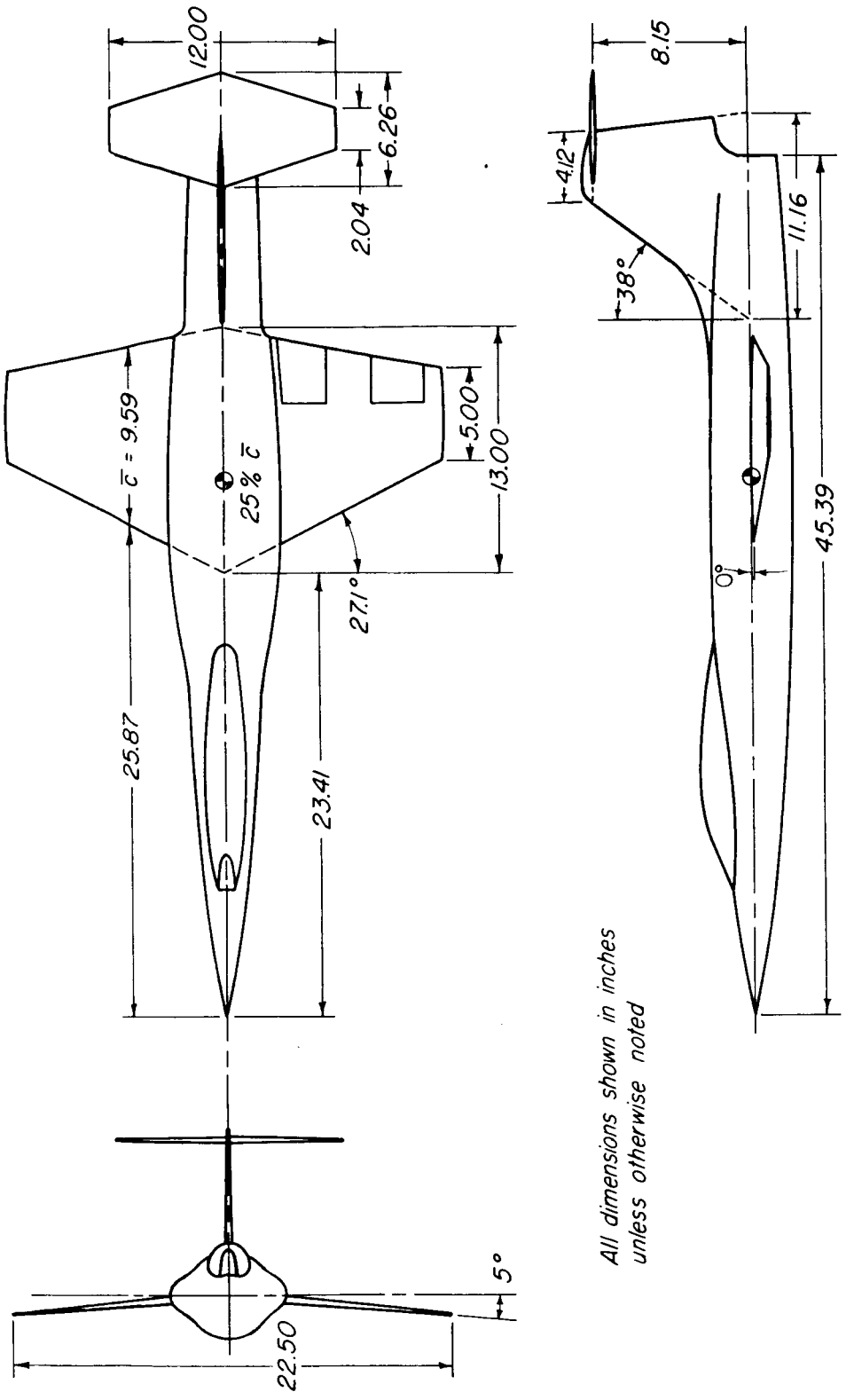

(a) Three-view drawing.

Figure 10.- Dimensional sketch of model B.

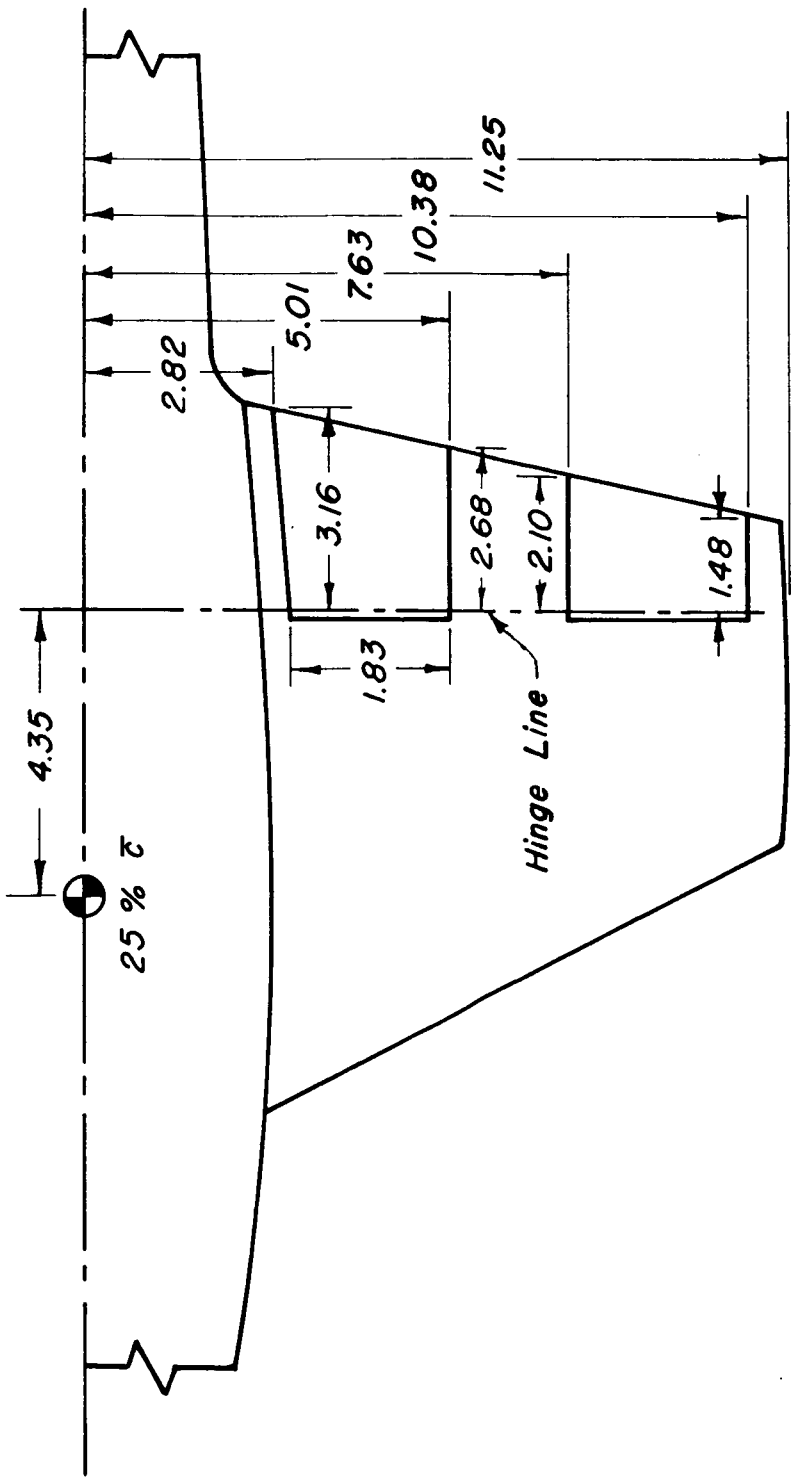

(b) Aileron detail.

Figure 10.- Concluded.

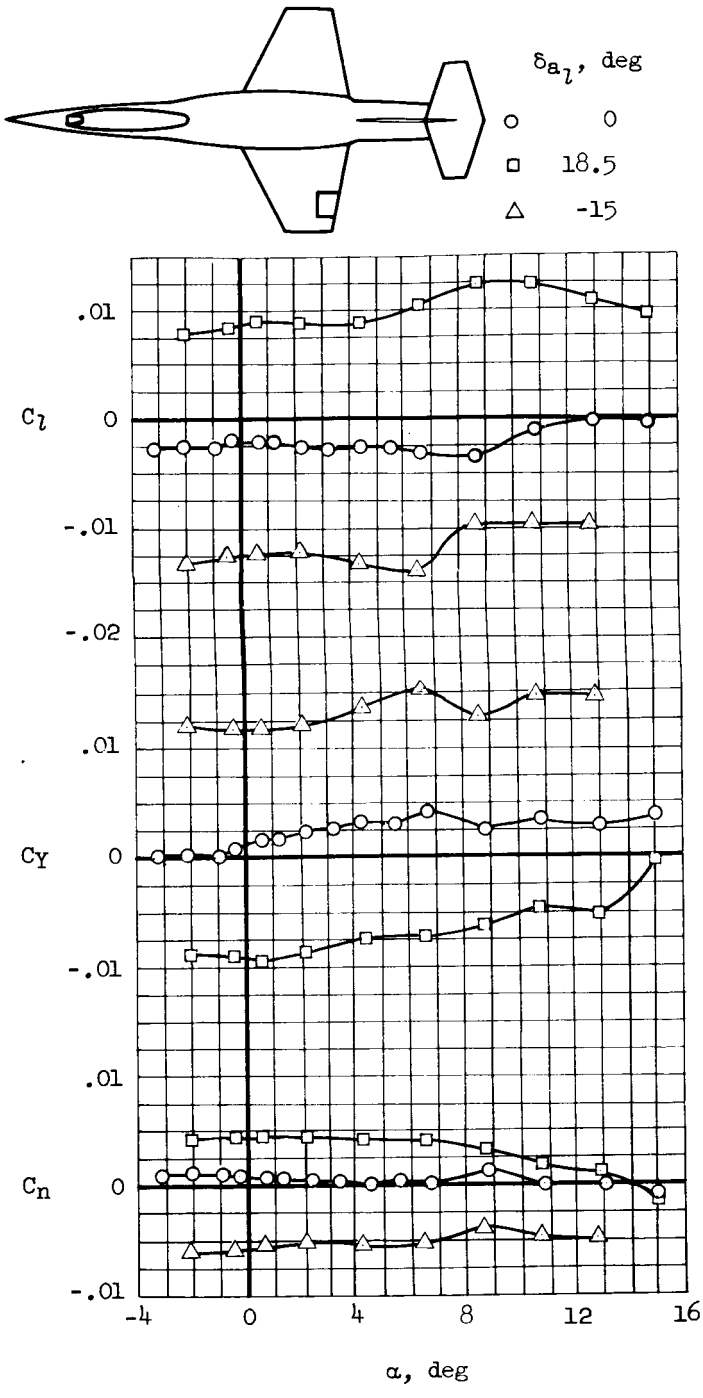

(a) M = 0.80

Figure 11.- Variation of C_l, C_Y, and C_n with angle of attack for model B with outboard aileron.

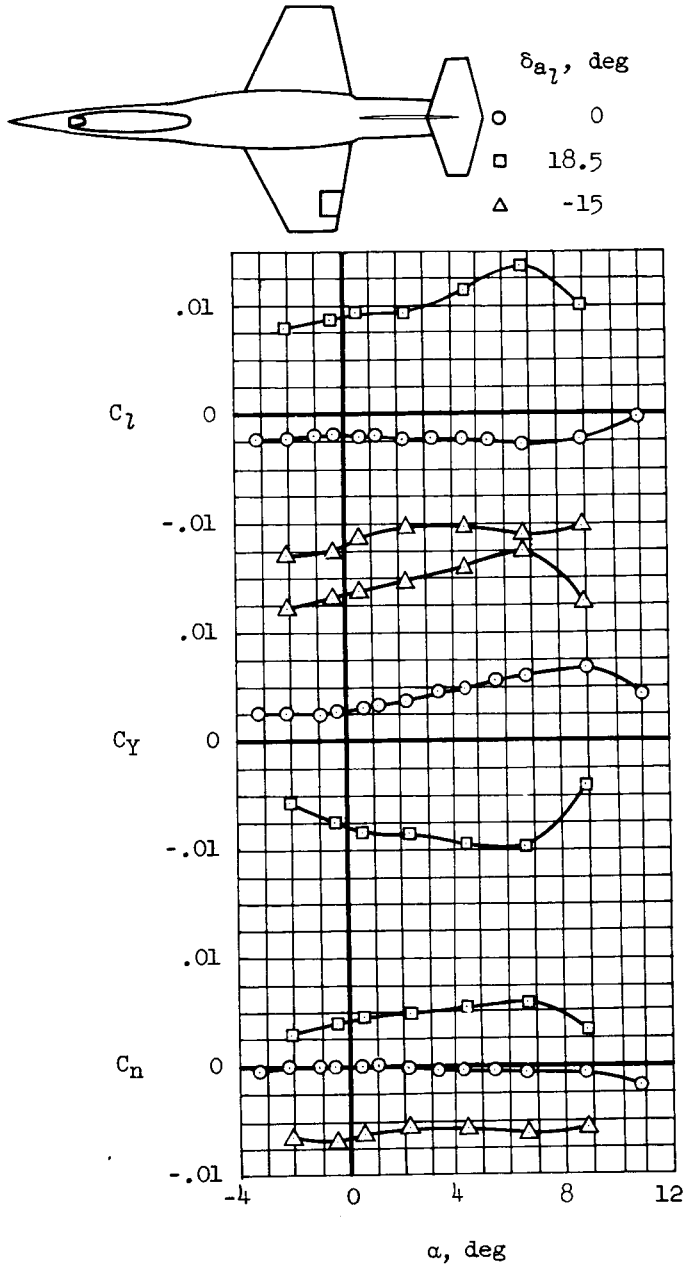

(b) M = 0.90

Figure 11.- Continued.

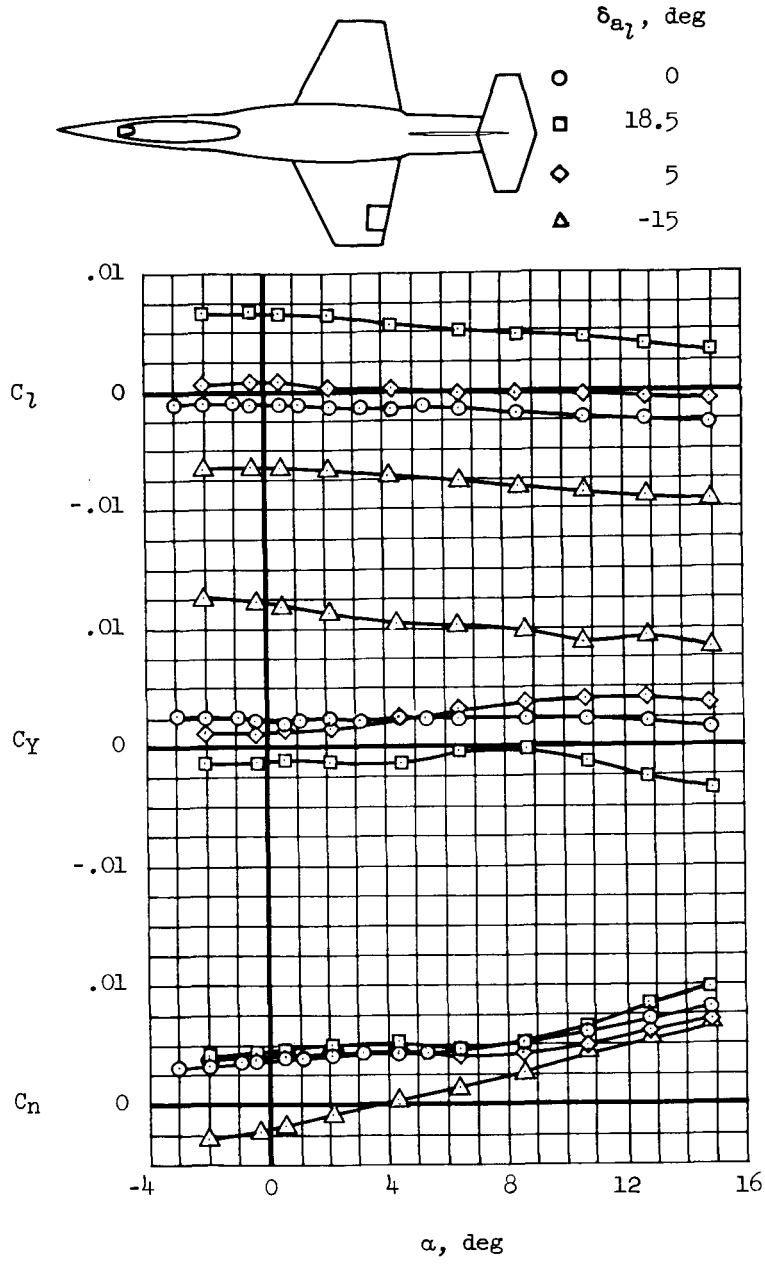

(c) M = 1.35

Figure 11.- Continued.

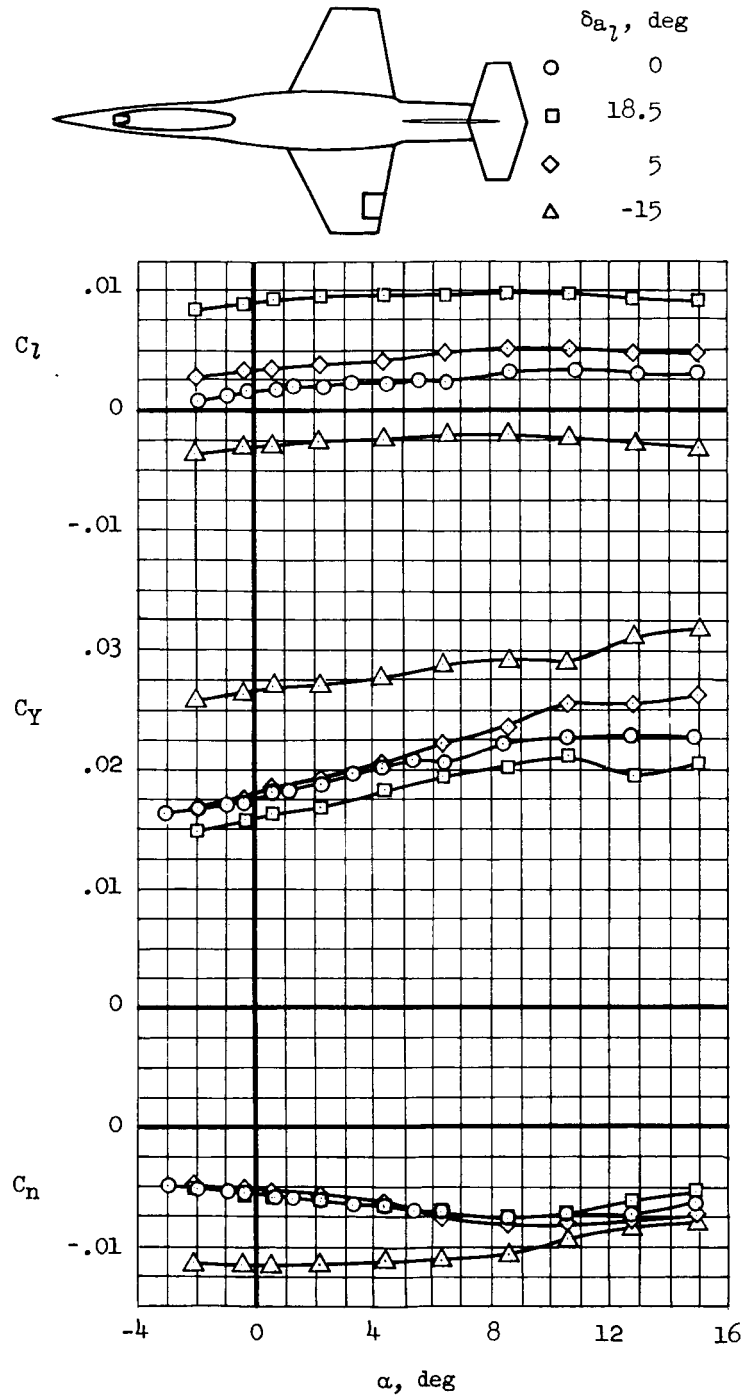

(d) M = 1.45

Figure 11.- Continued.

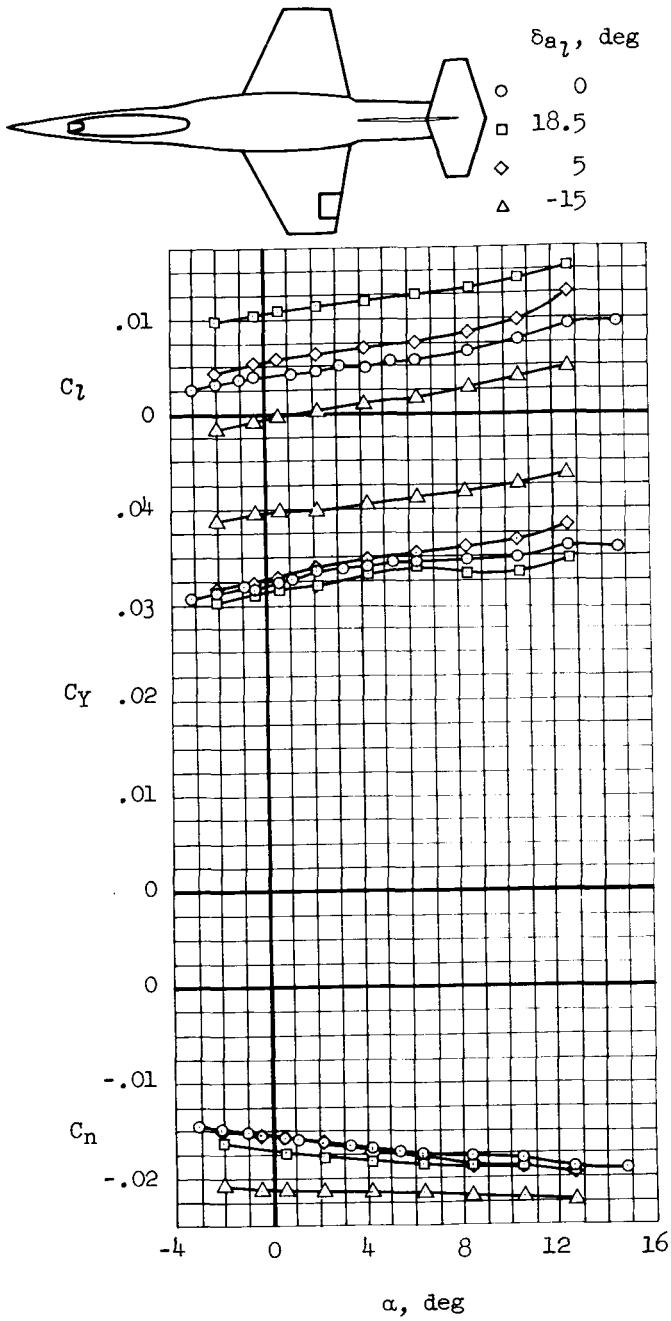

(e) M = 1.60

Figure 11.- Continued.

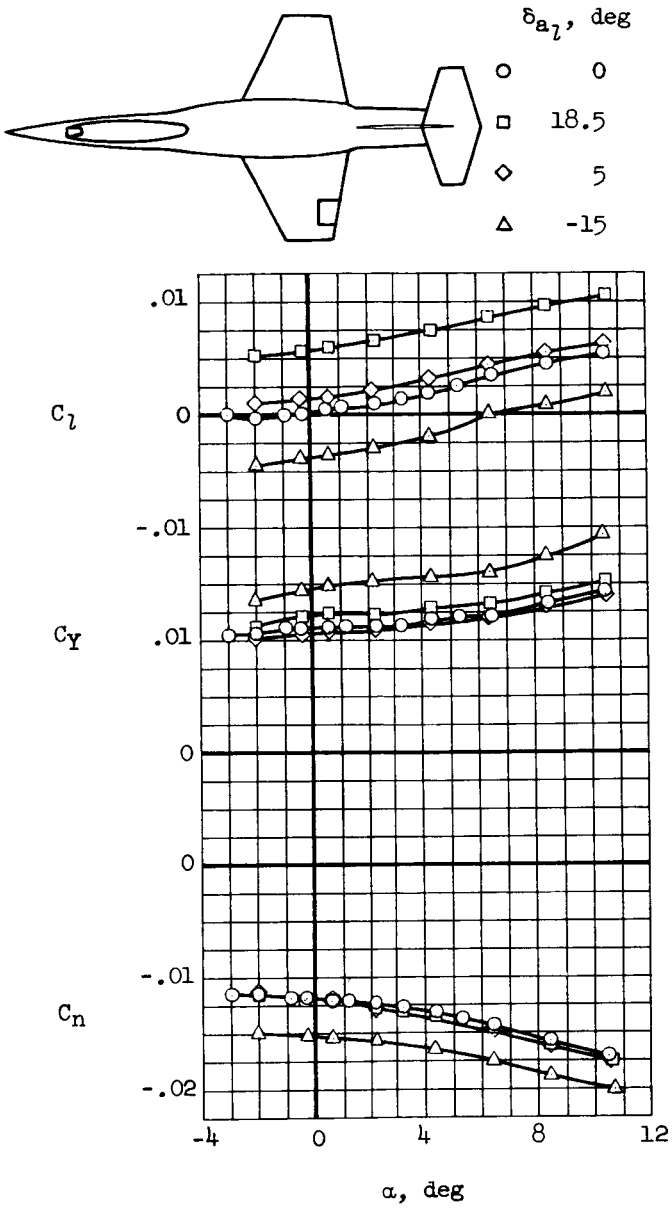

(f) M = 1.90

Figure 11.- Concluded.

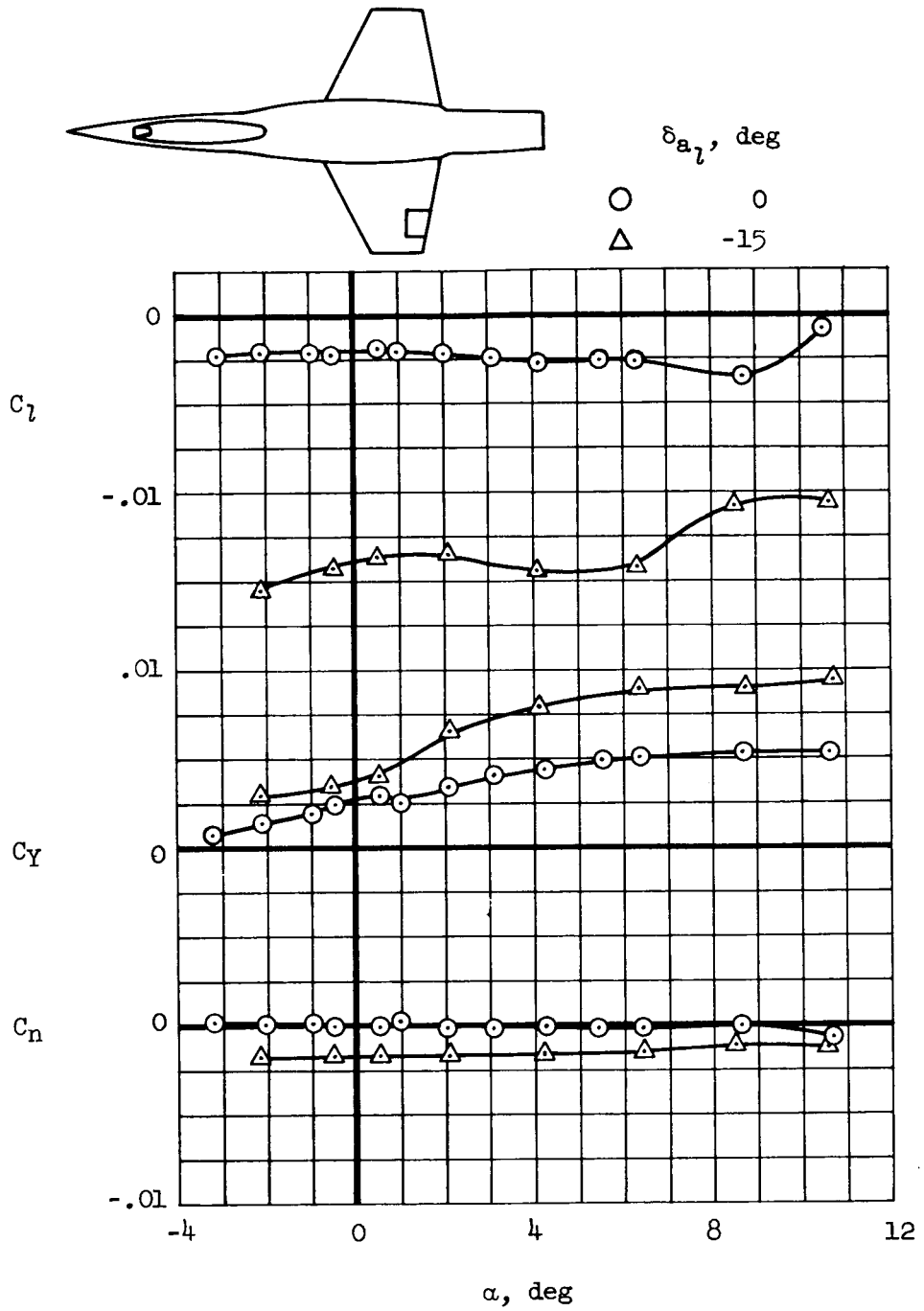

(a) M = 0.80

Figure 12.- Variation of C_l, C_Y, and C_n with angle of attack for model B with outboard aileron with the tail removed.

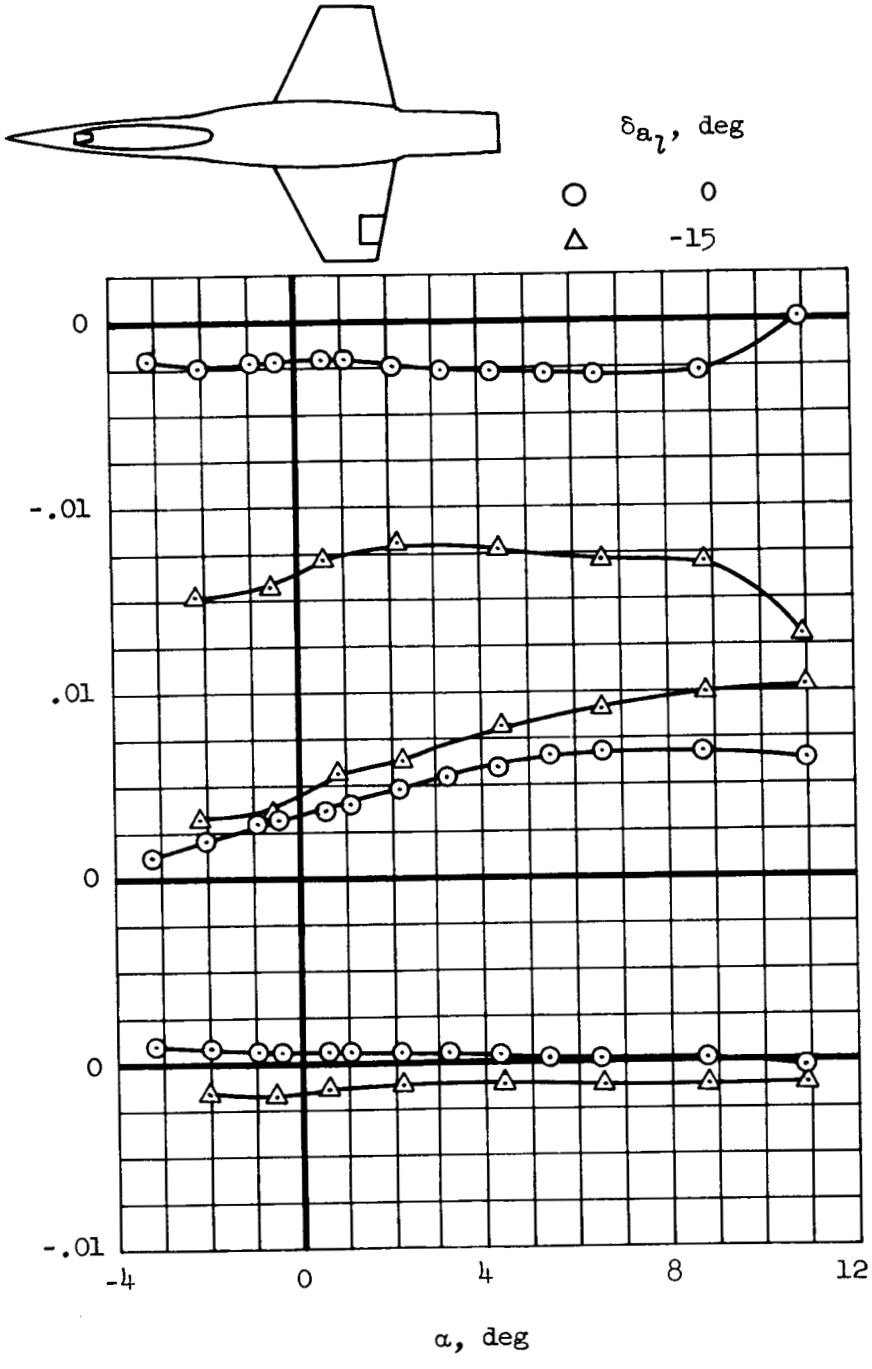

(b) M = 0.90

Figure 12.- Continued.

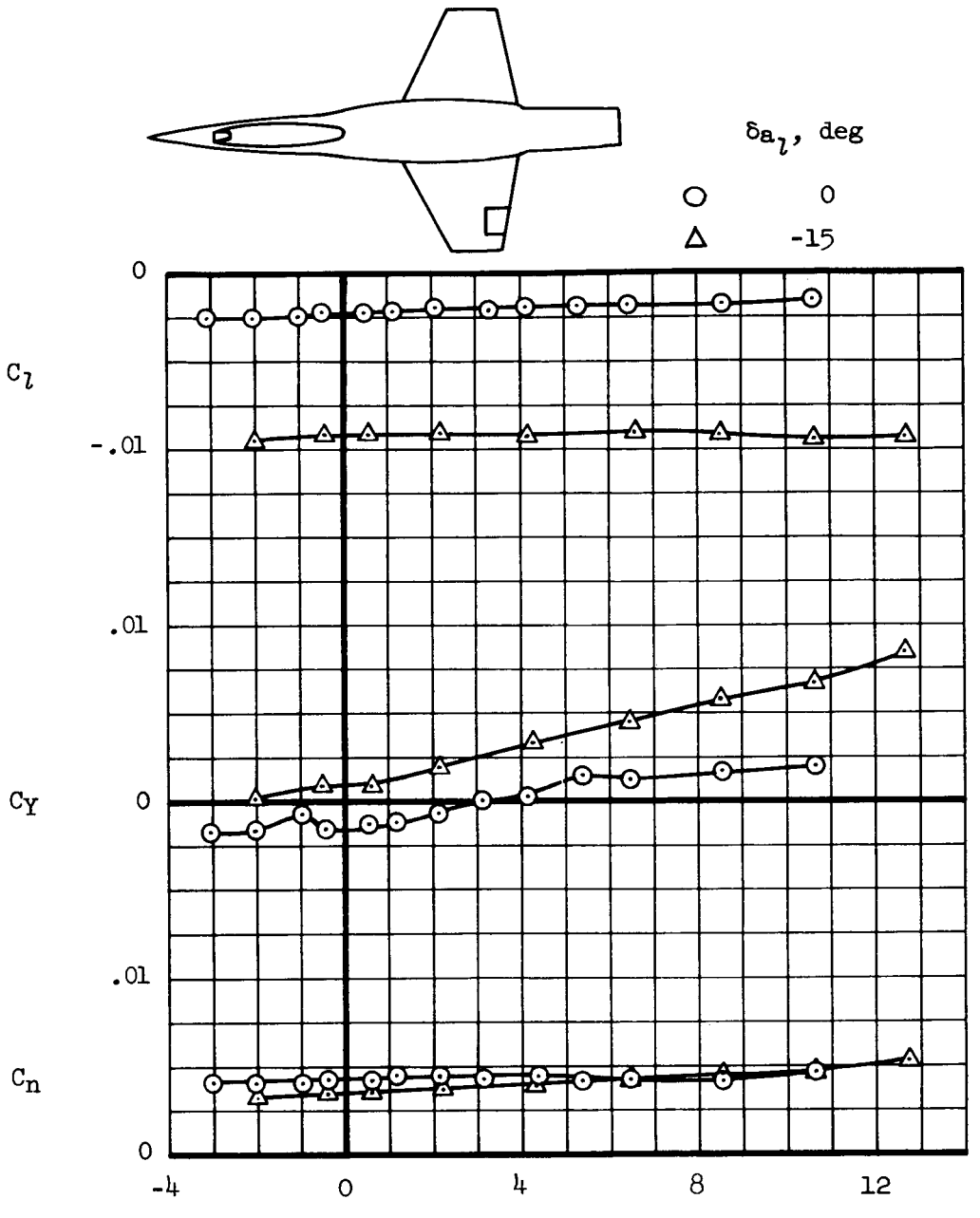

(c) M = 1.35

Figure 12.- Continued.

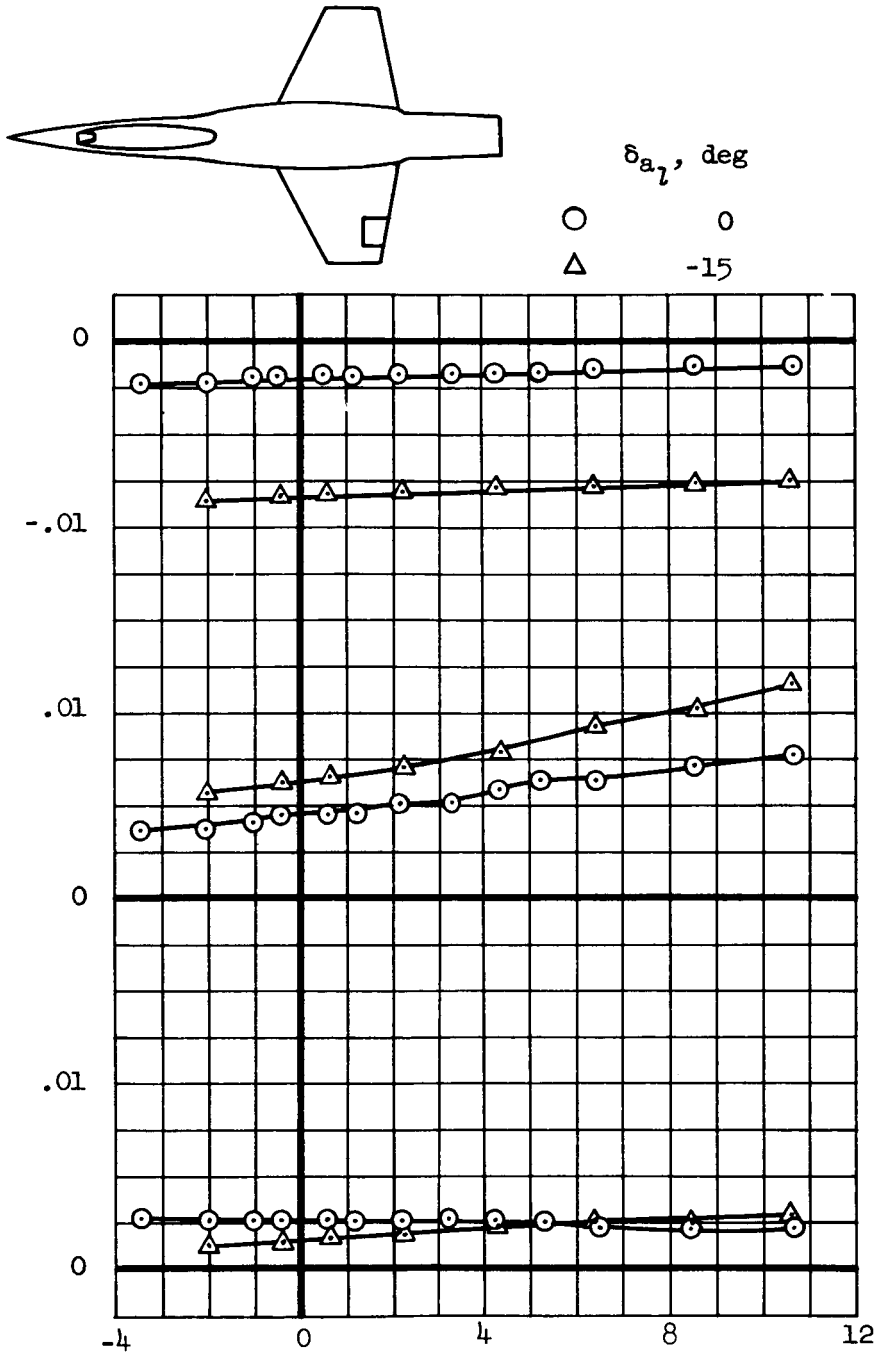

(d) M = 1.45

Figure 12.- Continued.

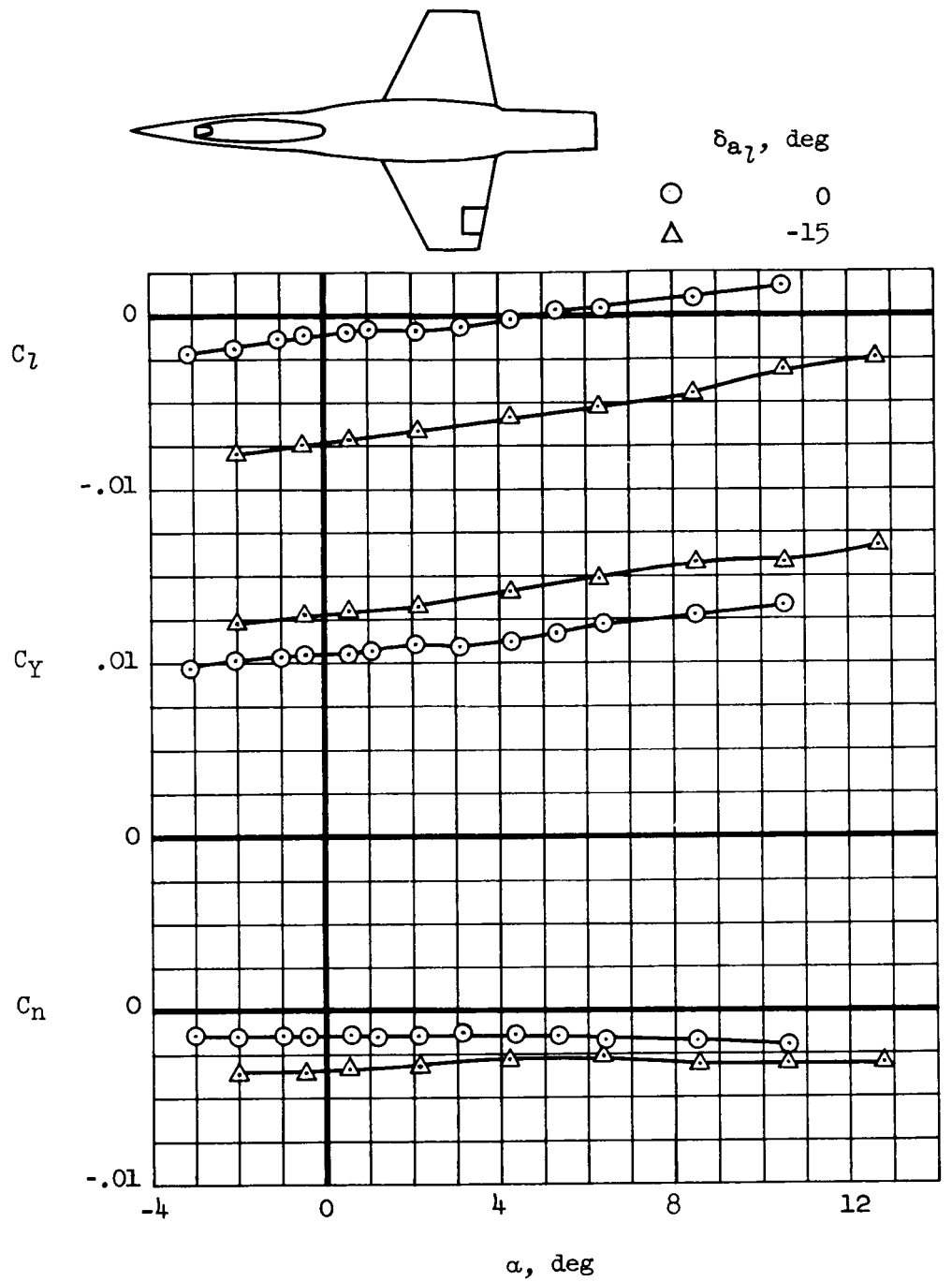

(e) M = 1.60

Figure 12.- Continued.

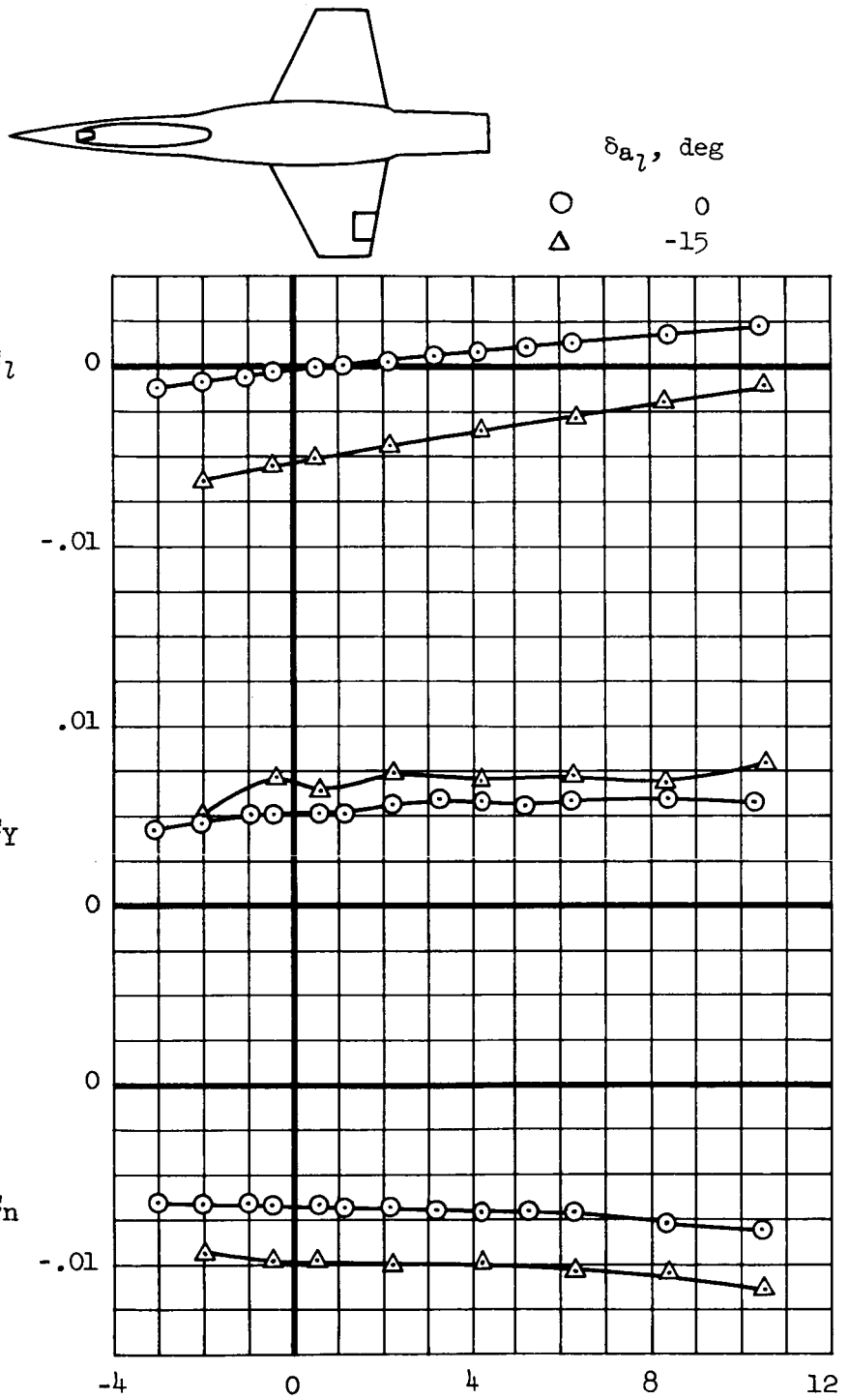

(f) M = 1.90

Figure 12.- Concluded.

[redacted]

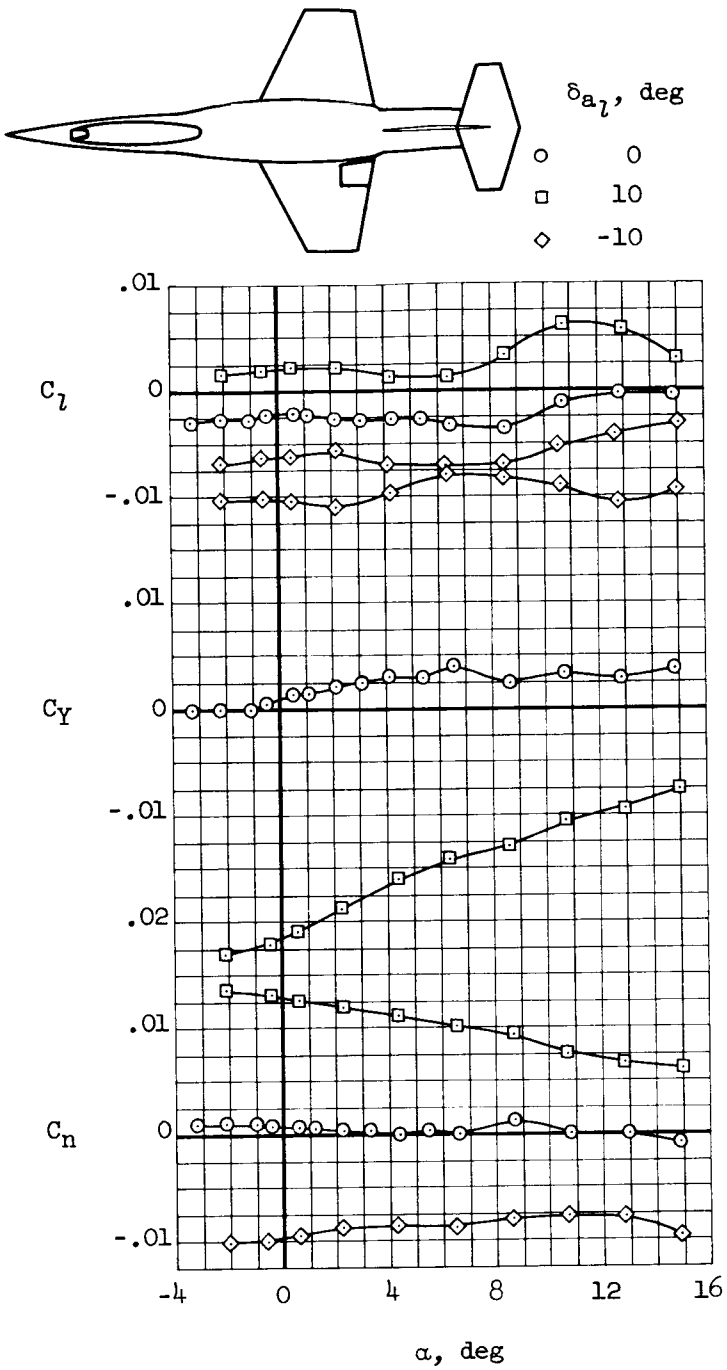

(a) M = 0.80

Figure 13.- Variation of C_l, C_Y, and C_n with angle of attack for model B with inboard aileron.

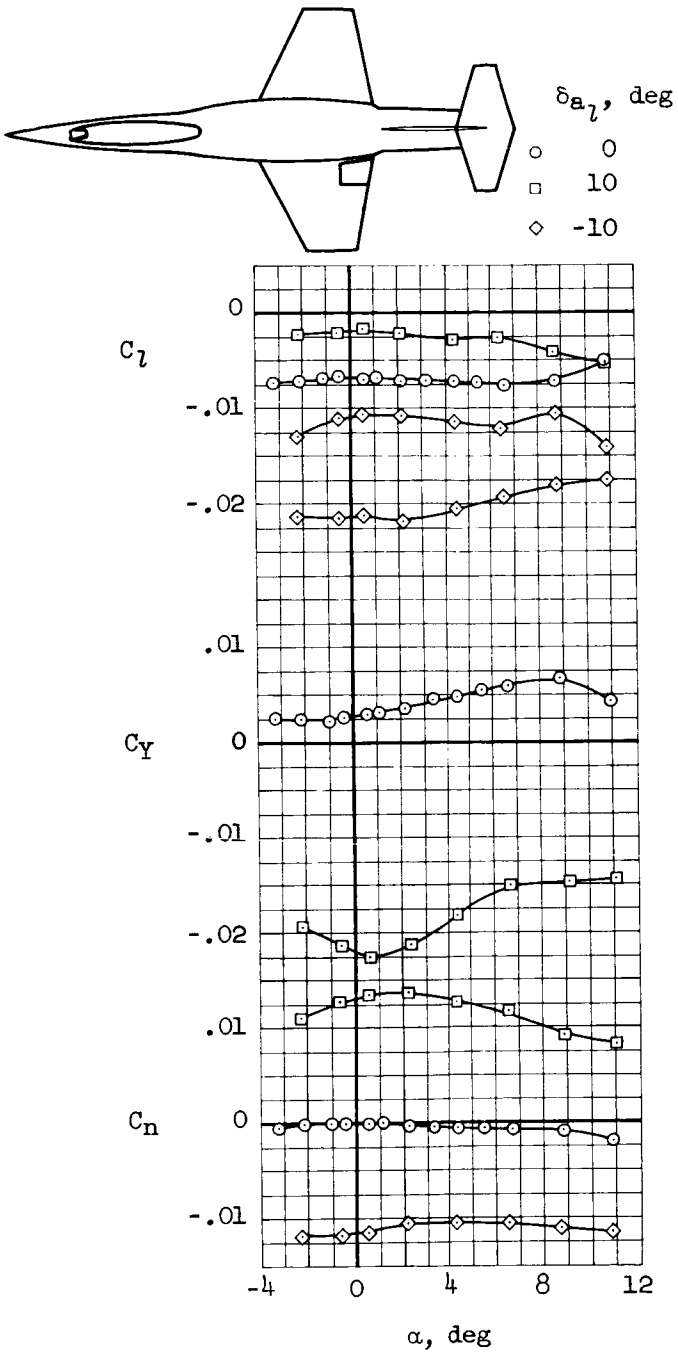

(b) M = 0.90

Figure 13.- Continued.

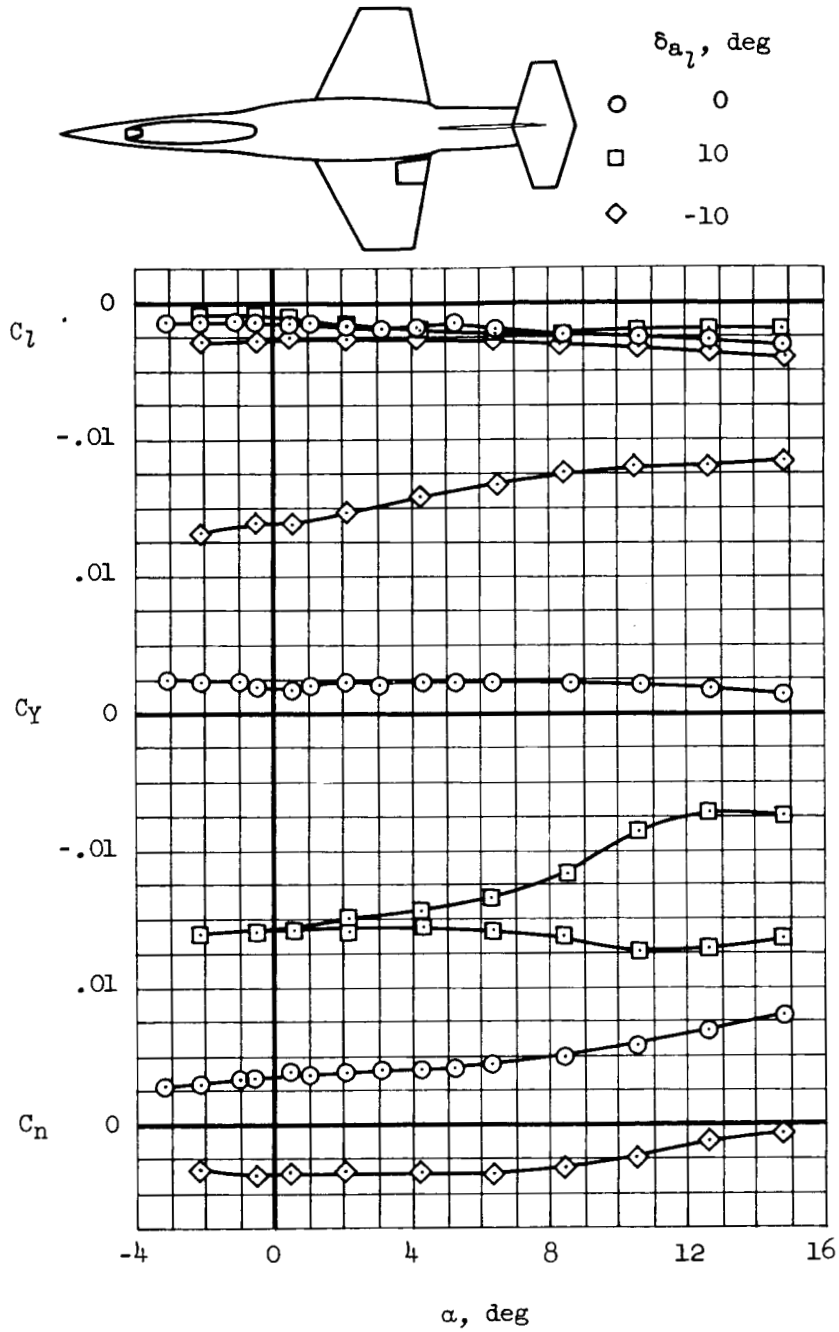

(c) M = 1.35

Figure 13.- Continued.

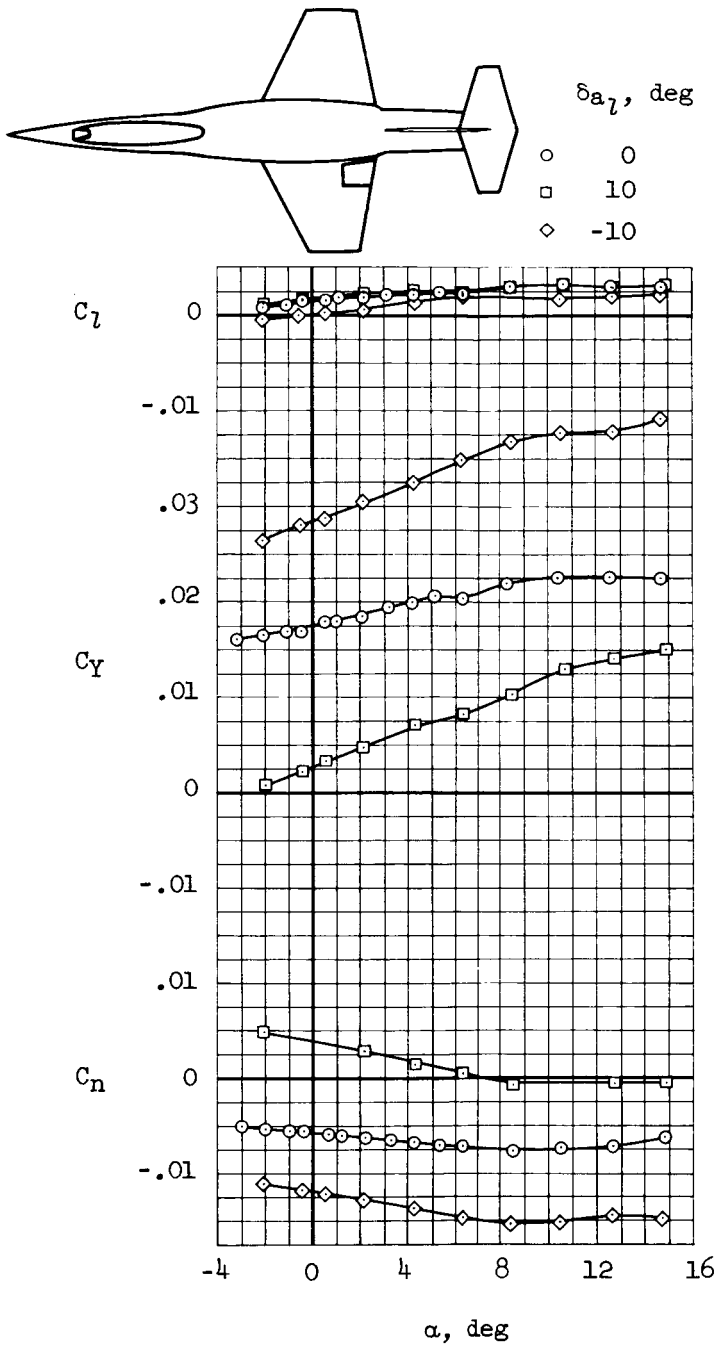

(d) M = 1.45

Figure 13.- Continued.

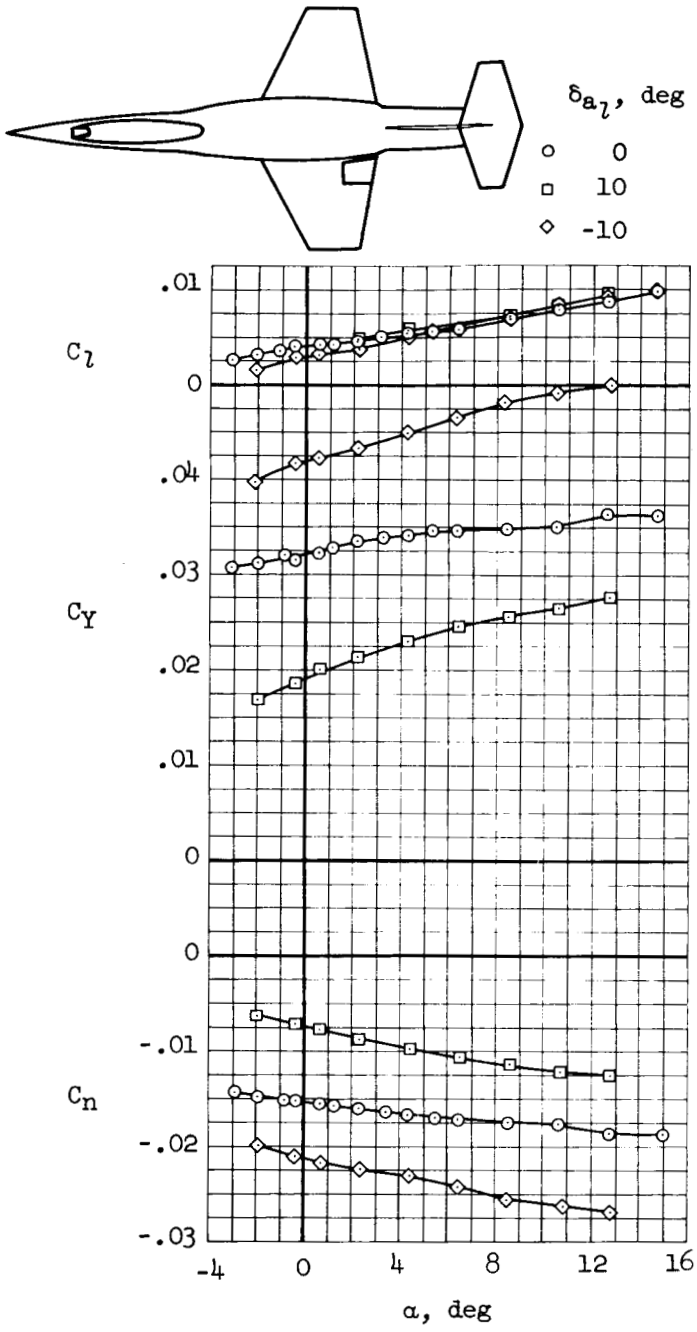

(e) M = 1.60

Figure 13.- Continued.

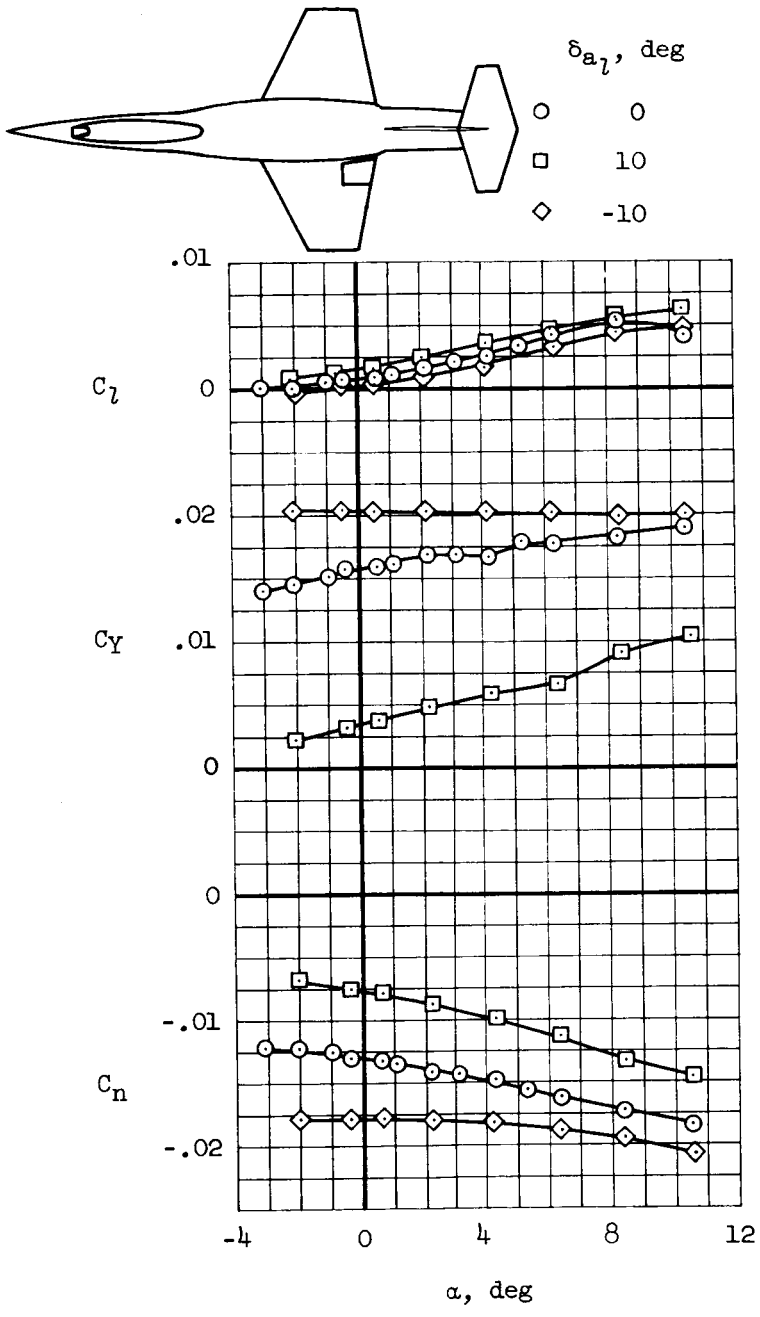

(f) M = 1.90

Figure 13.- Concluded.

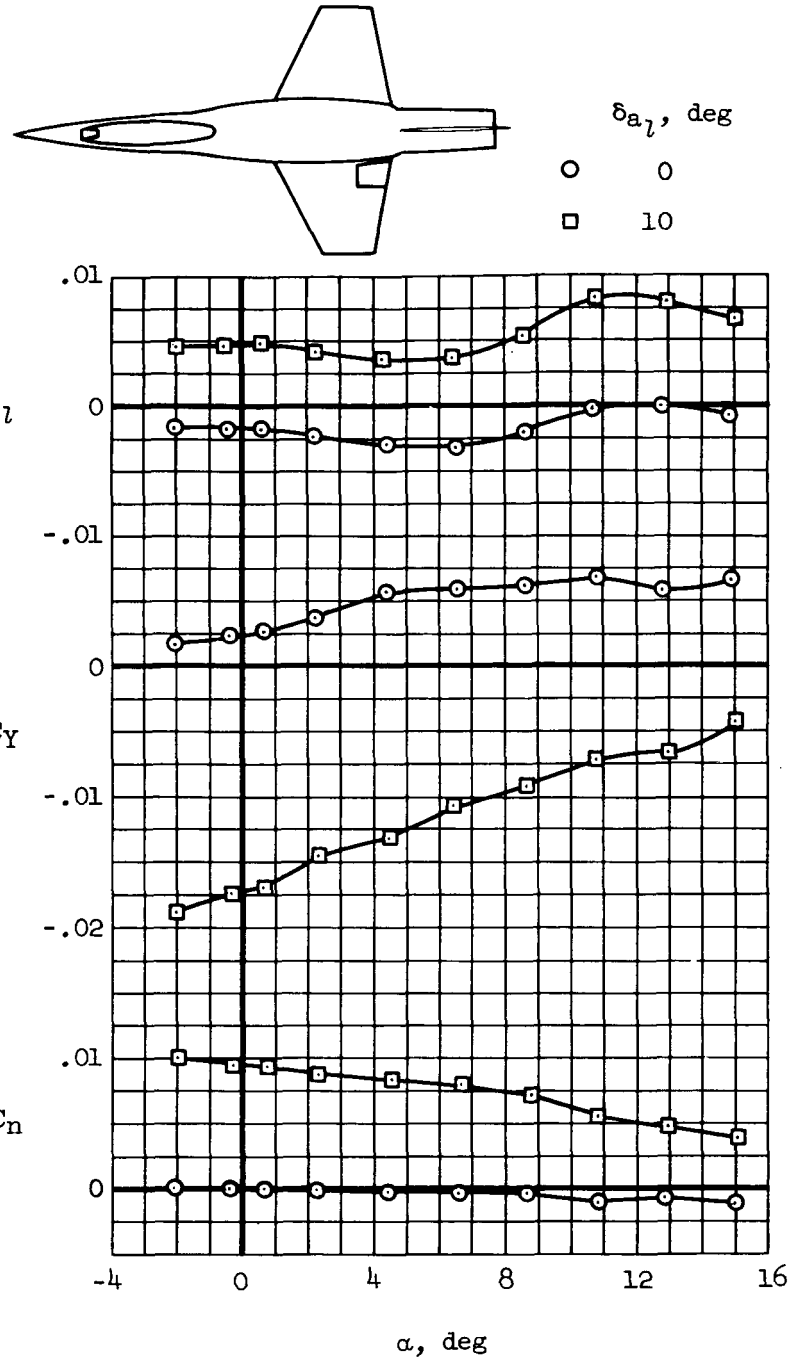

(a) M = 0.80

Figure 14.- Variation of C_l, C_Y, and C_n with angle of attack for model B with inboard aileron with the horizontal tail removed.

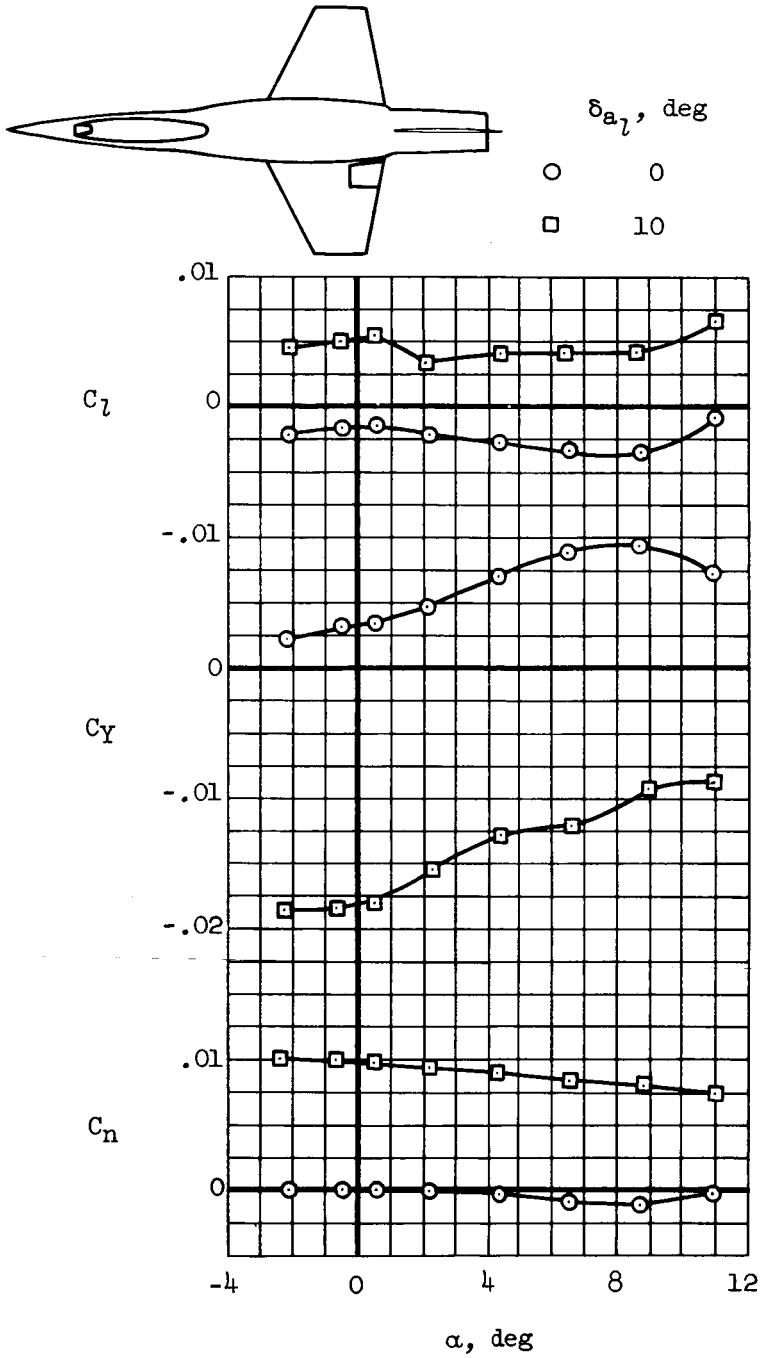

(b) M = 0.90

Figure 14.- Continued.

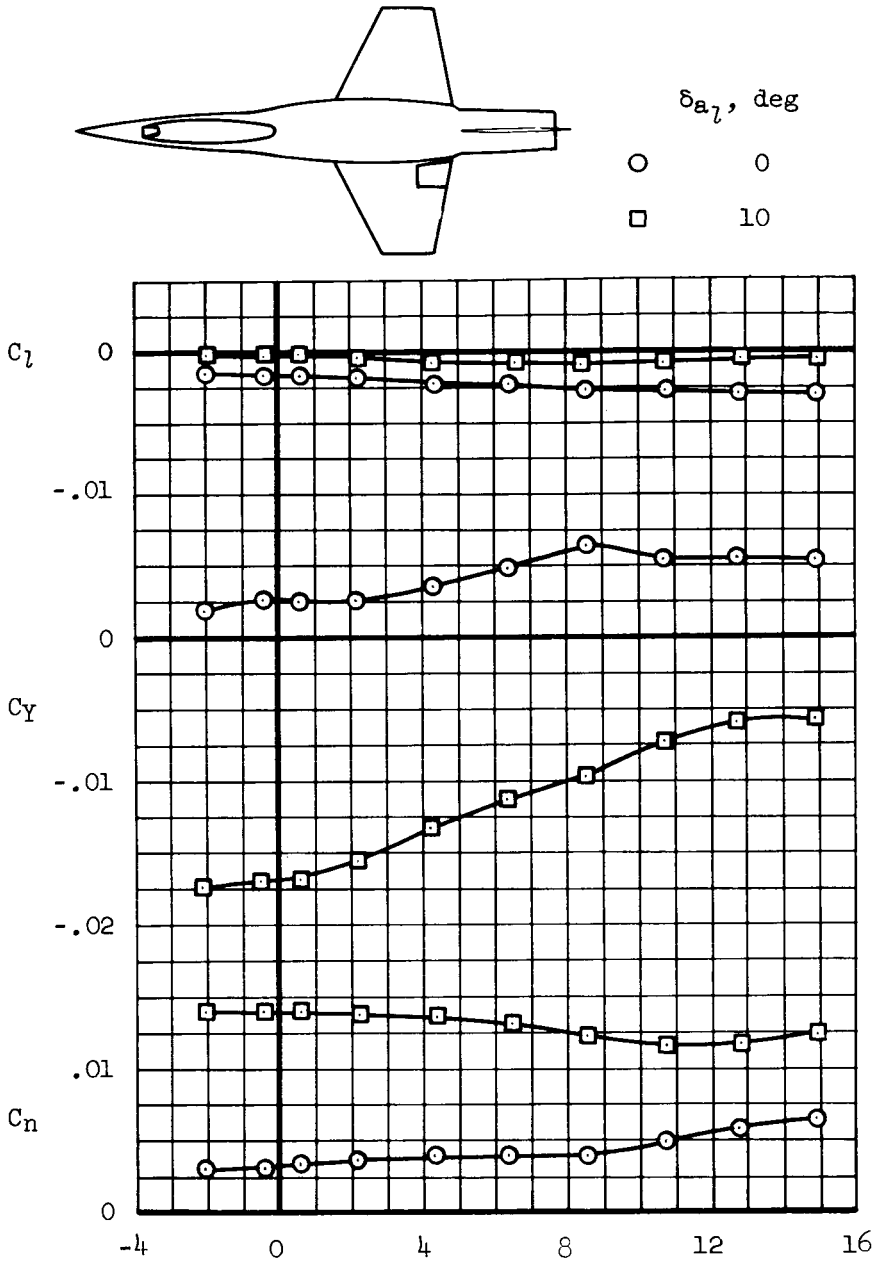

(c) M = 1.35

Figure 14.- Continued.

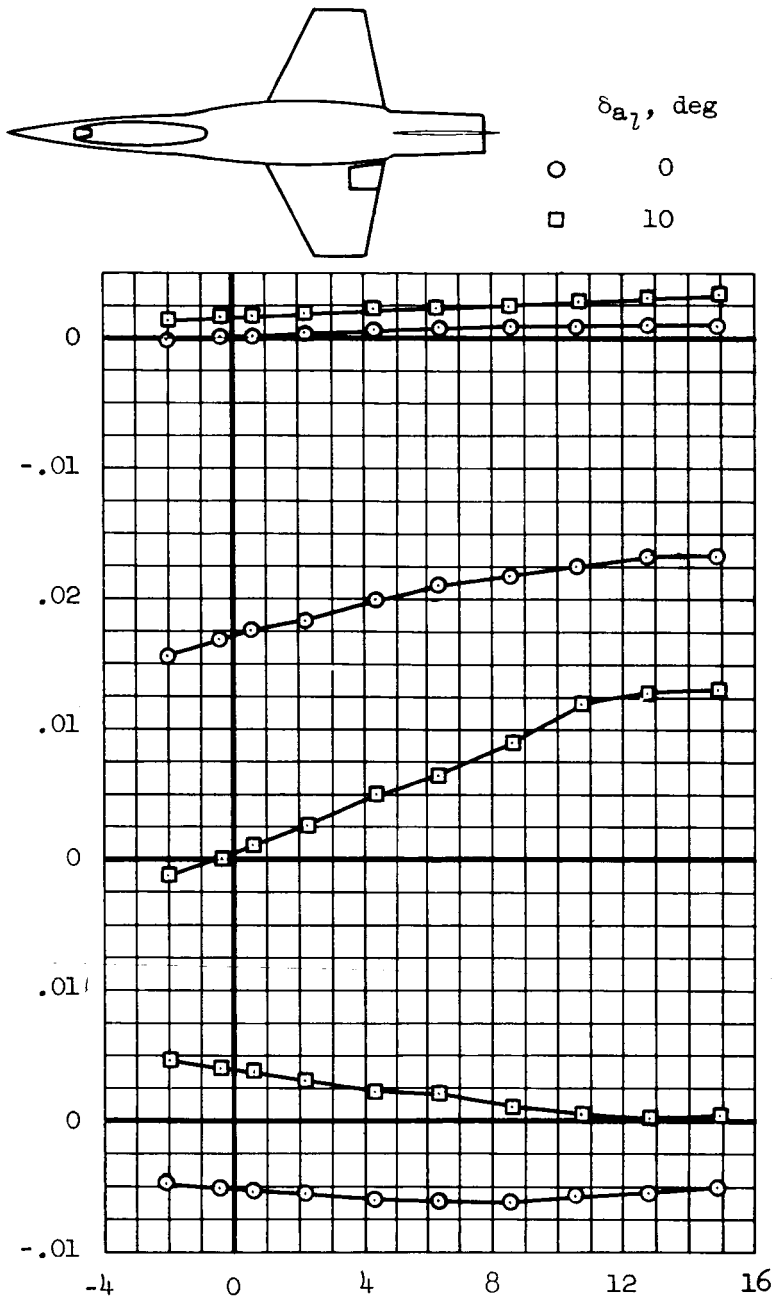

(d) M = 1.45

Figure 14.- Continued.

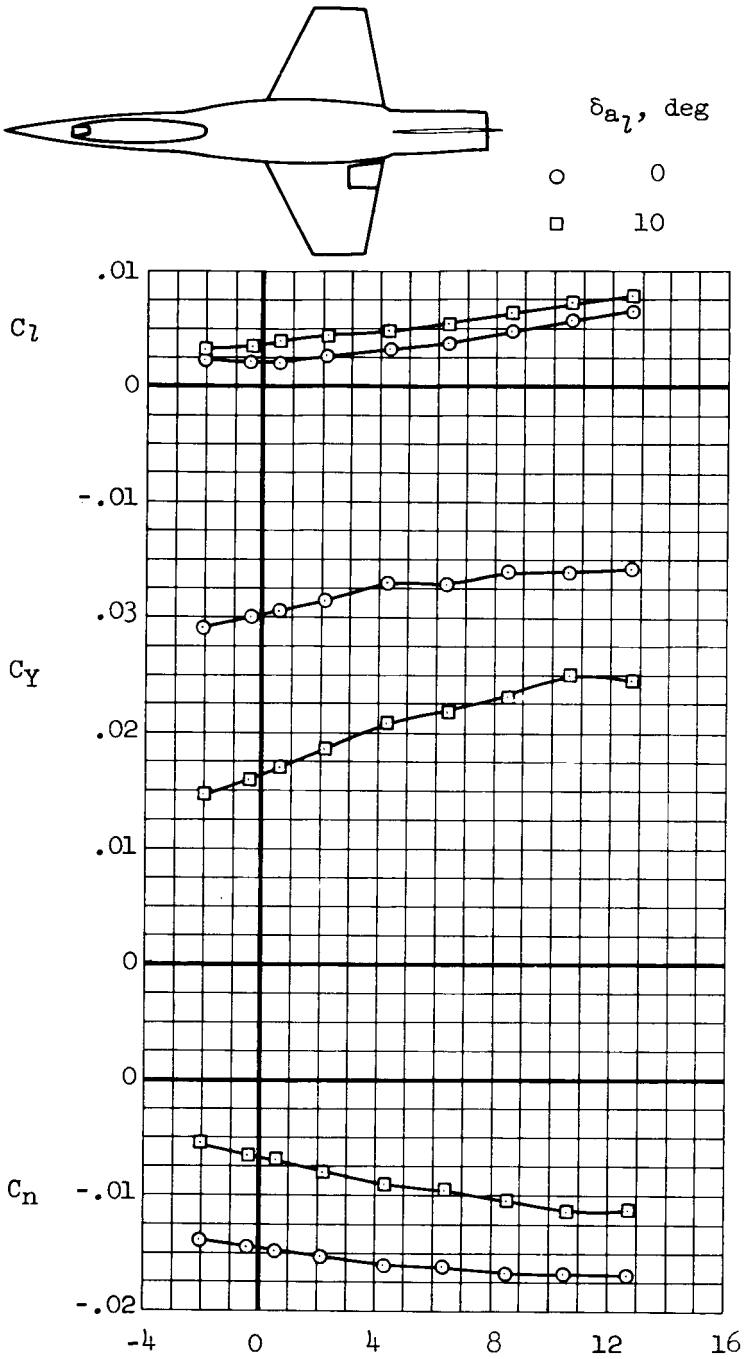

(e) M = 1.60

Figure 14.- Continued.

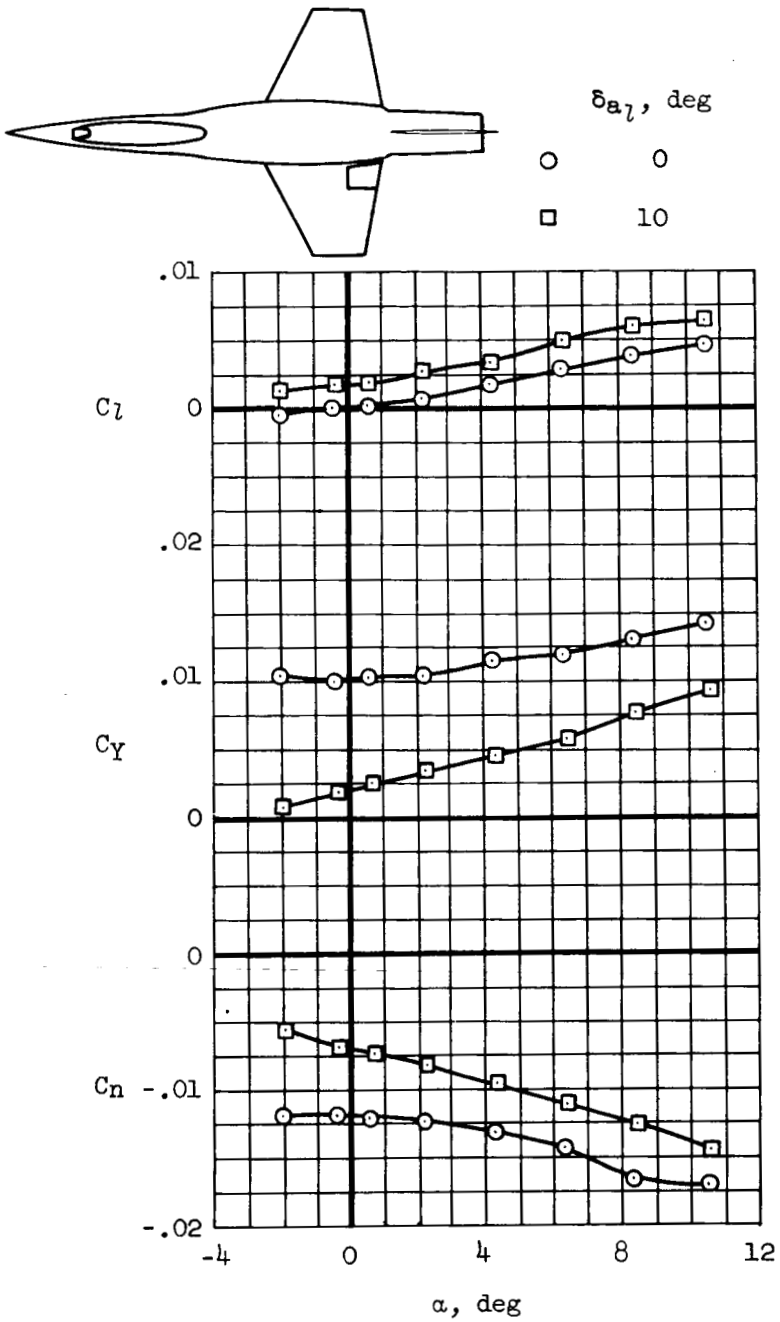

(f) M = 1.90

Figure 14.- Concluded.

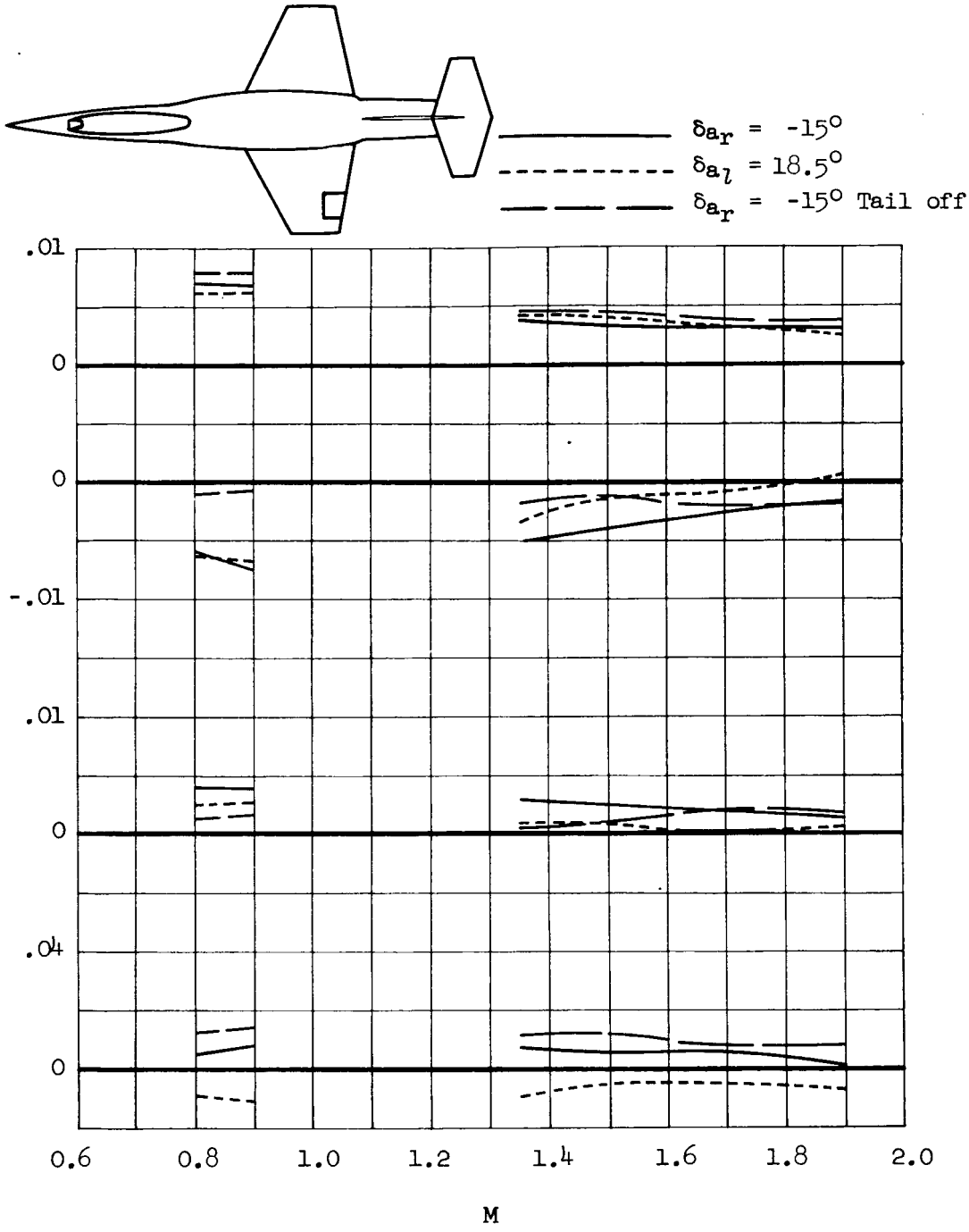

(a) Outboard aileron.

Figure 15.- Variation of ΔC_l, ΔC_Y, ΔC_n, and ΔC_m with Mach number for model B; $\alpha = 0°$.

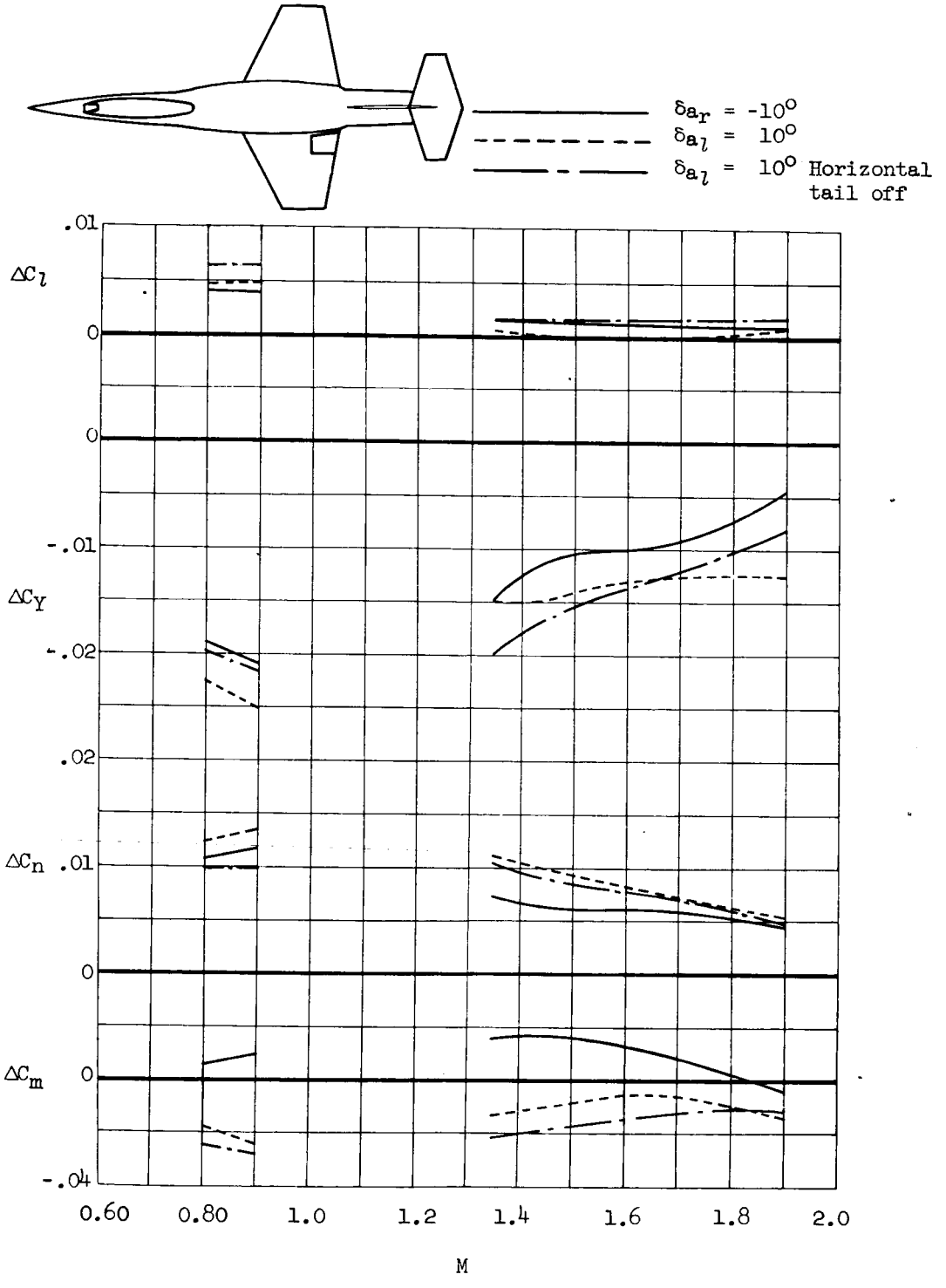

(b) Inboard aileron.

Figure 15.- Concluded.

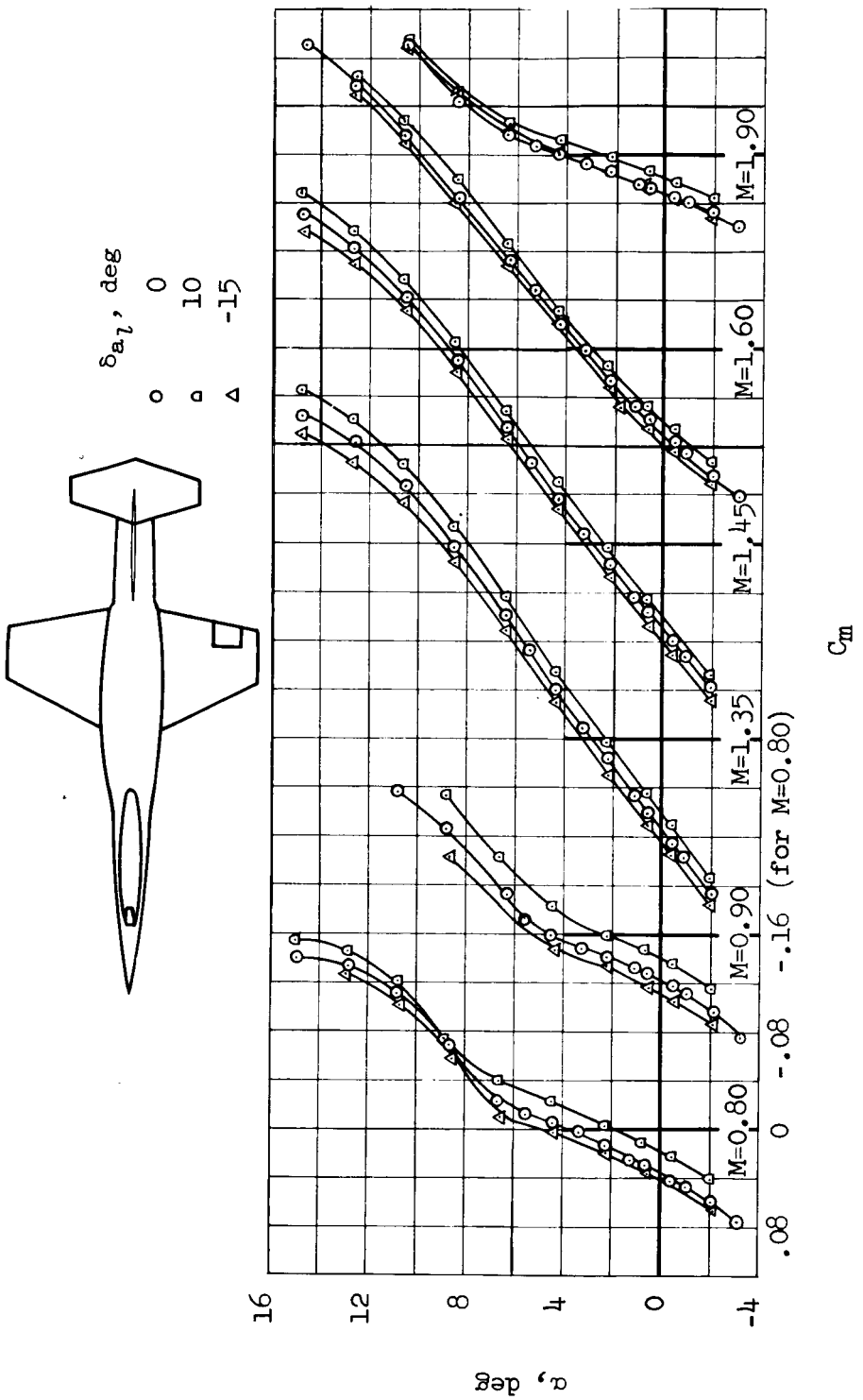

(a) Outboard aileron.

Figure 16.- Variation of C_m with angle of attack for model B.

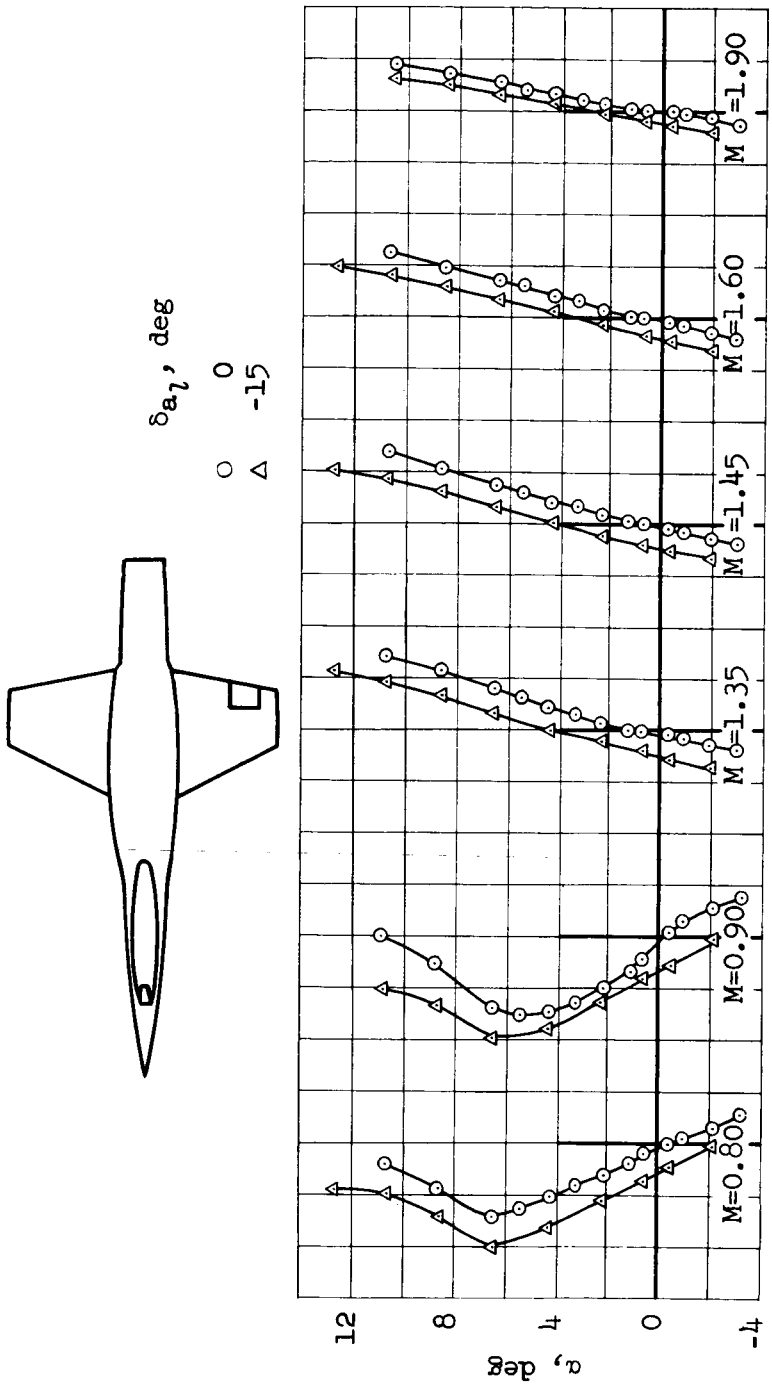

(b) Outboard aileron, tail off.

Figure 16.- Continued.

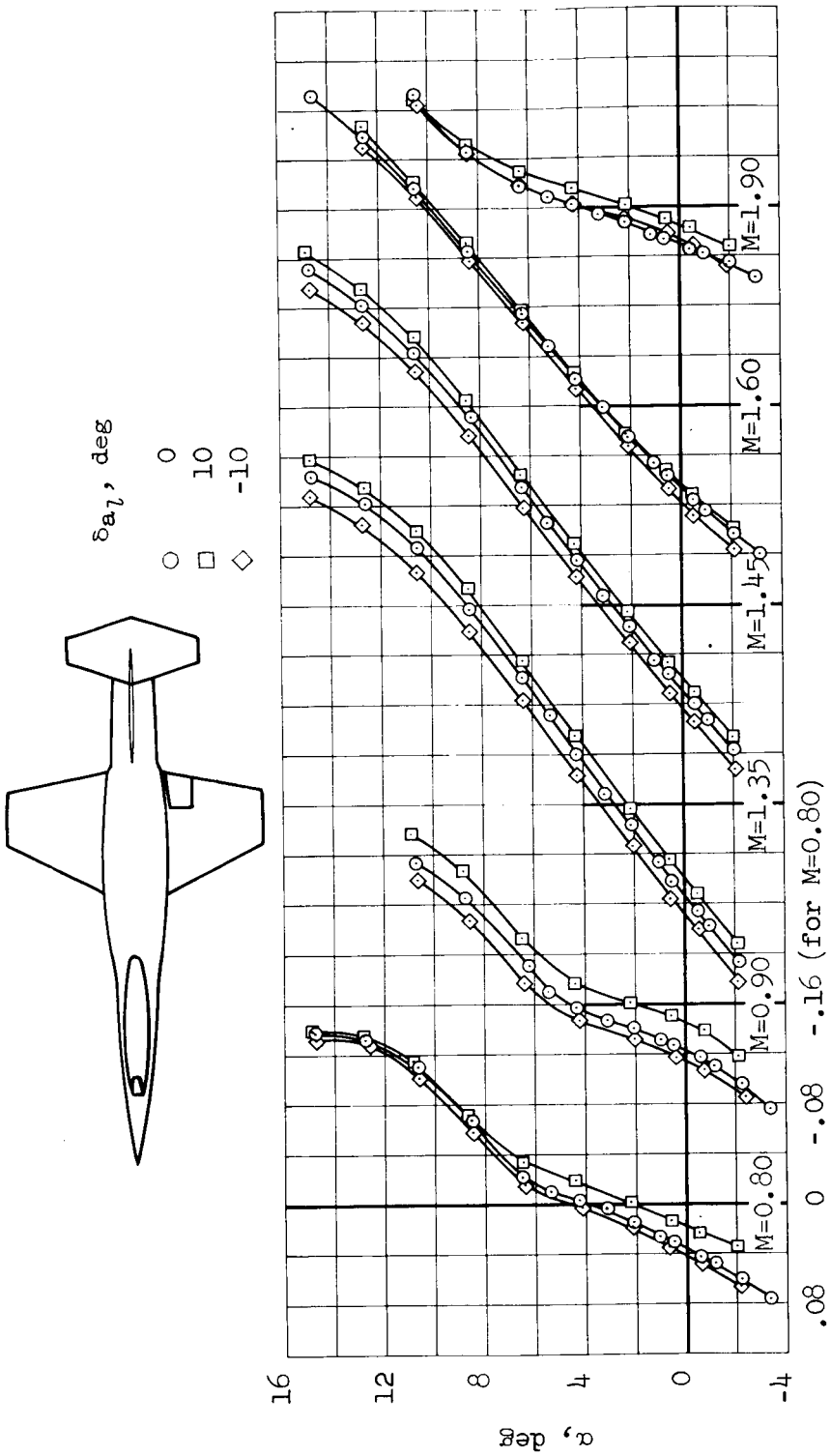

(c) Inboard aileron.

Figure 16.- Continued.

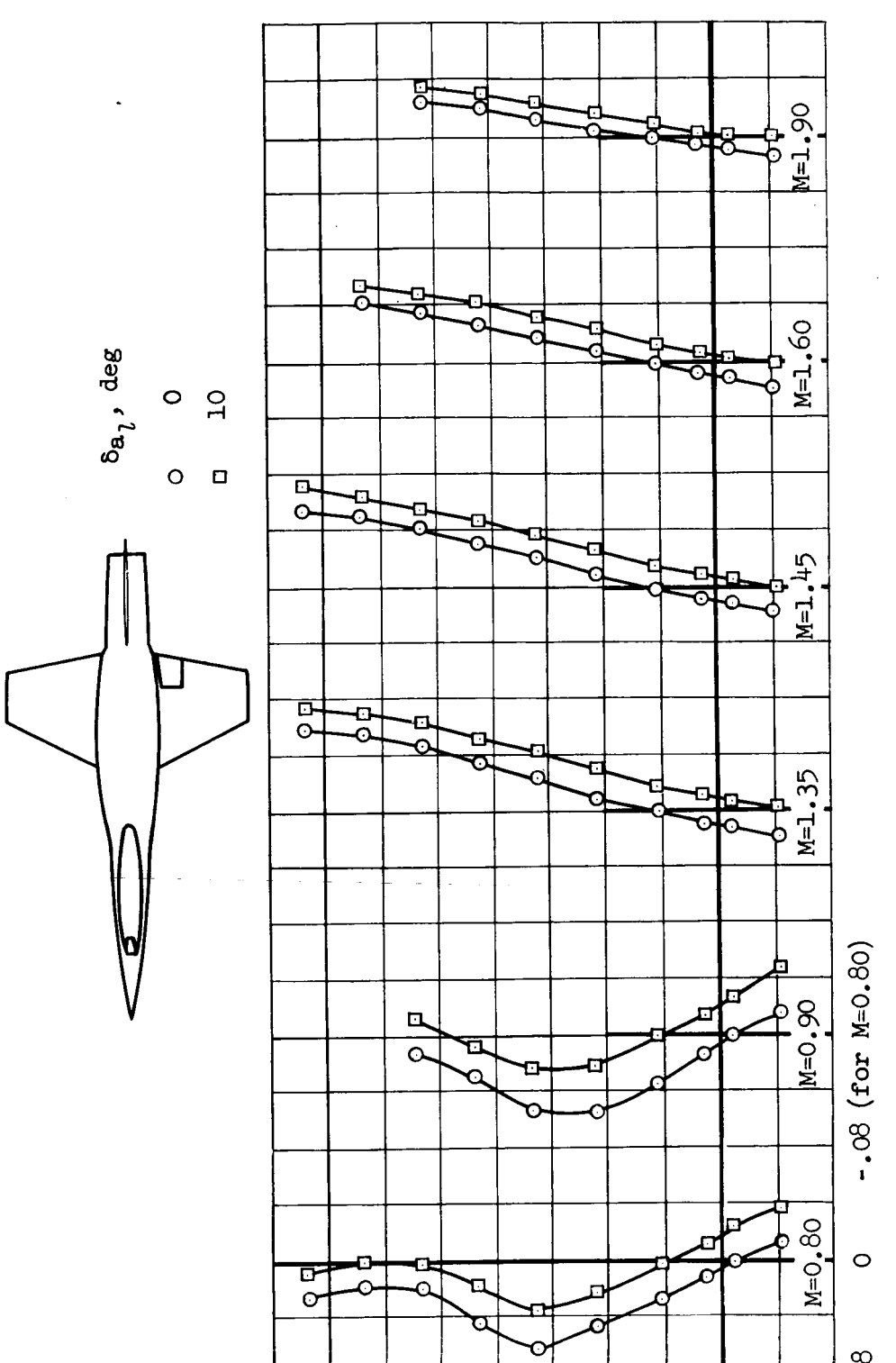

(d) Inboard aileron, horizontal tail off.

Figure 16.- Concluded.

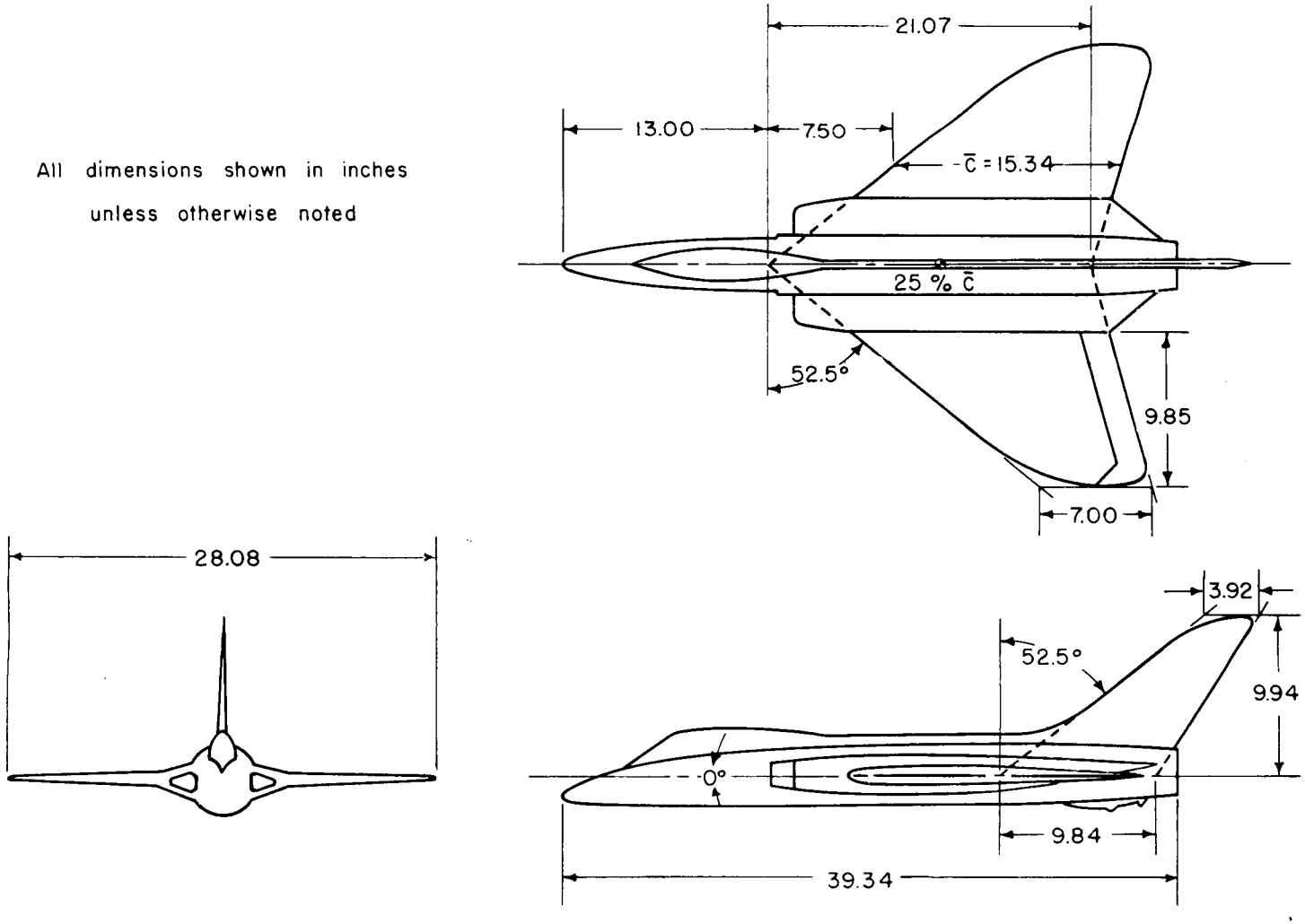

(a) Three-view drawing.

Figure 17.- Dimensional sketch of model C.

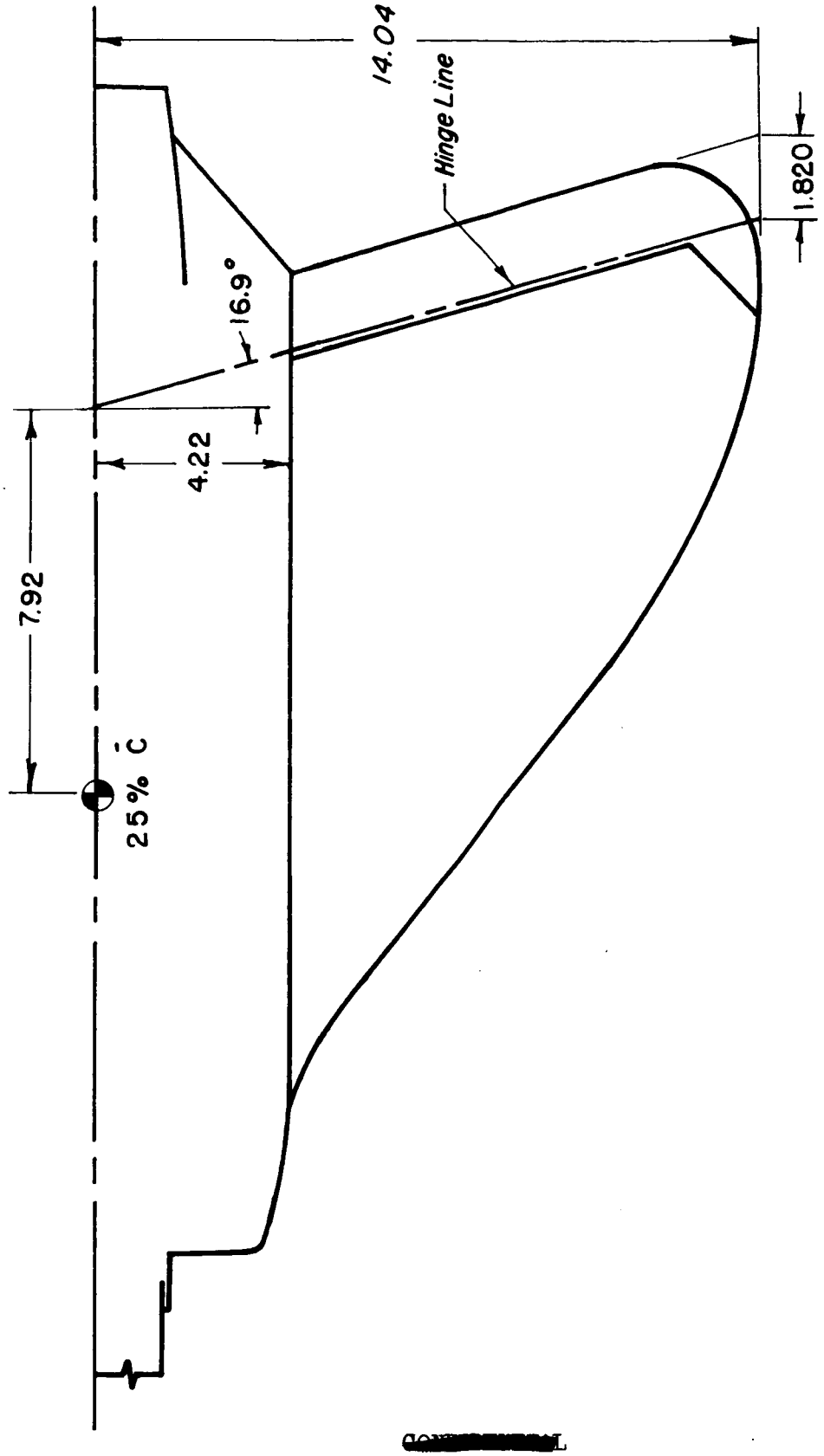

(b) Aileron detail.

Figure 17.- Concluded.

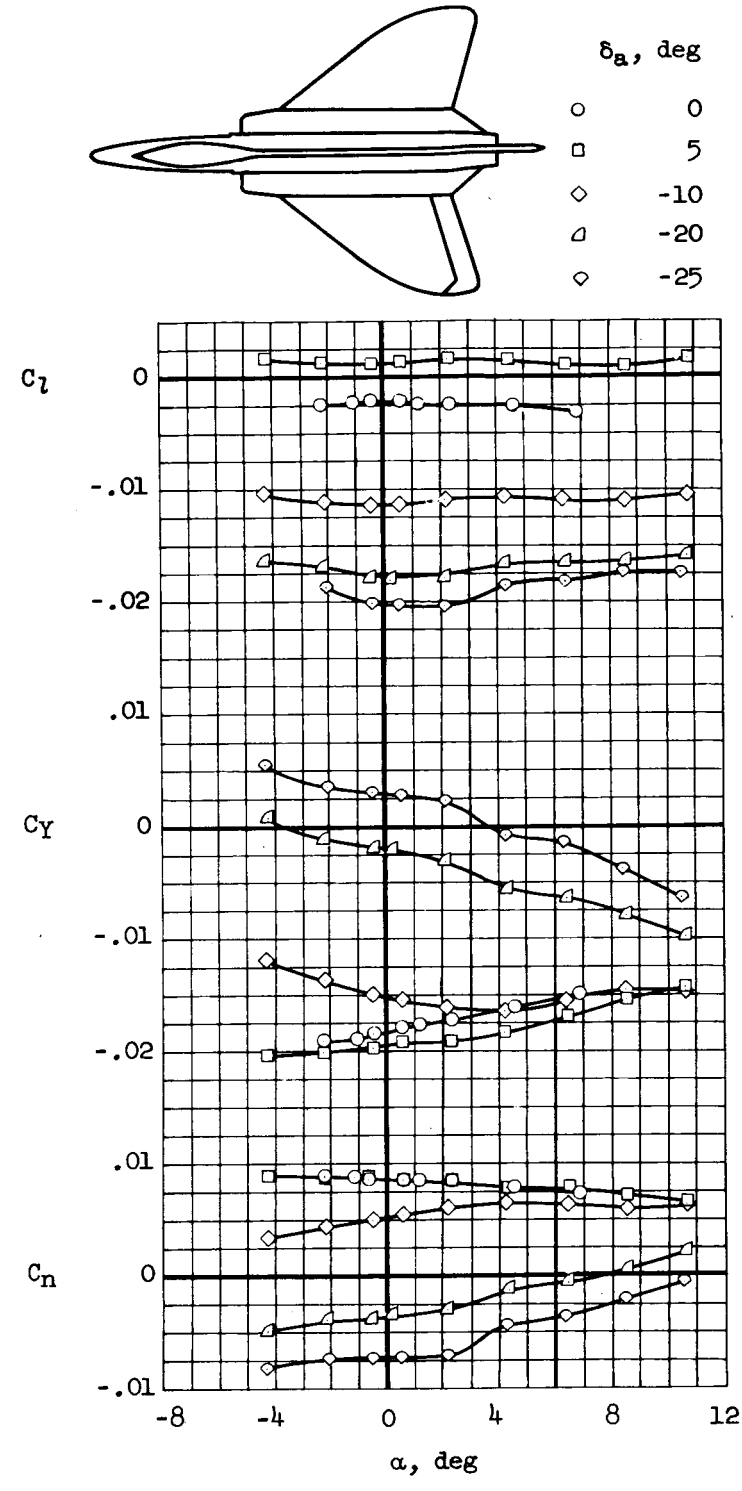

(a) M = 1.25

Figure 18.- Variation of C_l, C_Y, and C_n with angle of attack for model C.

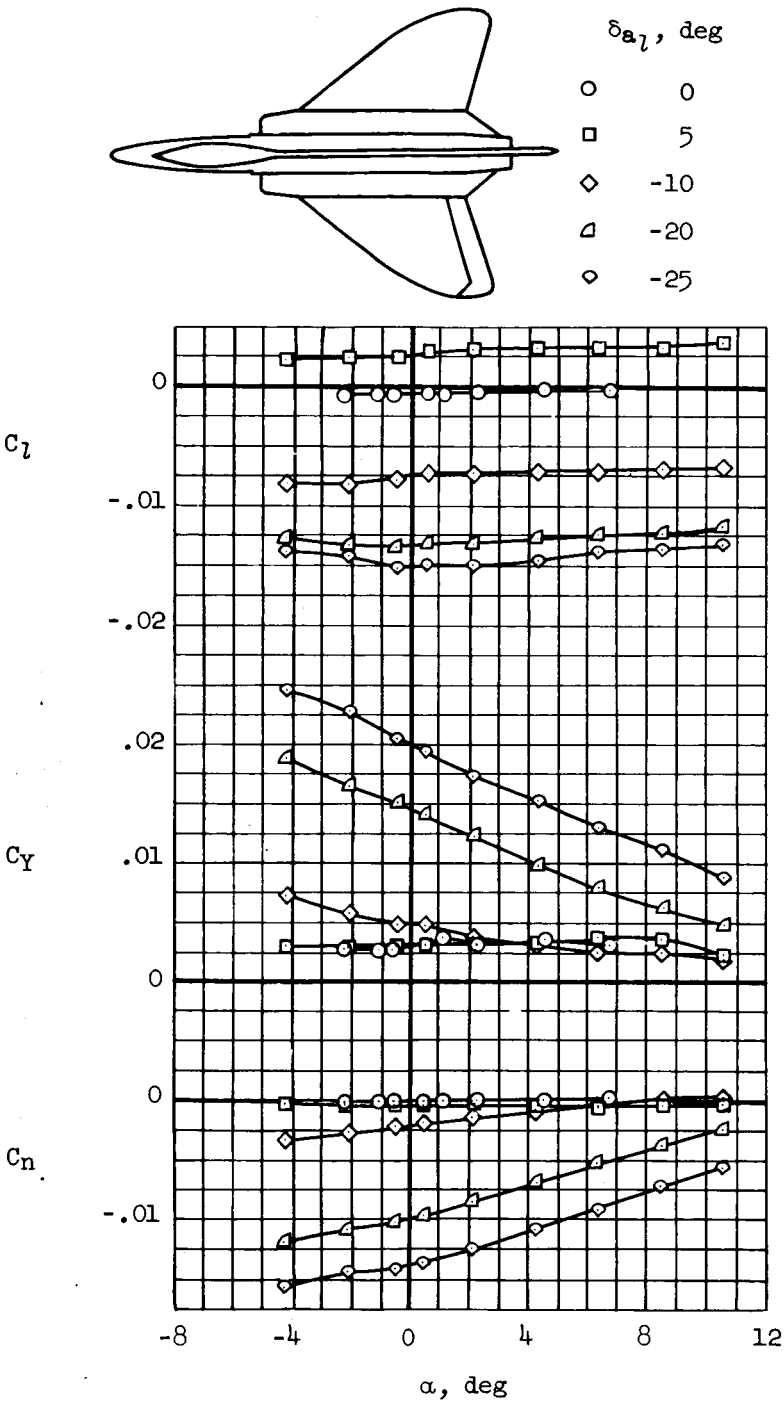

(b) M = 1.40

Figure 18.- Continued.

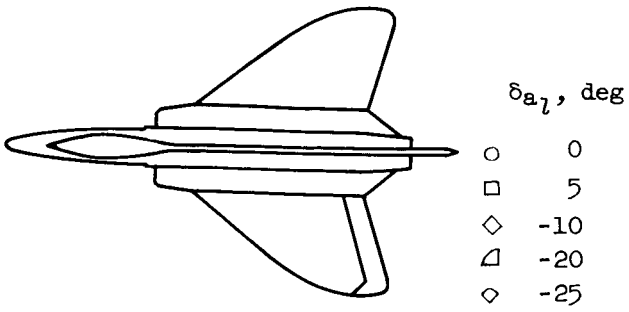

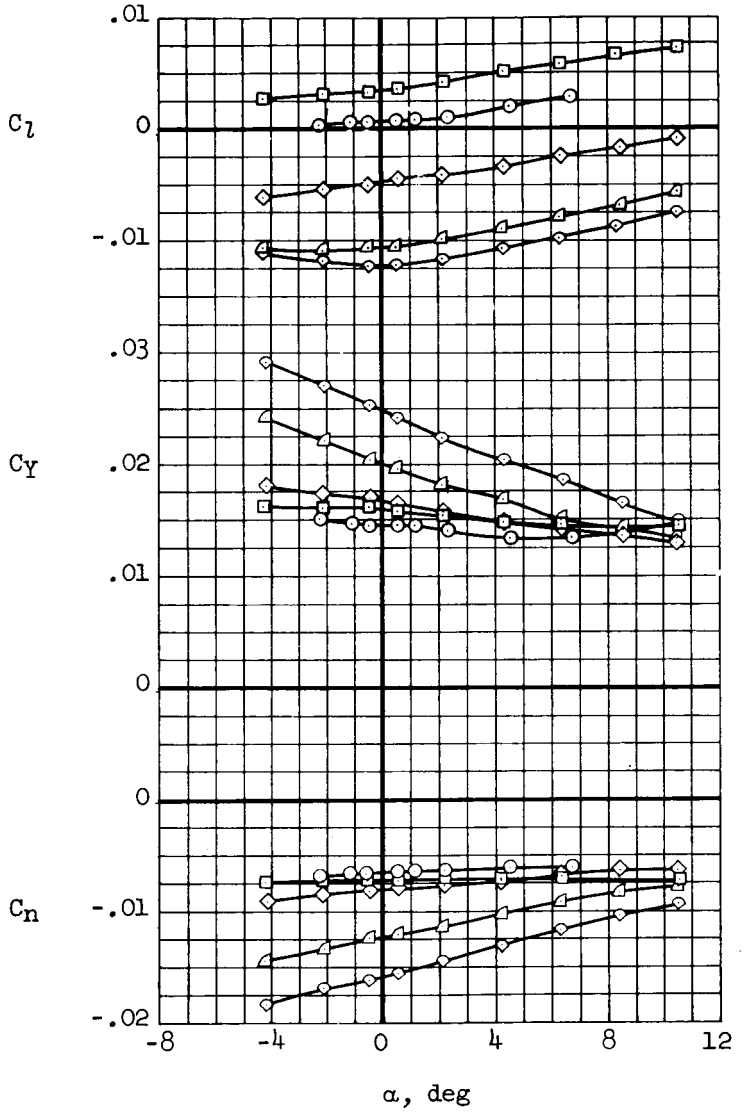

(c) M = 1.65

Figure 18.- Continued.

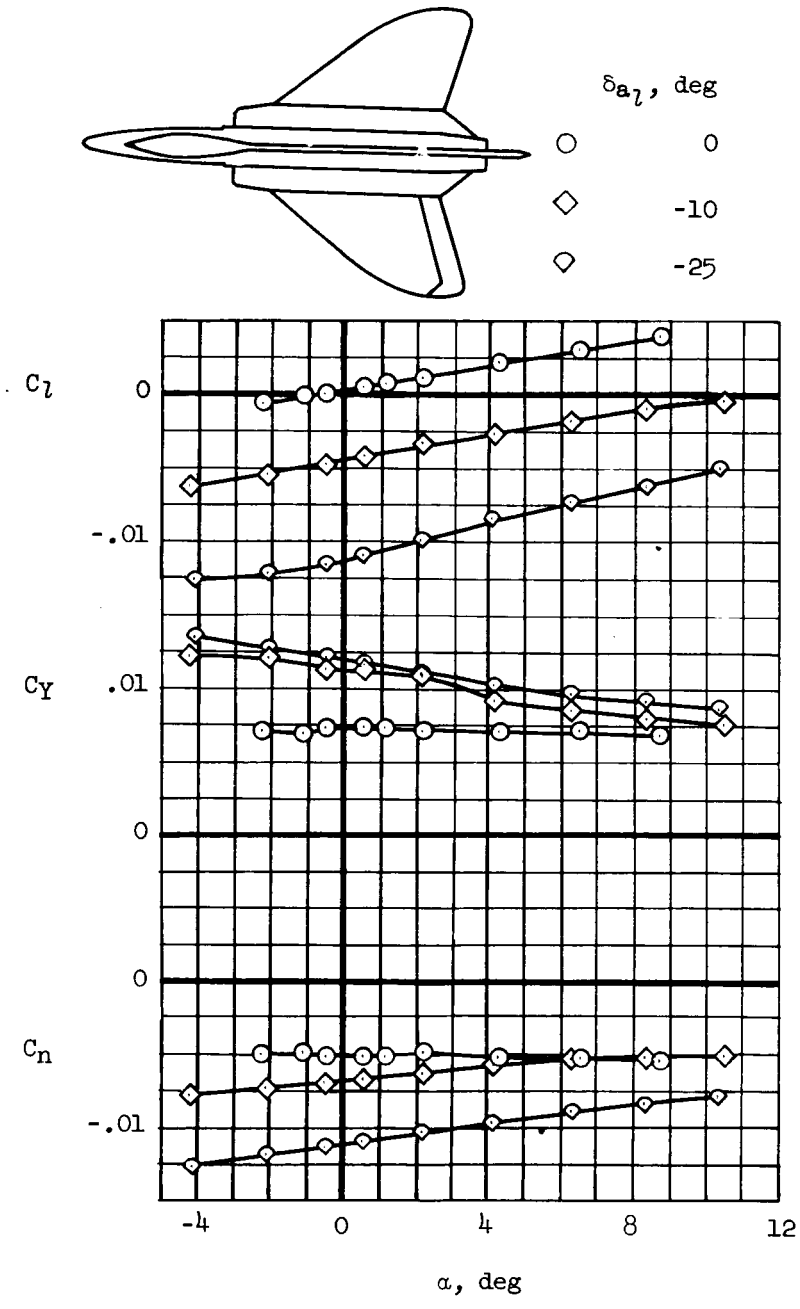

(d) M = 1.90

Figure 18.- Concluded.

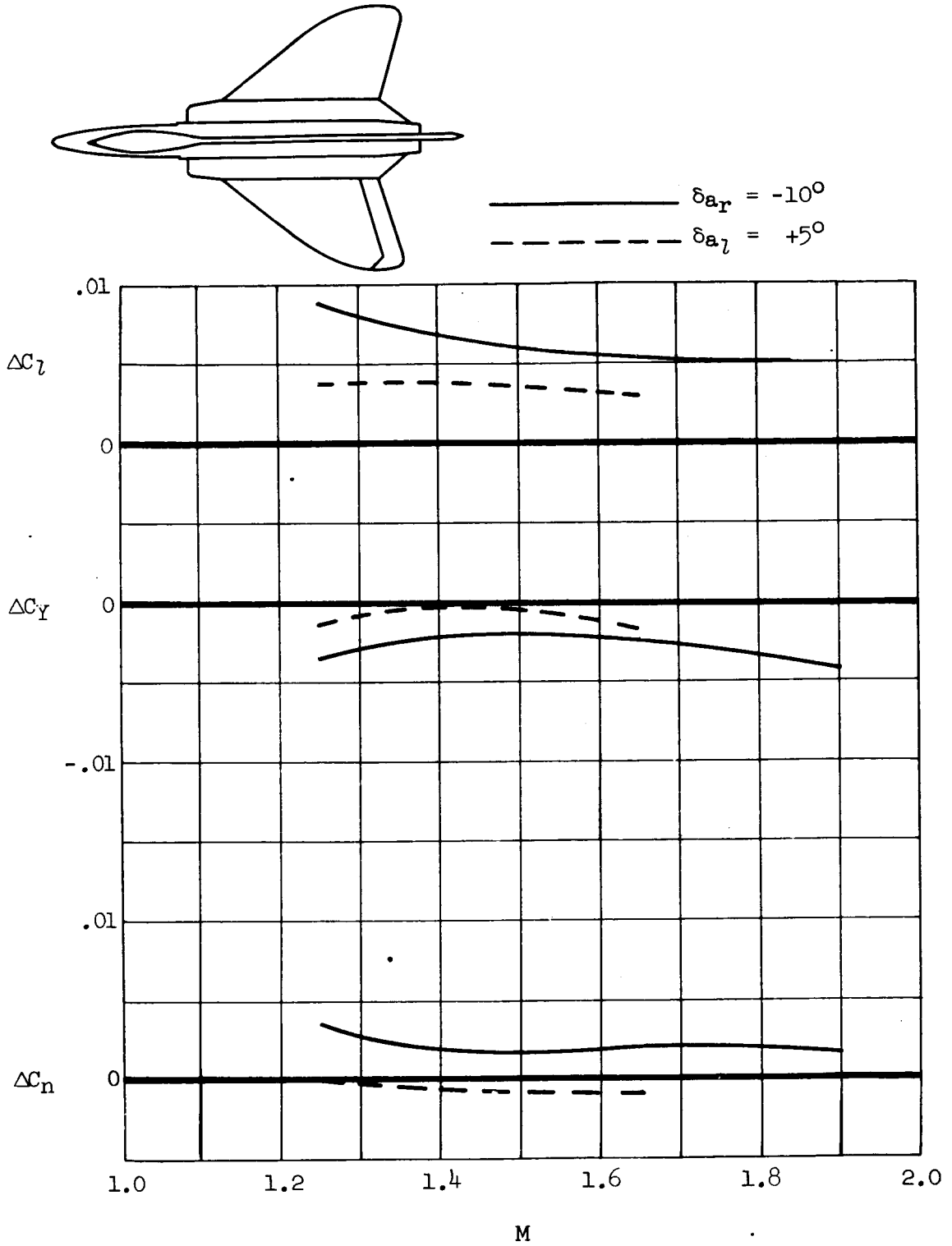

Figure 19.- Variation of ΔC_l, ΔC_Y, and ΔC_n with Mach number for model C; $\alpha = 0°$.

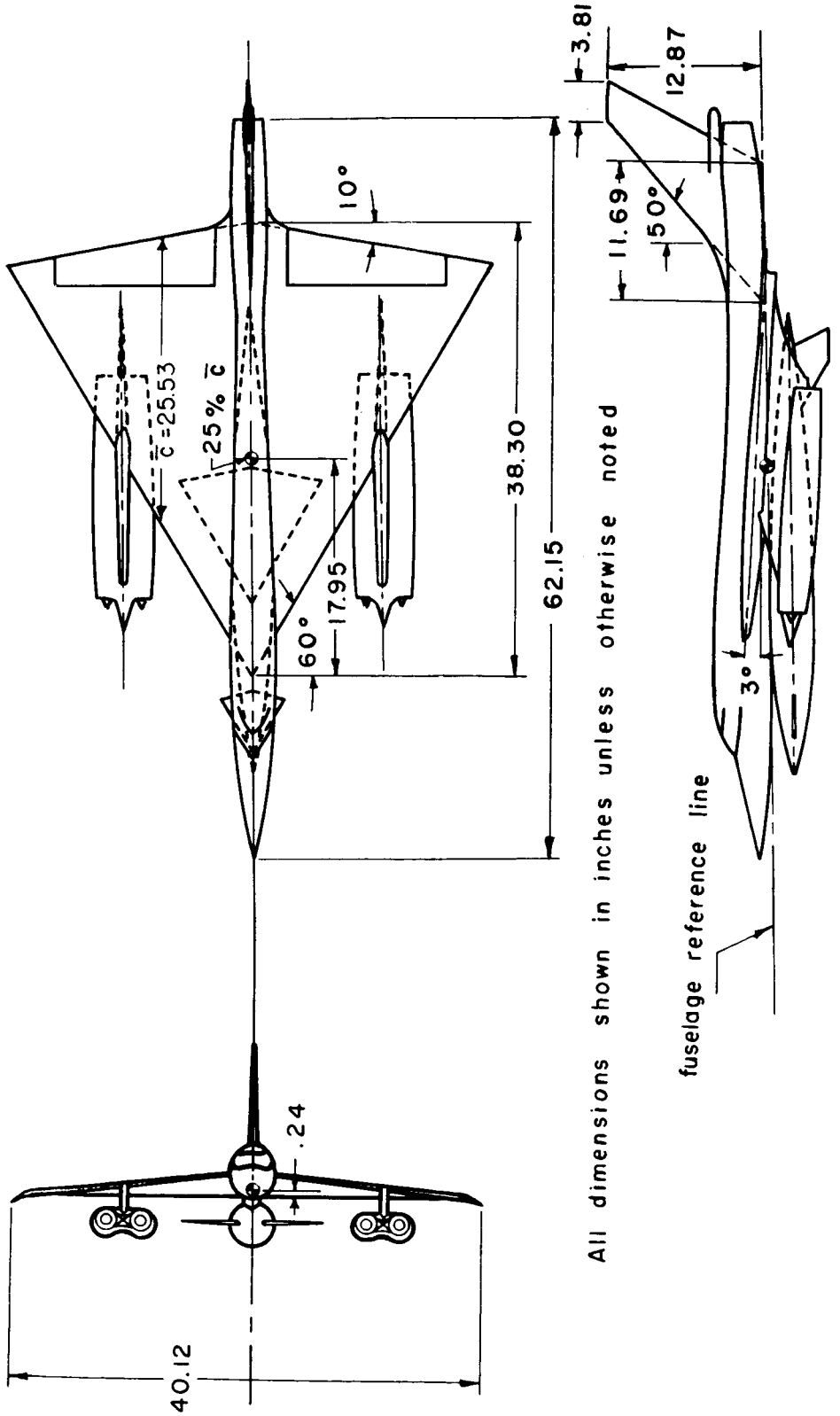

(a) Three-view drawing.

Figure 20.- Dimensional sketch of model D.

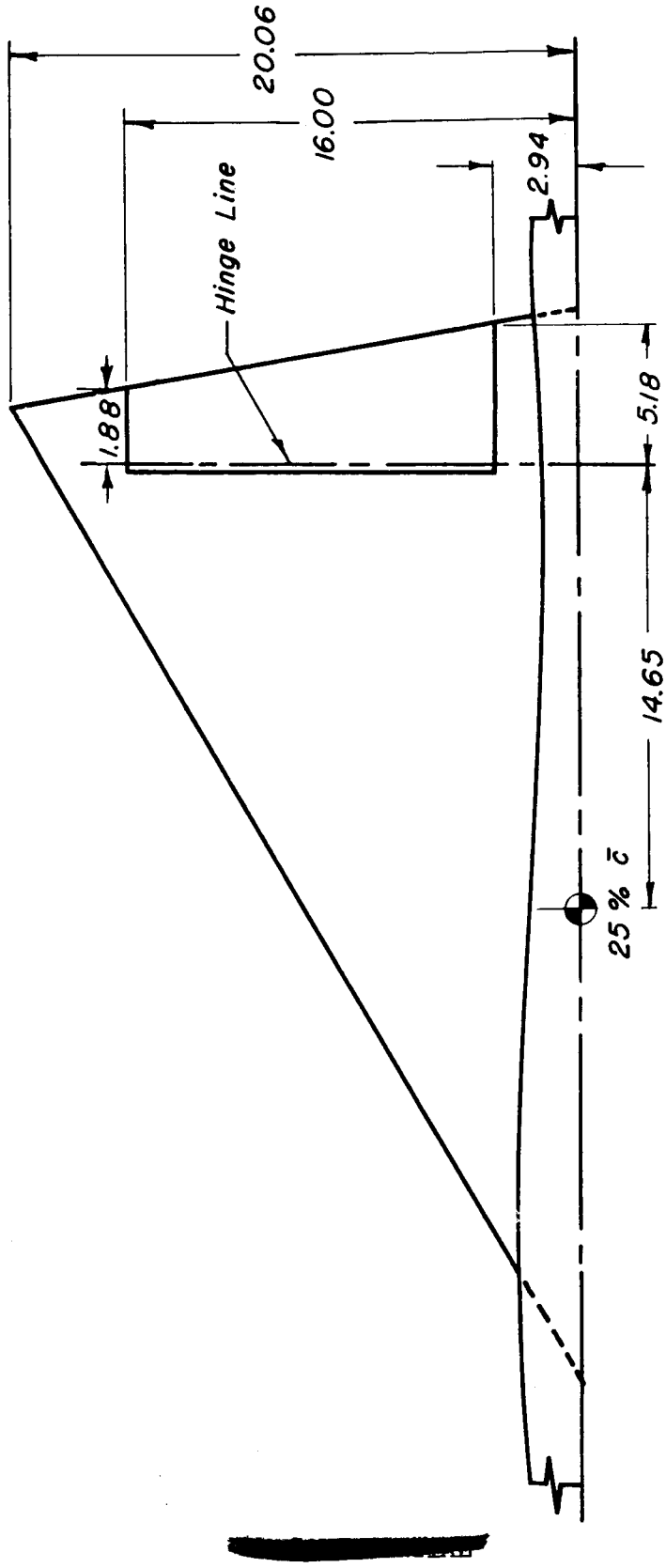

(b) Aileron detail.

Figure 20.- Concluded.

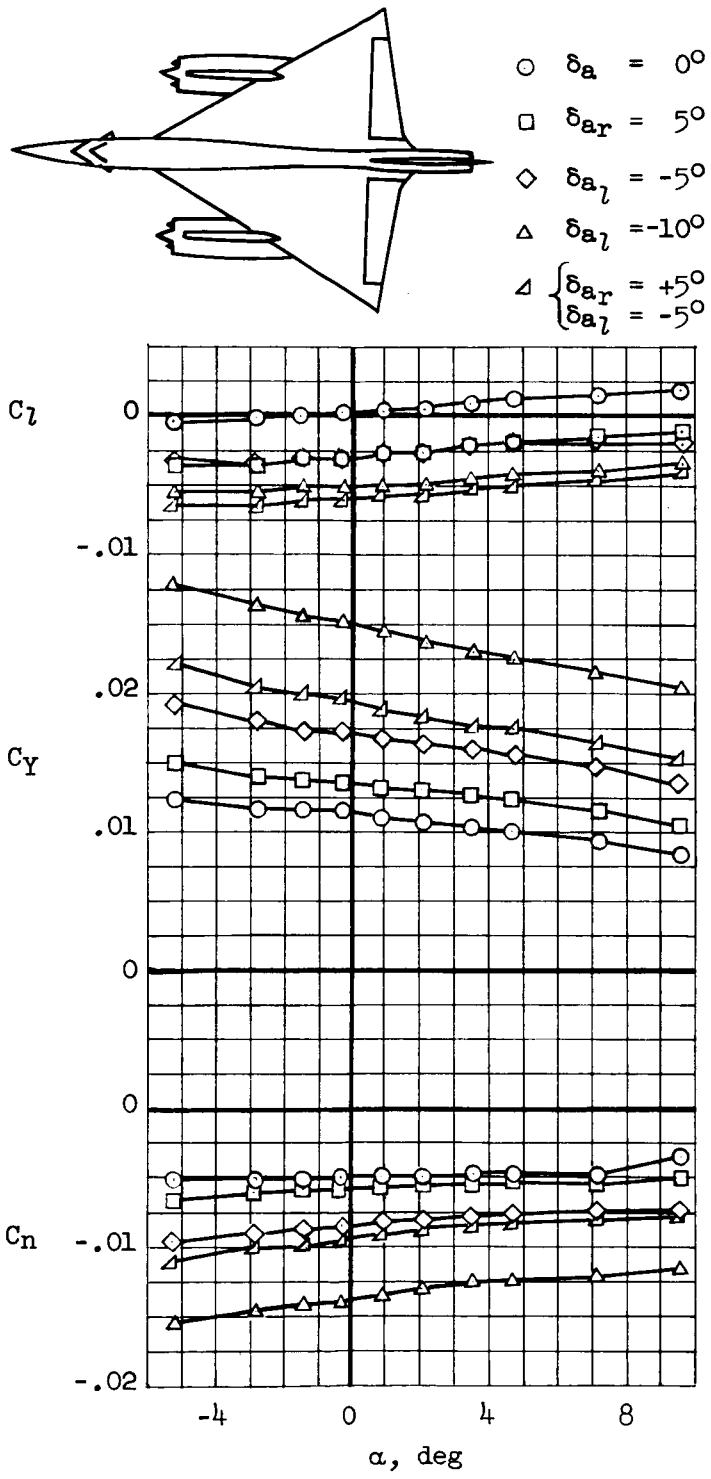

(a) M = 1.60

Figure 21.- Variation of C_l, C_Y, and C_n with angle of attack for model D.

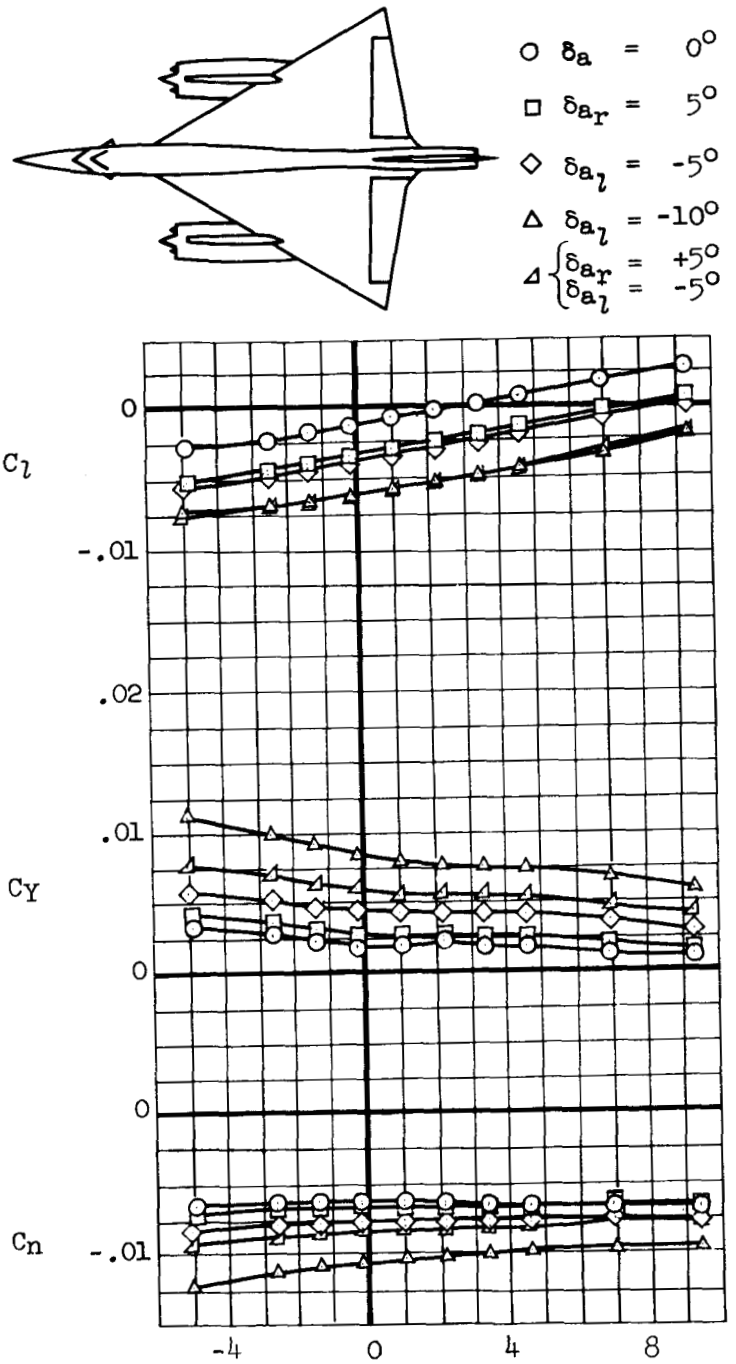

(b) M = 1.90

Figure 21.- Concluded.

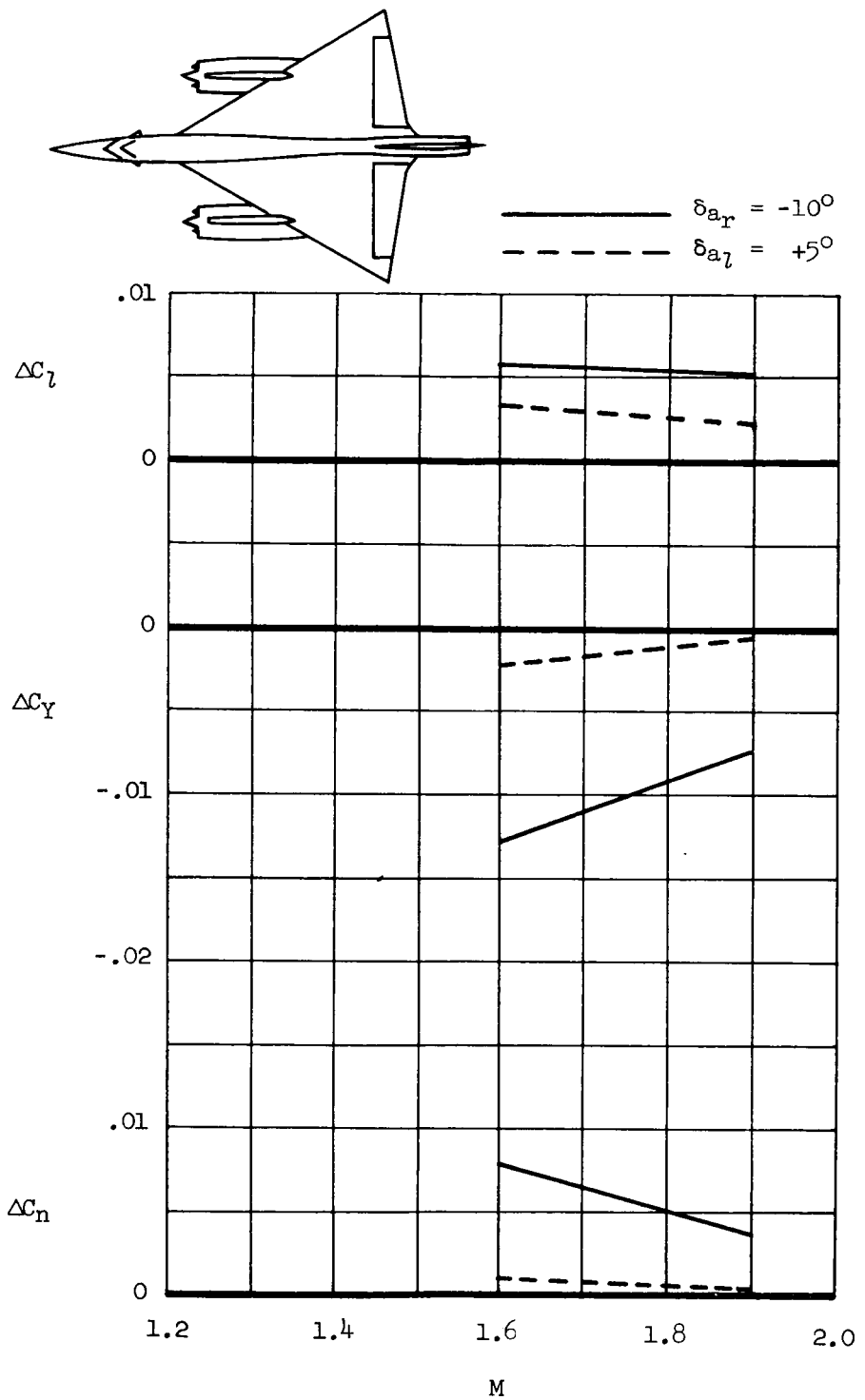

Figure 22.- Variation of ΔC_l, ΔC_Y, and ΔC_n with Mach number for model D; $\alpha = 0°$.

NACA - Langley Field, Va